

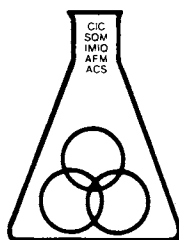
Biocatalysis and Biomimetics

Biocatalysis and Biomimetics

James D. Burrington, EDITOR
B.P. America Research and Development

Douglas S. Clark, EDITOR
University of California

Developed from a symposium sponsored
by the Divisions of Petroleum Chemistry, Inc.,
and of Industrial and Engineering Chemistry, Inc.,
as part of the program of the Biotechnology Secretariat
at the Third Chemical Congress of North America
(195th National Meeting of the American Chemical Society),
Toronto, Ontario, Canada,
June 5-11, 1988



American Chemical Society, Washington, DC 1989



Library of Congress Cataloging-in-Publication Data

Biocatalysis and biomimetics.

(ACS Symposium Series, 0097-6156; 392).

"Developed from a symposium sponsored by the Divisions of Petroleum Chemistry, Inc., and of Industrial and Engineering Chemistry, Inc., as part of the program of the Biotechnology Secretariat at the Third Chemical Congress of North America (195th National Meeting of the American Chemical Society), Toronto, Ontario, Canada, June 5-11, 1988."

Includes bibliographies and indexes.

1. Enzymes—Biotechnology—Congresses.
2. Biomimetics—Biotechnology—Congresses.
- I. Burrington, James D., 1951- . II. Clark, Douglas S., 1957- . III. American Chemical Society. Division of Petroleum Chemistry. IV. American Chemical Society. Division of Industrial and Engineering Chemistry. V. American Chemical Society. Biotechnology Secretariat. VI. Chemical Congress of North America (3rd: 1988: Toronto, Ont.). VII. American Chemical Society. Meeting (195th: 1988: Toronto, Ont.). VIII. Series.

TP248.65.E59B56 1989 660.2'995 89-307
ISBN 0-8412-1611-8

Copyright © 1989

American Chemical Society

All Rights Reserved. The appearance of the code at the bottom of the first page of each chapter in this volume indicates the copyright owner's consent that reprographic copies of the chapter may be made for personal or internal use or for the personal or internal use of specific clients. This consent is given on the condition, however, that the copier pay the stated per-copy fee through the Copyright Clearance Center, Inc., 27 Congress Street, Salem, MA 01970, for copying beyond that permitted by Sections 107 or 108 of the U.S. Copyright Law. This consent does not extend to copying or transmission by any means—graphic or electronic—for any other purpose, such as for general distribution, for advertising or promotional purposes, for creating a new collective work, for resale, or for information storage and retrieval systems. The copying fee for each chapter is indicated in the code at the bottom of the first page of the chapter.

The citation of trade names and/or names of manufacturers in this publication is not to be construed as an endorsement or as approval by ACS of the commercial products or services referenced herein; nor should the mere reference herein to any drawing, specification, chemical process, or other data be regarded as a license or as a conveyance of any right or permission to the holder, reader, or any other person or corporation, to manufacture, reproduce, use, or sell any patented invention or copyrighted work that may in any way be related thereto. Registered names, trademarks, etc., used in this publication, even without specific indication thereof, are not to be considered unprotected by law.

PRINTED IN THE UNITED STATES OF AMERICA

ACS Symposium Series

M. Joan Comstock, *Series Editor*

1989 ACS Books Advisory Board

Paul S. Anderson
Merck Sharp & Dohme Research
Laboratories

Alexis T. Bell
University of California—Berkeley

Harvey W. Blanch
University of California—Berkeley

Malcolm H. Chisholm
Indiana University

Alan Elzerman
Clemson University

John W. Finley
Nabisco Brands, Inc.

Natalie Foster
Lehigh University

Marye Anne Fox
The University of Texas—Austin

G. Wayne Ivie
U.S. Department of Agriculture,
Agricultural Research Service

Mary A. Kaiser
E. I. du Pont de Nemours and
Company

Michael R. Ladisch
Purdue University

John L. Massingill
Dow Chemical Company

Daniel M. Quinn
University of Iowa

James C. Randall
Exxon Chemical Company

Elsa Reichmanis
AT&T Bell Laboratories

C. M. Roland
U.S. Naval Research Laboratory

Stephen A. Szabo
Conoco Inc.

Wendy A. Warr
Imperial Chemical Industries

Robert A. Weiss
University of Connecticut

Foreword

The ACS SYMPOSIUM SERIES was founded in 1974 to provide a medium for publishing symposia quickly in book form. The format of the Series parallels that of the continuing ADVANCES IN CHEMISTRY SERIES except that, in order to save time, the papers are not typeset but are reproduced as they are submitted by the authors in camera-ready form. Papers are reviewed under the supervision of the Editors with the assistance of the Series Advisory Board and are selected to maintain the integrity of the symposia; however, verbatim reproductions of previously published papers are not accepted. Both reviews and reports of research are acceptable, because symposia may embrace both types of presentation.

Preface

BIOCATALYSIS AND BIOMIMETICS presents a cross section of recent advances in catalytic science and biotechnology. The chapters that follow will serve to illustrate how many of the key challenges in biotechnology can only be addressed by bringing together traditionally "separate" disciplines within chemistry and biology.

A subtitle for this volume might read, "A View of Biotechnology Through the Eyes of a Catalysis Scientist". As such it is not intended as an all-encompassing view of chemical opportunities for biotechnology, nor will it cover the recombinant-DNA or monoclonal antibody methods normally associated with modern biotechnology. Many such reviews are already available. Rather, it is meant to focus on emerging enabling technologies at the interfaces of catalysis and biology that will provide new opportunities for the chemicals industries. Key aspects to be presented within this major theme of catalysis and biotechnology are biomimetics and hybrid catalysts, biocatalytic applications of computers and expert systems, enzyme solid-state structure and immobilization, enzyme structure-activity relationships, and the use of enzymes under novel conditions.

The editors have been fortunate to have assembled contributions from world-class authorities in this field. We sincerely thank all who participated to make this not only a successful symposium, but an important contribution to the literature as well. We also thank the Biotechnology Secretariat for coordination of the symposium cluster on Biocatalysis and Biomimetics and the sponsoring Divisions of Petroleum Chemistry, Inc., and of Industrial and Engineering Chemistry, Inc. We greatly appreciate the contributions from E. I. du Pont de Nemours and Company, Monsanto Company, Eastman Kodak Company and B.P. America. The gracious support and understanding of our wives, Cindy Burrington and Molly Clark, and that of our families is most warmly acknowledged.

JAMES D. BURRINGTON
B.P. America Research
and Development
Cleveland, OH 44128
November 11, 1988

DOUGLAS S. CLARK
Department of Chemical
Engineering
University of California
Berkeley, CA 94720

Introduction

Biotechnology: Chemistry Is at the Heart of It

by Mary L. Good

Biotechnology is the study and application of genetic engineering techniques to improve the value of such things as crops, livestock, and pharmaceuticals. It is the adaptation of living systems to produce higher value-added products and processes. Planned are applications in medicine and agriculture that were considered impossible only 15 years ago. They include:

1. genetically altered bacteria for producing medicinals
2. alfalfa engineered to produce valuable proteins
3. livestock as factories for a human blood-clotting protein
4. cleanup of industrial wastes by bacteria
5. bacteria engineered as diagnostic tools

Chemistry is at the core of this fantastic new science of biotechnology. Jacqueline K. Barton of Columbia University has said, "You may notice that neither the words 'chemical' nor 'molecular' is incorporated into 'biotechnology', but the heart of what I think is exciting about this area is indeed chemical." Biotechnology depends on our ability to manipulate chemical structure in biological systems on the molecular level. We are learning how the structures of large biological molecules determine their functions. By altering chemical structure, we are learning how to design molecular properties with increasing precision and predictability.

We have also begun to understand that how well we manipulate these chemical structures may ultimately determine our nation's status in the global economy.

Several pharmaceutical and diagnostic products produced using recombinant DNA techniques are already on the market and more are on the way. It has been estimated that by the year 2000, the biotechnology market could reach \$100 billion. The predictions are that high value-added specialty products are likely to appear first, followed by production of chemicals and feedstocks, and later, biomass conversion.

The U.S. chemical industry has been quick to recognize the potential of this new technology and invest in it. Howard E. Simmons of DuPont tells us that his company spends one-third of its billion-dollar research budget for biotechnology-related research. In the company's Central Research & Development Department, for instance, half of the scientists working on biotechnology programs are chemists. Dow, Monsanto, American Cyanamid, and Eastman Kodak are a few of the other companies following suit.

The U.S. lead in most areas of biotechnology research has been challenged by West Germany, Great Britain, Switzerland, Sweden, and France, but most aggressively by Japan. In the United States, although large companies are forming or acquiring their own biotechnology divisions, the biotechnology development effort is led by small start-up firms that derive early technology from government-sponsored research at the universities. In Japan, large firms such as brewing companies with extensive bioprocess experience lead in biotechnology R&D. Their time scale for strategic planning is 10–15 years, a long-term view compared with the usual 3–5-year planning period in the United States. The National Science Foundation has concluded that the quality of biotechnology research performed in Japan matches that done in the West.

A study commissioned by the U.S. Department of Commerce predicts that Japan will offer the United States stiff competition in biosensors for the medical market. According to the study, Japan already is competitive in cell culture technology; is now fourth in the world and gaining in protein engineering; and is scaling up its lagging effort in recombinant DNA technology.

What is the role of the American Chemical Society? We have the capabilities and resources, and in terms of our charter an *obligation*, to make a positive contribution toward solving our nation's economic problems and to lead the chemical profession into new areas. Biotechnology will be one of the significant areas for the employment of chemists in the future and will greatly affect our standard of living. The establishment of this Biotechnology Secretariat, which presented its first technical program two years ago, is one proof of ACS' commitment. We have also:

1. presented a Select Conference on Advances in Biotechnology and Materials Science to many of those who make and interpret national science policy.
2. considered launching a new journal in biotechnology.
3. developed *CA Selects* in several areas of biotechnology.
4. considered a definition for a new certified B.S. degree with an emphasis on biochemistry.

These initiatives, because they have broken new ground, presented a challenge to the Society, one that we have met. Quite frankly, a driving force for change has been the recognition that many trained as chemists are already working in biotechnology fields. As a result, new program initiatives in biotechnology will go through more easily. All we have to do is dream them up.

Allied-Signal, Inc.
Morristown, NJ 07960-1021

October 19, 1988

Chapter 1

Biocatalysis and Biomimetics

New Options for Chemistry

James D. Burrington

B.P. America Research and Development, Cleveland, OH 44128

As a dominant technology in the chemicals industries, catalysis provides an important long-term commercial target for biotechnology. While enzymes represent the most efficient catalytic systems known, their impact on the chemicals industry relative to traditional catalysts is still small. Developments at the interface of biology and chemistry will be key to overcoming the major barriers to broad industrial application of enzyme catalysis.

The Impact of Catalysis

The overwhelmingly dominant technology in chemicals-related industries is catalysis. Commercial catalytic processes account for over half of all fuels production and for 60% of the 135 MM metric tons of organic chemicals produced annually in the U.S. In fact 20% of the nation's GNP can be attributed to catalytic processes (1). Thus, from a technical standpoint, advances in the chemicals industry are strongly linked to advances in catalysis.

A key property of catalytic processes is selectivity. Catalysis has revolutionized process chemistry by replacement of wasteful, unselective (i.e. multiple-product-forming) reactions with efficient, selective (i.e. one-product-dominating) ones. For example, selective catalytic methanol carbonylation (practiced by BP, BASF Monsanto, Eastman) has to a large extent substituted unselective non-catalytic n-butane oxidation (Celanese, and Union Carbide processes).

Control of reactivity by catalysis provides the capability to shift to lower cost feedstocks. In the twentieth century, advances in catalysis have allowed the substitution of acetylene with olefins and subsequently with synthesis gas as primary feedstocks. For example, production of acrylic acid, traditionally produced by the Reppe process from acetylene and CO, has now been replaced by catalytic oxidation of propylene. The emergence of paraffins, the hydrocarbon feedstock of the future, will depend on development of catalysts for selective alkane C-H activation (2).

0097-6156/89/0392-0001\$06.00/0

© 1989 American Chemical Society

Catalysis has also had a major impact on the functional and specialty chemicals businesses, providing lower cost routes and higher performance materials than would have otherwise been possible. Major examples are from polymer syntheses including Ziegler-Natta, anionic, cationic polymerization processes, for formation of polyolefins, ABS resins, polyesters and other synthetic materials. Future materials areas include high temperature composites, electronic materials and conducting organics.

The role of catalysis in the petroleum industry has been equally revolutionary. Metal-supported systems (e.g. of Topsoe and Shell) for catalytic reforming, hydrodesulfurization and hydrodenitrification, alkylation catalysts and shape selective systems (e.g. zeolites and pillared clays) for catalytic cracking (FCC) and production of gasoline from methanol (Mobil MTG) all represent significant technical and commercial achievements.

Thus, the impact of new technologies on the chemicals industries can be assessed to a large extent by its impact on the commercial practice of catalysis.

Nature's Catalysts

At the molecular level, nature's catalysts, the enzymes (isolated or as microbial systems) provide tremendous rate increases over the corresponding uncatalyzed reactions and virtually quantitative selectivity. The capability to both improve selectivity to a single product and utilize alternate feedstocks is well documented (3-4).

A major selectivity advantage of biological catalysts over traditional systems includes the ability to form single products (chemical selectivity) as well as single optical isomers (stereoselectivity). Specific examples where biological routes are preferred commercially include fermentative processes for the amino acids monosodium glutamate (MSG), lysine, aspartic acid, citric acid and phenylalanine (5). Many other chemicals have also been produced by fermentative processes (6).

Enzymes also provide a potential means to utilize alternate feedstocks which cannot be selectively activated by conventional catalysts, or to improve selectivity over traditional systems. For example, the hydroxylase enzymes convert paraffins to alcohols with virtually 100% selectivity, a reaction which has no analogue in traditional catalysis (7). The Nitto acrylonitrile to acrylamide process is an example of how biocatalysis can improve selectivity over traditional catalysis (8-10).

Coaxing Nature to Work Harder

The exciting technical opportunities in biocatalysis are tempered by the major barriers to commercialization which still exist. Most notably, these include low stability of an expensive catalyst, and the high separation and capital costs associated with low concentrations of reactants and products.

These significant barriers are largely responsible for the lack of substantial commercial impact of enzyme and microbial catalysts on the chemicals-related industries. High fructose corn syrup and amino

acids by fermentation remain the only significant chemicals produced by biotechnology and represent only a tiny fraction of industrial chemicals output.

Prospects

Advances in the life sciences over the past 30 years have produced the new enabling technologies normally associated with modern biotechnology, namely genetic engineering and monoclonal antibody methods. While these will surely be key to many new products, particularly in health care and agricultural markets, these methods alone are not likely to permit a major impact on the chemicals industries.

Along with the development of these enabling biological methods, catalysis and other technologies (such as computer modeling and expert systems), which already have a major influence on the chemicals industries, have also made major technical advances. The integration of biotechnology with these more traditional areas represents a means to capture the technical advances across a number of chemicals-related disciplines.

For example, the importance of the complimentary roles of surface, bulk and interfacial structure in heterogeneous catalysis (11-13), also indicates the need to address these issues in explaining and predicting catalytic behavior of enzyme systems as well.

From this cross-disciplinary approach a number of new enabling technologies are now emerging. The combination of biological and chemical catalysts to produce hybrid catalysis or "biomimetic" systems has shown some promise in capturing the high selectivity of enzymes with the favorable processing characteristics of traditional catalysts (see D. Clark, R. H. Fish, R. DiCosimo contributions, this publication). The growing body of information on structure/function relationships of enzymes is being accelerated by advanced crystallographic methods and the use of computer modeling and expert systems (see G. A. Petsko, G. Klopman, W.A. Goddard contributions, this publication). New methods of enzymology, including novel immobilization and reaction conditions (see T. A. Hatton, N. Herron, R. Sipehia contributions, this publication) have demonstrated the potential to improve catalytic performance.

These advances can collectively be viewed as the growing field of biocatalysis and biomimetics. Along with the biotechnical developments, these provide another option for exploiting the potential of enzyme catalysis in the chemicals industry. The following chapters present representative examples of current advances in this emerging field.

Literature Cited

1. Witcoff, H. Chem. Systems Report, Third Annual Review Meeting; New York, Jan. 17-18, 1985.
2. Weissermel, K.; Arpe, H. J., eds., Industrial Organic Chemistry, Verlag Chemie: New York, 1978, p 254.
3. Stiefel, E. I. Chemical Engineering Process, Oct 21, 1987.
4. Whitesides, G. M.; Wong, C-H. Angew. Chem. Int. Ed. Eng., 1985, 24, 617.

5. Sedovnikova M. S.; Belikov, V. M. Russian Chemical Reviews, 1978, 47, 357.
6. Quелlette, R. P.; Cheremisinoff, P. N. Applications of Biotechnology, Technomic Publishing Co.: Lancaster, 1985, p 72.
7. Leak, D. J.; Dalton, H. Biocatalysis, 1987, 1, 23.
8. Nitto Chemical Industry. U.S. Patent 4 414 331, 1983.
9. Nitto Chemical Industry. U.S. Patent 4 421 855, 1983.
10. Nitto Chemical Industry. U.S. Patent 4 343 900, 1982.
11. Gates, B. C.; Katzer, J. R.; Schuit, G. C. A. The Chemistry of Catalytic Processes, McGraw-Hill: New York, 1979.
12. Grasselli, R. K.; Brazdil, J. F. Solid State Chemistry in Catalysis, ACS Symposium, Series 279, American Chemical Society: Washington, D. C., 1985.
13. Vedrine, J. C.; Coudurier, G.; Forissier, M.; Volta, J. C. Catalysis Today, 1987, 261.

RECEIVED October 17, 1988

Chapter 2

Biomedical Science and Technology

The Interdisciplinary Challenge

Paul B. Weisz

Departments of Chemical Engineering and Bioengineering, University
of Pennsylvania, Philadelphia, PA 19104-8393

Interdisciplinary bridges across chemistry, chemical engineering science and medicine are compelling challenges to progress basic insights and solutions for major problems in the life sciences and technologies. An analysis of the molecular spectrum identifies some trends, basic phenomena and skills involved, and examples of basic focal points for the joining of existing but largely segregated skills.

Interdisciplinary Research - Vogue or Reality?

"Interdisciplinary" is a word used frequently these days. Perhaps some of us think -or even hope- that it is a vogue that will pass. It is a fact, however, that our institutions, communications and activities in the sciences have become increasingly subdivided into "specialties". As researchers, we generally keep drilling deep in our own specialty parcels, with but occasional excursions to adjacent fields. Our institutions (organizational units, departments, course structures, journals, funding organizations, "peer" groups, etc.) are neatly subdivided, categorized, organized. All these factors, by interdependence and mutual perpetuation, mold the character of education, attitudes, professional language, and the opportunities as well as constraints in the choice, type and execution of research, career, the structure of knowledge, etc.

Perhaps the word "interdisciplinary" will go away. But the concept will not, because society needs it. There is a growing awareness that real problems in our society

NOTE: This chapter was presented as the plenary address of the symposium, Impact of Surface and Interfacial Structure on Enzyme Activity.

0097-6156/89/0392-0006\$06.00/0
• 1989 American Chemical Society

are not optimally served by the convenience (and comforts) of orderly compartmentation. We recall (1) a 1979 meeting in Princeton, attended by leading scientists from diverse fields, including Nobel Laureates, in which the keynote speaker, Ashly Montagu, observed that

"The present degree of specialization has resulted in a condition of intellectual isolationism. This manifests itself in inability to see ... relevance of content, methods and models of other ... disciplines, existence of an inbred ... philosophy ... largely irrelevant to ... problems of modern life."

Ten years before that, an observation, outspoken but humorously true, was that of E. Haskell (2) (Connecticut Review, p. 84, April, 1969):

"The multiversity has now become the modern tower of Babel, each of whose departmental languages grows ever less understandable to members of all other departments."

The evolving field of biomedical science and technology appears to be one that recognizes from the outset that it must deal with "real" and "relevant" problems of health, life, and, literally, with survival; that there is little time or value to engage in moral debate over what is "pure", basic, or applied research. Louis Pasteur, whom we could well call the father of biomedical science and technology, stated nearly a century ago "There is only one science: A basic science and its application."

As we address biomedical problems, as Pasteur did, we surely deal with "real" problems, "relevant" to society, and we are forced thereby to look to the skills of all the disciplines. It is significant that many of these most important pieces of knowledge to be embraced and used exist already at a quite basic level of the sciences, not buried in great depths of specialized sophistication.

In that spirit, let us examine some very basic science concerning the nature and behavior of the molecules that are the actors in all of life. From whatever we touch to the mechanisms of life itself, we deal with molecules and molecular processes. Figure 1 displays molecules, molecular complexes, and molecular systems of our world, in the order of their molecular weights (M.W.). From left to right we have molecular entities of ever increasing sizes and complexities.

Molecular Entities, Phenomena, Skills

Moving from simple gases, through inorganic and organic compounds, somewhere we get to peptides, oligomers and to polymers, macromolecules like proteins or polysaccharides; we move on to complexes or interacting systems of molecules, like neurons or cell organelles; to systems of systems, like cells, organisms, organs, people, and societies, each an associative, dynamic molecular system of ever increasing order. Mathematically and actually,

Under this spectrum, I have indicated where the center of gravity, or focus of interest has been of a few of our named disciplines.

Starting on the left (Figure 1), chemistry has first dealt with the realm of chemical (atomic) composition and structure of molecules, and focused on reactivity of molecules (or its parts), progressing from simple toward more complex structures. At the other end of the spectrum, medicine has always dealt with the vast biological complexity of people.

Early in this century, a few chemical and medical scholars of a few universities in Austria-Hungary and southern Germany crossed the constraints of disciplinary boundaries. It led to the beginnings of biochemistry (3), to at least four Nobel Prizes (4), and to vitamins. It was a decisive step toward bridging the vacuum between the right and the left of our spectrum, by applying the chemical skills of composition and structure to various biological entities of relatively small to fair molecular complexity, with a growing and, finally, a major emphasis on the complexity of proteins.

Molecular biology is certainly a prominent outgrowth of that trend and discipline, with its center of gravity heavily in the realm of structural detail of proteins, and the significance and relationship of that sophistication to informational phenomena (recognition, immune response, replication, genetics, etc).

We face the challenge of increasingly bridging the large remaining gaps. We might say that we know many pieces, but we know too little of how they effect the whole. What are some of the phenomena that are fundamental to a successful march across this bridge?

As we progress from left to right, we move from problems of composition, structure and reactivity of *compounds* to those of the dynamics of interacting *processes* and *process systems*; generally we move from individual entities to systems, and these become directed to very specific *missions* to be achieved, with mandatory *efficiency*, and within the constraints of many physical and chemical parameters acting upon the process system as a whole.

During the last few decades, the study of processing systems, their constraints, behavior and performance for specific missions has centered largely in the compartments of chemical engineering science. It is important to discard any image of 100 foot towers that may arise at the word "engineering". Fortunately, the fundamentals of chemical engineering science are equally applicable to chemical process systems of any dimension.

Chemical Engineering and Bio-Medicine

For example, chemical engineering science has evolved much basic knowledge, qualitative and quantitative guidelines for the understanding and design of porous, heterogeneous

catalysts for chemical processes. They deal with criteria that define how large the catalytic materials or regions may be to support a desired conversion rate; how that relationship depends on the concentration of the molecules undergoing conversion; how the size and geometry of catalytic regions can effectively accomplish a sequence of reactions, inhibit it, or side-track it (5,6).

All these considerations are basic and equally applicable to the broad variety of biochemical reaction systems. We can use them to determine the optimal size of catalyst particles in a giant petroleum cracking process; but they have interdisciplinary, i.e. universal applicability to any molecular process systems (7) including the biochemical transformation processes at the dimensions of organs, cells, organelles, and smaller molecular units.

By way of an example illustrated in Figure 2, "chemical engineering" criteria can provide relationships between the maximum allowable dimensions of the intracellular enzymatic reaction systems, or the minimum concentrations of metabolic intermediates they are to process, required to achieve certain desired magnitudes of turnover numbers (6b). At the time of this publication, applying chemical engineering science useful in the chemical process industry to cellular processes was an excursion with a very small audience, in spite of the universal applicability of its criteria. Only occasionally, the biochemist has applied the concepts, often after independent efforts; for example, Nevo and Rikmenspoel showed that such an "engineering" criterion links the optimal (and actual) physical length of the tail of spermatozoa firmly to the concentration of the ATP generated at its base (6c).

Today, chemical engineering science is logically able to apply its skills to phenomena of the molecular processing systems characteristic of bio-medicine and to their "modelling" to develop rigorous and quantitative foundations. The basic need for the bridges in our spectrum of knowledge (Figure 1) to span the territory of chemical systems, promises fruitful results from an increasing partnership between the sciences of medicine, chemical engineering and chemistry.

Quite in line with the above quoted comment by Haskell, such partnership will mainly require courage, effort and patience to overcome a divisive language barrier. It is, I believe, the only barrier that stands in the way to a meeting of minds, and to an explosive acceleration towards major insights and revelations.

The detailed interaction and dynamics of several molecular entities and parameters in an entire process system, is of crucial importance throughout biology and medicine. It is well illustrated by the battle of an army of macrophage, seeking, meeting and annihilating invading pathogens. A recent study of my chemical engineering and medical colleagues (8) is another example of the

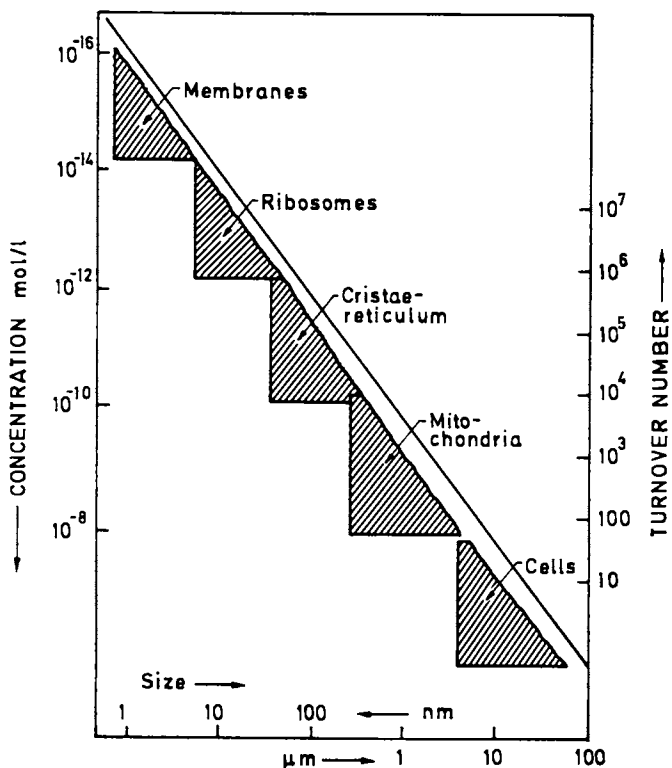


Figure 2. Basic relationships between maximum dimension of biochemical apparatus (e.g. cell component), achievable turnover number, and concentration of metabolic intermediate to be processed (see ref. 7).

combination of "chemical engineering" modelling with medical inquiry (9). The success of the vital process involves invasion rates, pathogen and macrophage concentrations, mobility behavior etc.. The results of their analysis, sketched in Figure 3, demonstrates the dramatic importance of the macrophage having a slight but critical chemotactic directivity superimposed on its general mobility. Below that critical value, the required time of battle goes to infinity, i.e. the war is lost.

By way of such insights, we can see how, like diffusion coefficients in chemical technology, cell motility and chemotactic coefficients are becoming fundamental parameters with rigorous significance. Aided by a symbiosis between the skills of chemical process science and medicine, they are bound to become routinely accessible by experiment, as rigorous descriptive parameters for biomedical research, and potentially for medical, diagnostic purposes .

Trends

There are currently at least three notable and important trends observable that work in the direction of narrowing the gaps between the simple and the complex molecular world we described in Figure 1.

One is the increasing number of demonstrations that some less complicated chemical things on the left can do some things best known in the complex medical sector on the right. The best representatives of that trend are the researches devoted to chemical mimics for molecular recognition or enzymatic action. An example is the demonstration by Myron Bender and co-workers (10) of b-benzoyl-L-glutamate, a relatively simple molecule pictured in Figure 4A, as an efficient mimic of the enzyme chymotrypsin, a protein containing 245 amino acid residues. The reaction rate equals or exceeds that of the natural enzyme. In addition, its stability to denaturation is superior over a vast range of pH conditions, as shown in Figure 4B.

There is now a complementary trend quietly reaching from the complex right to the far left of our working spectrum (Figure 1). The bulk of biochemical science has focused on the nucleic acids and complex macromolecules, proteins, DNA and RNA. The skills of sequencing and determination of ever increasing structural detail have grown rapidly. We have become accustomed to expect, as a matter of routine, that all or most of such detail is essential for the functioning of any prominent bioactive entity, such as growth factor or any other "factor".

Now, the word *fragment* is beginning to make a dominant appearance. In diverse instances, smaller molecular entities derived from an important and complex macromolecule are found to have similar biochemical functions as the prominent parent, sometimes displaying one of the parent's several (desirable and undesirable) functions.

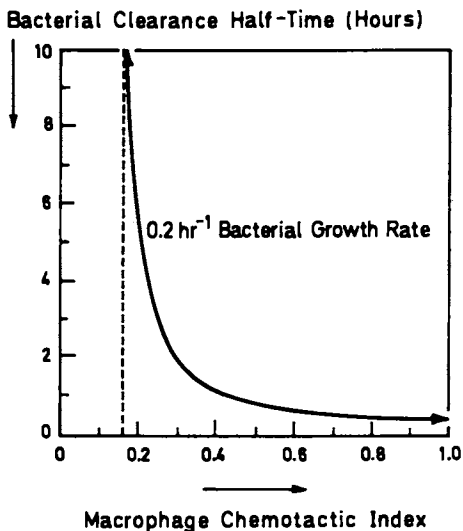
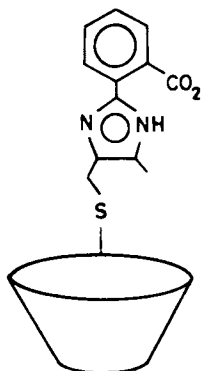


Figure 3. Clearance of Bacterial Attack by Macrophage on the Lung Surface. Success (represented by the time required for clearance, the ordinate) depends critically on the coefficient of chemotactic motility (abscissa). Initial macrophage and bacterial densities = 10^3 cm^{-2} ; random motility coeff. = $10^{-8} \text{ cm}^2/\text{sec}$; speed = $3 \mu\text{m}/\text{min}$.

(A)

CHYMOTRYPSIN:

245 amino acid
sequence β - BENZYME:

Cyclodextrin

Figure 4. Enzyme mimic for chymotrypsin. (A) Structure and molecular weights. (Continued on next page.)

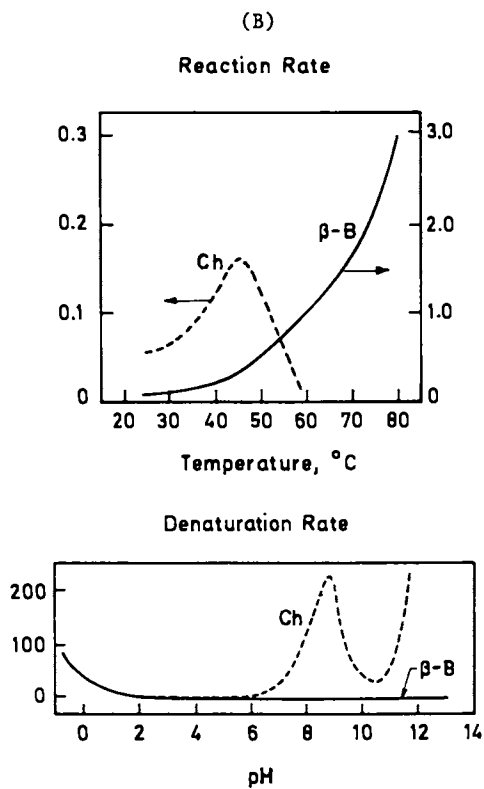


Figure 4. *Continued.* (B) Comparative reaction rates and stability to denaturation.

Soon after the discoveries by J. Folkman and his associates, of the powerful role heparin could play in promoting tumor induced angiogenesis (11, 13), and its dramatic capability, when combined with certain steroids, to inhibit such angiogenesis and thereby arrest tumor growth (12, 13), the modulating effects of the complex, 10,000 to 40,000 M.W. glycosaminoglycan, were shown to be obtainable from a fragment of but five to seven sugar units (12, 13). Similarly, the antithrombic activity traditionally associated uniquely with heparin was shown to be obtainable from a small (five to seven glucose oligomeric) fragment of heparin (14, 15, 16).

We have some fascinating analogies in animal and plant biology. We are familiar with the release of biochemical factors (growth factors, glycosaminoglycans, etc.) that results from tissue injury and their vital role in the subsequent repair mechanisms. We now note that the destruction of plant cell walls also leads to important products. They are relatively small oligo-saccharide fragments. They have important functions in plant growth regulation and antibiotic defense (17).

Fragments of hyaluronic acid, in contrast to the whole parent compound, have been reported to be promoting neo-vascularization (18). Sub-fragments of myosin have been shown to be sufficient to cause movement of actin filament (19). Nicotinamide and nicotinamide group containing fractions of a tumor derived ethanol extract were reported to have angiogenic activity and would represent the first non-proteinic low molecular weight molecules tumor derived growth factor (20).

A third trend, now following the mushrooming discoveries of growth factors, is a phase of discovery of growth inhibitors. This, in turn, leads logically to a heightened awareness (21) that the condition for the normal, i.e. the non-pathological state, is the achievement of balance in a dynamic network of kinetics involving a number of stimulating and inhibiting molecular participants (factors) seeking to act upon one, perhaps more receptors. It is analogous, if not equivalent to the systems of heterogeneous catalytic chemistry, where receptors become sites, stimulating and inhibiting factors become promoters and poisons, and the role of more than one receptor in the accomplishment of a task becomes known as polyfunctional catalysis (6a).

Challenges

In the first two trends, we recognize indications of ripeness and fertility that awaits us in exploring the gap between "simple" chemistry and "complex" medicine. The third observation re-emphasizes the important role of evolving rigorous kinetic models which become essential, first for "keeping track" of, and subsequently for "making sense" out of the many interactive events in a multicomponent system, of promoters, inhibitors,

protagonists and antagonists, in the real kinetic systems of biomedical chemistry. It underlines the future utility of the linking of skills between the biomedical and the chemical "engineering" sectors.

Linkages progress in many ways and instances. Many are catalyzed by ever widening capabilities of instrumental skills, exemplified by the study and use of nuclear magnetic resonance techniques. The joining of intellectual approaches and skills between disciplines will create major and basic advances such as to have multiple impacts on many branches of biomedical science.

Angiogenesis is an example of a *basic* process in biomedicine: It impacts on many aspects and branches of health and disease: Wound healing, ovulation and menstrual activity, inflammatory diseases including arthritis, tumor growth and management, neovascular ophtamological diseases, psoriasis, to name a few. It is a basic process *system*, where the biomedical and the chemical 'engineering' researcher can apply their respective *skills* for 'modelling' to advance the understanding of behavior, balance, and control of complex kinetic networks (and three interacting components already suffice to produce a "complex" network!). Dr. J. Folkman and I will report some results from such a cooperation in the following paper.

I will close with an example of where the pooling of knowledge from segregated disciplines could be of great potential importance:

Silicon and aluminum oxides and hydroxides are the most abundant compounds on our earth. They exist in rock, soil, the dust we breathe, and as components or trace components in just about all we touch or consume. Over decades, they have made their appearance in a number of segments of medicine such as fibrotic diseases, tumor induction, Alzheimer's disease, and aluminum related bone diseases. Of these Alzheimer's disease is perhaps one of the most serious diseases in our society. Here a still mysterious role of "aluminum" is observed and acknowledged by many researchers.

In traditional teaching of chemistry these oxides are considered among the stablest materials. On the other hand, in another discipline, namely in modern catalytic chemistry and technology, we know of and utilize the catalytic capabilities of trace amount of aluminum associated with silica (22). A major portion of petro-chemical technology depends on these sites (receptors). Yet the potential relevance of that extensive experience in catalytic chemistry of the rugged hydrocarbons, remains largely unrecognized and segregated from the world of delicate and diverse biochemical entities and processes.

Acknowledgment

Support by the Mobil Foundation for the initiation of interdisciplinary studies is hereby gratefully acknowledged.

Literature Cited

- (1) Ashly Montagu, Keynote Address, "Crisis in Scientific Research", Princeton, N.J., October, 1979;
- (2) E. Haskell, Connecticut Review, p.84, April, 1969;
- (3) "The Origins of Modern Biochemistry", P.R. Srinivasan, J.S. Fruton, J.T. Edsall, Ed.'s, Ann. N.Y. Acad. of Sciences, Vol. 325, 358, 1979;
- (4) H. Fischer (Vienna); O. Loewi (Graz); F. Pregl (Graz); A. Szent Györgyi (Szeged)
- (5) P. B. Weisz and C.D. Prater, "Interpretation of Measurements in Experimental Catalysis", Adv. in Catalysis, Vol.6, Academic Press, New York, 1956; C.N. Satterfield, "Mass Transfer in Heterogeneous Catalysis", MIT Press, Cambridge, 1970; R. Aris, "The Mathematical Theory of Diffusion and Reaction in Permeable Catalysts", Clarendon Press, Oxford, 1975;
- (6) (a) P.B. Weisz, "Polyfunctional Heterogeneous Catalysis", Adv. in Catalysis, Vol. 13, 1962; (b) P.B. Weisz, "Enzymatic Reaction Sequences and Cytological Dimensions, Nature, 195, 772, 1962; (c) A.C. Nevo and R. Rikmenspoel, J. Theor. Biol. 26, 11, 1970.
- (7) P. B. Weisz, "Diffusion and Chemical Transformation: An Interdisciplinary Excursion", Science, 179, 433, 1973;
- (8) E.S. Fisher, D.A. Lauffenburger and R.P. Daniele, "The Effect of Alveolar Macrophage Chemotaxis on Bacterial Clearance from the Lung Surface", Amer. Rev. of Respiratory Diseases, in publ., 1988;
- (9) D.A. Lauffenburger, "Mathematical Analysis of the Macrophage Response to Bacterial Challenge in the Lung", in "Mononuclea Phagocytes: Characteristics, Physiology and Function", R. van Furth, Z. Cohn and S. Goron, Ed.'s, Martinus Nijhoff, 1985;
- (10) V.T. D'Souza, X.L. Lu, R.D. Ginger and Myron L. Bender, Proc. Natl. Acad. Sci. USA, 84, 673, 1987;
- (11) S. Taylor and J. Folkman, "Protamine is an inhibitor of angiogenesis", Nature, 297, 307, 1982;
- (12) J. Folkman, R. Langer, R. Linhardt, C. Haudenschild, and S. Taylor, "Angiogenesis Inhibition and Tumor Regression caused by Heparin or a Heparin Fragment in the Presence of Cortisone", Science 221, 719, 1983;
- (13) J. Folkman, "Regulation of Angiogenesis: A new Function of Heparin", Biochem. Pharmacology, 34, 905, 1985;
- (14) R.J. Linhardt, A. Grant, C.L. Cooney, and R. Langer, "Differential Anti-Coagulant Activity of Heparin Fragments Prepared Using Microbial Heparinase", J. Biol. Chem., 257, 7310, 1982;
- (15) J. Choay, J.C. Lormeau, M. Petitou, P. Sinaÿ and J. Fareed, "Structural Studies on a Biologically Active Hexasaccharide Obtained from Heparin", Ann. N.Y. Acad. Sci. 370, 644, 1981;

- (16) L. Thunberg, G. Bächström and U. Lindahl, "Further Characterization of the Antithrombin Binding Sequence in Heparin", *Carboh. Res.*, 100, 393, 1982;
- (17) K.T.T. Van, P. Toubart, A. Cousson, A.G. Darvill, B.J. Gollin, P. Shelf, and T. Albersheim, "Manipulation of the Morphogenetic Pathways of Tobacco Explants by Oligosaccharins", *Nature* 314, 615, 1985; see the overview: P. Albersheim and A.G. Darvill, "Oligosaccharins", *Scient. American* 253, 58, 1985;
- (18) D.C. West, I.N. Hampson, F. Arnold and S. Kumar, "Angiogenesis induced by Degradation Products of Hyaluronic Acid", *Science* 228, 1324, 1985;
- (19) Y.Y. Toyoshima, S.J. Kron, E.M. McNally, K.R. Neibling, C. Toyoshima and J.A. Spudich, "Myosin Subfragment-1 is Sufficient to Move Actin Filaments in vitro", *Nature* 328, 536, 1987;
- (20) F.C. Kull, D.A. Brent, I. Parikh and P. Cuatrecasa, *Science* 236, 843, 1987;
- (21) Jean L. Marx, "Cell Growth Control Takes Balance", *Science* 239, 975, 1988;
- (22) J. Folkman, P.B. Weisz, M.M. Joullié and W.R. Ewing, in publication, *Science*;
- (23) W.O. Haag, R.M. Lago, P.B. Weisz, "The Active Site of Acidic Aluminosilicate Catalysts", *Nature* 309, 589, 1984.

RECEIVED January 25, 1989

Chapter 3

Interdisciplinary Challenges

Control of Angiogenesis

Judah Folkman¹ and Paul B. Weisz²

¹Departments of Surgery, Anatomy, and Cell Biology, Harvard Medical School and Children's Hospital, Boston, MA 02115

²Departments of Chemical Engineering and Bioengineering, University of Pennsylvania, Philadelphia, PA 19104-8393

Angiogenesis is the normal process of growth of capillary blood vessels, but unabated angiogenesis is the basis to many diseases. Heparin administered together with certain steroids can inhibit angiogenesis. In investigations guided by a "simplest possible" chemical kinetic model for the interaction in the heparin/steroid/cell system, we demonstrate that low molecular weight molecules of minimal chemical complexity can take the function of heparin. A polysulfated seven membered cyclopyranose is shown to be nearly a hundred times more effective than heparin.

We will briefly discuss the meaning, role and importance of angiogenesis, and report recent progress concerning angiogenesis inhibition, identifying chemical structures of minimal complexity in the role of heparin, but equally or more effective in antiangiogenic activity.

Angiogenesis

In the adult, new capillary blood vessels are normally not formed except in females, during ovulation, menstruation and pregnancy. Otherwise blood vessels remain quiescent. Endothelial cells which constitute the lining of the vessels divide slowly, if at all. Their turnover time may be as much as ten years. By contrast, other cell systems proliferate rapidly. For example, there are some 10^{10} cell divisions per hour in bone marrow, and the whole bone marrow mass is replaced in some five days.

During angiogenesis (1), however, endothelial cells can change their resting condition into rapid cell proliferation with similarly fast turnover times of a few

0097-6156/89/0392-0019\$06.00/0

• 1989 American Chemical Society

days. Angiogenesis is the phenomenon of inducing sprouting and proliferation of endothelial cells from an existing vascular component, resulting in the generation and growth of new capillaries and vessels; see Figure 1.

Angiogenesis is an active, desirable and necessary phenomenon during healing processes after injury or after myocardial infarction, i.e. after heart attack. On the other hand, there are more than fifty diseases in which angiogenesis turns on abnormally, continues out of control, and causes devastating tissue damage. Therefore, angiogenesis is a basic physiological process, with wide ranging consequences in life and biomedicine.

For example, in ophthalmology, angiogenesis is the most common, basic physiological phenomenon that causes blindness. The capability of adequate control of that condition would have enormously beneficial consequences. In another realm of medicine, tumors induce the most intense angiogenesis by release of its own growth factors (2). It is becoming increasingly evident that progressive tumor growth and metastasis is dependent on angiogenesis for its maintenance and growth, due to its dependence on the endothelial network for nutrient transport (3,4). In view of this linkage of tumor cell and endothelial cell proliferation, successful agents for angiogenesis inhibition would impact importantly on oncology. Targeting the control of the endothelial process, as compared to tumor cell biochemistry, offers an attractive and general strategy (5), especially since tumor species release different and often several angiogenic molecules. At least four angiogenic polypeptides have been analyzed for their complete amino acid sequence (4), but many more factors exist.

Inhibition of Angiogenesis

Inhibition of angiogenesis has been demonstrated to be possible by the unique, simultaneous action of two compositions, a steroid of specific structure and heparin (6,7,8,9). The steroid by itself has little or no effect; heparin also has no inhibiting effect, and at some concentrations may promote angiogenesis. Only the simultaneous application of both agents can result in successful inhibition.

Hydrocortisone has been used most frequently in studies of antiangiogenesis. In view of the well known clinical side effects of hydrocortisone it is of interest that the angiostatic function can be separated from these other steroidal activities by moving the 11-OH group from its beta-position to the alpha-position (i.e. below the plane of the molecule), to produce 11-alpha epicortisol. Such variants of that steroid structure are now potentially available to serve as "angiostatic steroids" (7,8,9).

Angiogenesis inhibition is most conveniently demonstrated and measured in the chick embryo bioassay (CAM assay, see further below). It sets in upon introduction of

about 10 μg of heparin (in 10 μl solution, containing 50 μg of hydrocortisone), for a "good" heparin or heparin fraction. Increasing heparin concentration leads rapidly to an optimal effect, followed by a decline.

On the other hand, the attainable effectiveness and usefulness of the heparin varies greatly with its source (6,10). It is usually manufactured from pig intestine. The product is a heterogeneous, polydisperse composition, its molecular weight in a range from some 10,000 to 40,000, varying among manufacturers, and from batch to batch. Furthermore, studies with heparin administered subcutaneously to mice have shown that heparin's anticoagulant activity is sufficiently close to its antiangiogenic dose requirement to risk bleeding as a serious side effect.

In view of these problems, the fact that heparins have been the only source of an effective co-factor for the anti-angiogenic pair effect, and the general importance of achieving reliable inhibition, we have examined potential mechanisms and structures for an effective alternative molecule.

The "Simplest Model" Approach

Heparin is a material of the family of glycosaminoglycans. Heparins contain some 20 to 60 sugar units bearing many and various substituents (O-sulfate, N-sulfate, glucuronic, N-acetyl, epimers of uronic acid residues) (11a,b,c). The polyionic substituents render the molecule hydrophilic and water soluble.

A customary approach to research concerning the biological activity of a macromolecule focuses on its very detailed chemical structure. If smaller portions of such a molecule exhibit the desired activity, one can more easily duplicate its detailed structure or vary and examine the significance of one or the other structural detail. Heparin fragments of 5 to 7 sugar units have indeed been shown to be active (6). However, the structural/chemical complexity is still so large that the creation of structural variants or duplicates by chemical synthesis requires an extraordinarily large number of synthetic steps (12,13).

We have undertaken an approach different but familiar in scientific system's analysis: Initial construction of a "simplest model" generally consistent with observed behavior and current knowledge, in terms of the smallest number of parameters and most basic (elementary) properties; in our case, the chemical system involves three participants, two molecular species and the cell. Adequacy of such "simplest" working model is tested experimentally, for either confirmation or added information for modification; but complexity is added only as required.

The necessity of simultaneous action of the two molecular components suggests involvement of a bimolecular complex. While the saccharide is highly hydrophilic in

nature, the anti-angiogenic steroids, hydrocortisone or structural variants, are hydrophobic structures. (This still applies to the bulk of the steroids' molecular structure, even when water solubility is attained for pharmaceutical practice by introduction of acetate, phosphate or other single polar group in 21-position). Superficially, this difference may discourage the thought of mutual interaction. However, an oligomeric chain of glucose rings, can and will attain a spiral (helical) configuration, especially with polar substituents directed outward to interact with the aqueous medium. Such helical configuration is observed for heparin (18,19). It offers an apolar, hydrocarbon-like region for hydrophobic interaction (14) within the configurational loops. This is, in fact, the basis for the strong inclusion of non-polar molecules by the cycloamyloses (cyclodextrins) where such a conformation is permanently offered (15,16,17).

A simple working model is based on the following assumptions:

1. Complex formation takes place between the steroid (the "angiostat") and portions of the saccharide. The saccharide thus facilitates fluid (aqueous) solubility and functions as the carrier;

2. The carrier saccharide adsorbs strongly at the cell surface by hydrophilic (ionic) bonding, and thereby presents a high surface concentration of the active steroid (either to surface receptors directly or for facilitated channel diffusion).

Experimental Approach

The cyclodextrins (CD's) have a proven capability for the formation of complexes with many hydrophobic structures (14,15,16). The α , β , and γ cyclodextrins are cyclic oligomers of 6, 7, and 8 glucose (anylose) rings, respectively. The center cavity of the β form can easily include a large portion of a steroid molecule. The α cyclodextrin cavity can capture at best a small portion. Each cyclodextrin sugar unit has three hydroxyl groups, and no other substituents. These materials are not known, by themselves, to have any particular biological functions.

Stability constants (equilibrium constants for complex formation, K_c) for many steroids in α -, β - and γ -cyclodextrin have been reported (17); for hydrocortisone and simple substitutions, they typically have magnitudes of $K_c = 2000$ to 4000 M^{-1} for β - and γ - CD's, and $K_c = 50$ to 200 for α - CD. They are hydrophilic and water soluble. We tested them for angiogenic activity in combination with hydrocortisone, with negative success.

Although, they should satisfy the first criterion, of complexing with the cyclodextrin of our "simplest model", bonding to the cell surface would have to rely entirely on

hydrogen bonding with hydroxyls of the cyclodextrin. On the other hand, it has been shown that in sulfated glycosaminoglycans, like heparin, sulfate plays a major role in strong cell adhesion (20); their importance is particularly well demonstrated by the observation that adsorbed sulfated species such as heparan sulfate is displaced by a similar species of still higher sulfate density, namely heparin (20).

We therefore proceeded to examine two polysulfated β -cyclodextrins, one with ca. 7 sulfate substitutions per molecule (β -CD-7S), and another with about 14, i.e. with two thirds of the available hydroxyl groups sulfated; this product is referred to as β -CD-14S, for β -cyclodextrin tetradecasulfate.

All of the angiogenesis inhibitors discovered have been found by using the chick embryo bioassay, also called the chorioallantoic membrane (CAM) assay: Using fertilized chicken eggs, the initial development and growth of blood vessels can be visibly observed and measured. On day 6, the angiogenesis inhibitor, contained in 10 ml of methylcellulose, is placed on the vascular membrane (the chorioallantoic membrane). Normally, its diameter doubles each day and new vessels grow with it. However, an angiogenesis inhibitor causes regression of growing capillaries over a period of 48 hours. The new capillaries disappear and leave an avascular zone of about 2 to 4 mm). The avascular zones are like those in a penicillin assay and can be used to generate dose-dilution curves.

Effective Replacement of Heparin for Angiogenic Control

The results (J. Folkman, P.B. Weisz, M.M. Joullié and W.R. Ewing, *Science*, in publication;) of antiangiogenic effectiveness measured by the CAM- assay (see below), using 25 mg saccharide with 60 mg hydrocortisone-21-phosphate (in 10 ml solution) are shown in the following table, together with the range of results with heparins (20 to 57 eggs per assay):

<u>Saccharide</u>	<u>%Avascular Zones (Antiangiogenic Activity)</u>
heparins	0 to 65
β - CD	5
β - CD-7S	7
β - CD -14S	62
α - CD	0
α - CD -12S	4

The β -CD-14S material is not only the first non-heparin material we have seen to have activity to promote

antiangiogenic activity with the steroid; it also produced the widest avascular zones in the chick embryo assay.

It is significant also that the alpha cyclodextrin, having a smaller hydrophobic cavity for complexing, and slightly smaller sulfate substitution showed very little activity.

A dose response study, keeping the hydrocortisone constant, but changing the concentration of β -CD-14S, gave the results shown in Figure 2. The % avascular zones are shown (bars represent results from 30 to 50 assays in each case. Five replicate experiments were carried out over 10 months. The shaded area represents the area of past experience with various heparins. The data obtained under this area include those from many heparins and CHOAY heparin pentasaccharide.

The β -CD-14S material is found to still maintain 40% percent of the activities achievable with the best of heparins, at two orders of magnitude concentrations.

An Example Application: Inhibiting Corneal Neovascularization

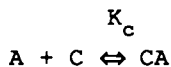
We have since confirmed the exceptional activity also using the rabbit corneal test (19), in which endotoxin from a corneal implant of a sustained release polymer induces neo-vascularization, and a second implant contains the test substances.

Moreover, with the cyclodextrin polysulfate, in contrast to heparin, we can obtain adequate transmembrane transport into the cornea using topical application (eye drops) to administer the anti-angiogenic pair of substances. The photographs of Figure 3, taken during the study, demonstrate: (a) the unabated corneal neo-vascularization (induced by an endotoxin pellet) as, in fact, it would be seen in a patient rejecting a corneal transplant; (b) hydrocortisone alone (0.5 mgm/ml drops) produces a slight suppression; (c) both components applied together completely stop all angiogenesis; (d) β -CD-14S alone (1.0 mgm/ml) causes some stimulation.

Model and Mechanism

The "simplest model" appears satisfactorily applicable to the results. The two steps assumed to be operative are familiar to chemical and biochemical interactions, subject to elementary formalisms:

The first step is the bimolecular equilibrium between the active component A (steroid) and the carrier C (saccharide), capable of forming the complex CA,



$$K_c = \frac{CA}{A \times C} = \frac{CA}{(A_0 - CA)(C_0 - CA)}$$

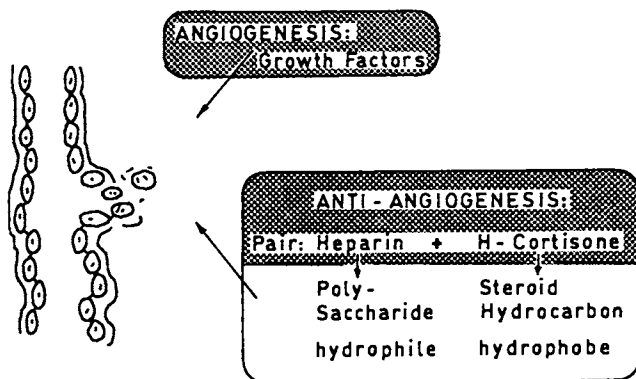


Figure 1. Angiogenesis and its Inhibition. Growth factors induce blood capillaries (left) to sprout; endothelial cells proliferate. Inhibition (anti-angiogenesis) is effected by the pair H-cortisone + heparin.

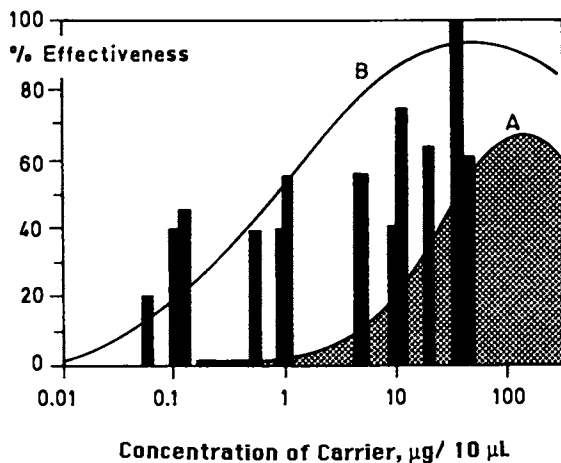


Figure 2. Anti-angiogenesis in the Chick Embryo Bioassay. Dose response for saccharide concentration (in µg in 10 µl sol.) with H-cortisone (60 µg in 10 µl sol.). For heparins the shaded area represents past experience; bars represent results with β-cyclodextrin tetradecasulfate. Curve A and B, see text.

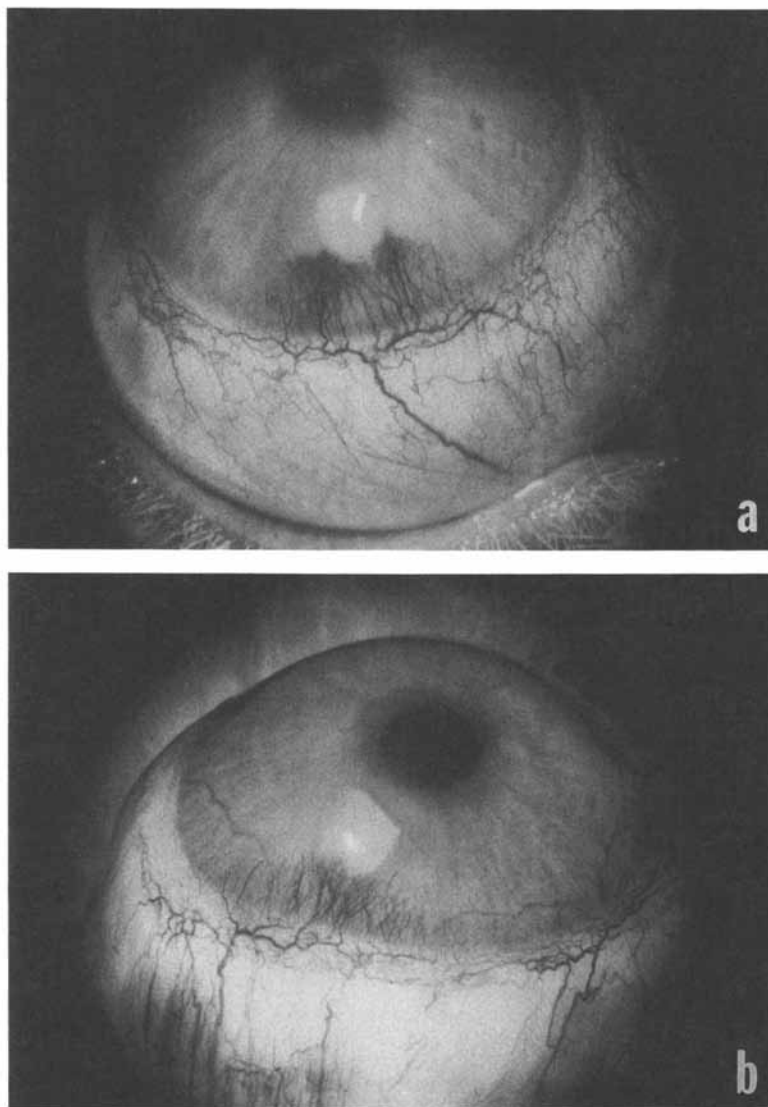


Figure 3. Inhibition of corneal vascularization by administration of H-cortisone (HC) with polysulfated β -cyclodextrin (CDS), by eye drops. (a) No intervention, (b) HC alone. (Continued on next page.)

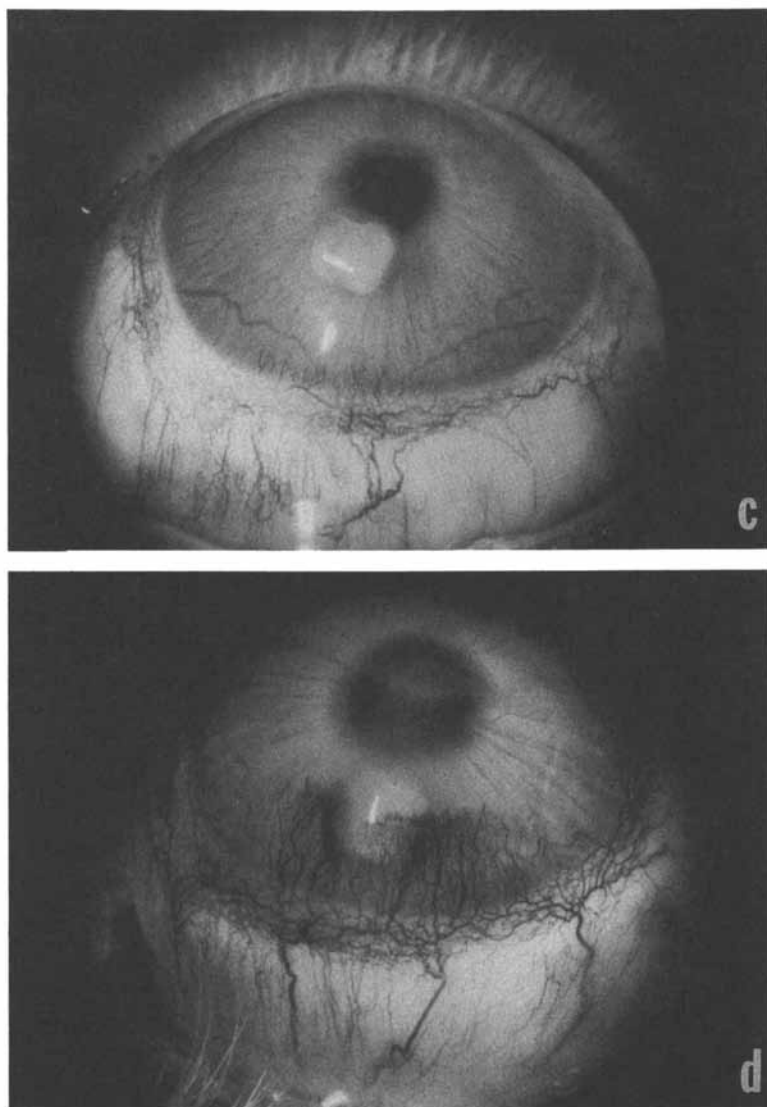


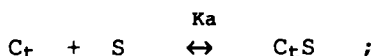
Figure 3. *Continued.* (c) HC + CDS, (d) CDS alone.

where each symbol represents molar concentration, and the last relationship applies to initial concentrations A_0 and C_0 . From this follows that the fraction ϵ of carrier which will be complexed as CA (will "carry" an A), $\epsilon = CA/C_0$, will be given by the relation

$$\epsilon^2 - \epsilon(1 + r + 1/C_0K_c) + r = 0, \quad (1)$$

where r is the initially available molar ratio $r = A_0/C_0$.

The second step involves the surface (adsorption) equilibrium between the carrier concentration in solution, $C_t = C + CA$, and the concentration of sorbed carrier species C_tS , on cellular surface sites (receptors) S:



We assume that K_a , dependent mainly on polar bonding substituents, will be similar in magnitude for the carrier, whether or not it is associated with the hydrophobe. For the case of excess carrier in solution, $C_t \approx C_0$, and elementary sorption dynamics (Langmuir, or Michaelis-Menten - depending on one's discipline) gives the fraction of total available adsorption sites η as

$$\eta = C_0 / (1/K_a + C_0). \quad (2)$$

The total effectiveness will be proportional to the fraction of cellular adsorption sites occupied by complexed (i.e. angio-stat bearing) carriers,

$$\text{Effectiveness} \approx \epsilon \times \eta.$$

In the CAM assay, the concentrations are in a dynamic state, i.e. they are not in a steady state. They ultimately dilute into an infinite volume. But the simple model can be expected to give at least semi-quantitative guidance for the early events, where the active volume is limited by the diffusion distance.

Figure 4 shows the character of the relationships (1) in A, and (2) in B, when plotted in terms of the variables as they appear in the CAM assay; the abscissa is measured in weight concentration of the saccharide.

To use the proper translation to molar quantities and ratios, we accept that complexing of the steroid molecule will involve a chain of about seven sugar units (as shown by molecular model or the performance of the 'preformed' cyclodextrins). Thus the effective molar saccharide unit has a molecular weight of about 2500 (a seven-membered, sulfated saccharide unit) even though the material used may have anominal molecular weight many times greater (heparin). This, in fact, is consistent with the

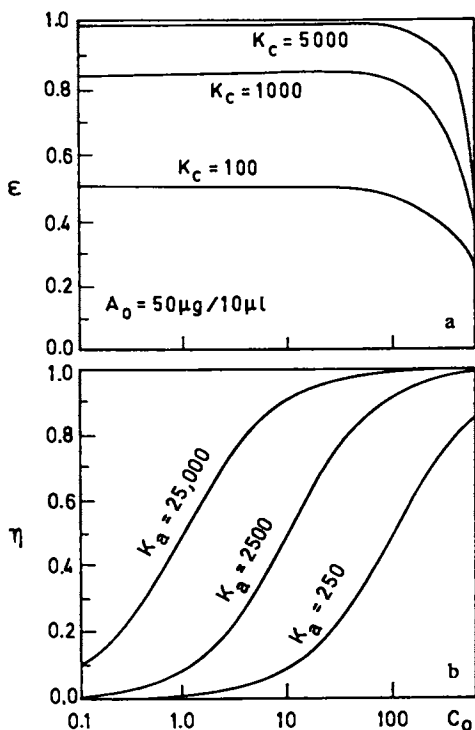


Figure 4. Basic Model Relationships for Interaction of the Steroid/Saccharide/Cell System. The abscissa is the saccharide concentration in $\mu\text{g}/10\mu\text{l}$ as used in the Chick Embryo Assay (CAM). a) ϵ is the fraction of saccharide complexed with (i.e. "carrying") steroid; b) η is the fraction of available cell surface sites occupied by saccharide (complexed or uncomplexed). Total effectiveness is proportional to the product of ϵ and η .

observation that the optimal effects of all active heparin materials, whether whole heparins or fragments (6), and now with cyclodextrins, appear at similar weight concentrations of the saccharide!

Figure 4A shows the course of the complexing phenomenon. Application of too large a saccharide concentration can diminish its effectiveness. B shows the commanding importance of the cell-saccharide binding equilibrium constant K_a for obtaining effectiveness at very low concentration. It is consistent with the need for sulfate anions and their observed role in cellular adsorption (20).

In the experimental CAM plots pictured in Figure 2, curve A, the envelop of past experience with the heparins, fits well the curve obtained from (3), with $K_c \approx 1500 \text{ M}^{-1}$, and a cell adsorption constant of $K_a \approx 800 \text{ M}^{-1}$. The performance of the β -CD-14S material (curve B) represents an increased adsorption equilibrium constant of $K_a \approx 50,000 \text{ M}^{-1}$, i.e. nearly a hundred times greater. (The shift in K_a is inversely proportional to the shift in concentration for the half-way point in effectiveness, due to formula (2)).

We can estimate an additional binding energy which is effective in the case of the cyclodextrin tetradecasulfate (consisting of seven sugar units) as compared to a seven-sugar fraction of the heparins from

$$\Delta E = RT \ln (K_{a,CD}/K_{a,heparin}) = RT \ln 100 = 2.9 \text{ kcal/mol}$$

This applies to a mole of seven-sugar-units and is a reasonable, added contribution shared between some 14 sulfate bonds sterically and rigidly positioned on our cyclic seven-unit oligomer.

Conclusions

The effective inhibition of angiogenesis by the co-action of heparin and a steroid action depends sensitively on the detailed structure of the angiostatic steroid (7,8,9). On the other hand, there is no need for much of the chemical complexity of heparin. The role of the saccharide appears to be that of a carrier of the active steroid to the endothelial cell surface. This action depends primarily on two overall physical/chemical properties: 1. the capacity to complex, in parts of its structure, a hydrophobic portion of the steroid molecule, and 2. the ability to form strongly interactive bonding with the cell surface protein. An oligosaccharide structure of seven (generally about five to eight) sugar units is sufficient to embrace a steroid for complexing; a minimum number of anionic sulfate groups alone suffice to provide sufficiently strong saccharide-cell bonding. No other saccharide substituents appear to be necessary.

A highly sulfated β -cyclodextrin (the tetradecasulfate) is a very effective, reliably

synthesizable heparin 'mimic' for angiogenesis control, and is, in fact, effective at nearly one hundredth of the dose required of heparin. Its use in at least one application, the inhibition of corneal neovascularization, is demonstrated, while its wider therapeutic usefulness seems promising.

The advances in mechanistic understanding and in the discovery of the heparin-alternatives (J. Folkman, P.B. Weisz, M.M. Joullié and W.R. Ewing, Science, in publication;) were intimately coupled in this interdisciplinary effort. Further reports, on corneal angiogenesis (J. Folkman, W.W. Li, in preparation) and other studies related to this work are in preparation.

Acknowledgments

The authors acknowledge the contributions of M.M. Joullié and W.R. Ewing (University of Pennsylvania) in synthesizing the sulfated cyclodextrins, and William Li (Harvard Medical School) in developing the early data on corneal antiangiogenesis. We thank Racheal Levinson and Geraldine Jackson (Harvard) for help with the chick embryo assays, and Dr. Yasuhiko Kiwano (Takeda Chemical Industries, Ltd.) for synthesizing additional β -cyclodextrin tetradesulfate. We acknowledge the gifts of various cyclodextrin raw materials by American Maize Products Company and Chinoin Pharmaceutical Co. (Budapest). We thank the Mobil Foundation for the encouragement and financial seed support for interdisciplinary research.

Literature Cited

- (1) D. Ausprunk and J. Folkman, *J. Microvasc. Res.* 14, 53, 1977;
- (2) J. Folkman, "Tumor Angiogenesis", in "Cancer", F.F. Baker, Ed., Plenum Publ. Co., New York, Vol.3, 1976;
- (3) J. Folkman, in "Advances in Cancer Research", G.Klein and S. Weinhouse, Eds., 175 - 203, Academic Press, New York, 1985
- (4) J. Folkman and K. Klagsbrun, *Science* 235, 442, 1987;
- (5) J. Folkman, in "Important Advances in Oncology", 197-211, V.T. Devita Jr., S.Hellman and S..A. Rosenberg, Eds., J.B. Lippincott, Philadelphia, 1985;
- (6) J. Folkman, R. LAnger, R. Linhardt, C. Haudenschild and S. Taylor, *Science* 221, 719-725, 1983;
- (7) R. Crum, S. Szabo and J. Folkman, *Science* 230, 1375-1378, 1985;
- (8) D.E. Ingber, J.A. Madri and J. Folkman, *Endocrinol.* 119, 1768-1775, 1986;
- (9) J. Folkman and D.E. Ingber, *Ann. Surg.* 206, 374-384, 1987;
- (10) J. Folkman, *Cancer Res.* 46, 467-473, 1986;

- (11) U. Lindahl, M. Hook, GH.Backstrom, I. Jacobsson, J. Riesenfeld, A. Malstrum, L. Roden and D.S. Feingole, Fed. Proc. 36, 19-23, 1977; b) T.C.Laurent, A. Tengblad, L. Thunberg, M.Hook and U. Lindahl, Biochem. J. 175, 691-701, 1978; c) R.J. Linhardt, A. Grant, C.L. Cooney and R. Langer, J. Biol. Chem. 257, 7310-7313, 1982;
- (12) J. Choay, M. Petitou, J. Lormeau, P. Sinay, B. Casu and G. Gatt, Biochem. Biophys. Res. Comm. 116, 492-493, 1983;
- (13) C.A.A. van Boeckel, T. Beetz and S.F. van Aelst, Tetrahedron Letters 29, 803-806, 1988;
- (14) J. Sejtli, "Cyclodextrins and their Inclusion Complexes", Akademiai Kiado, Budapest, 1982;
- (15) M.L. Bender and M. Komiyama, "Cyclodextrin Chemistry", Springer-Verlag, Berlin, 1978;
- (16) W. Saenger "Structural Aspects of Cyclodextrins and their Inclusion Complexes", in "Inclusion Compounds", Vol.2, J.L. Atwood, J.E.D. Davies and D.D. McNicol, Eds. Academic Press, New York, 1984;
- (17) K. Uekama, T. Fujinaga, F. Hirayama, M. Otagiri, and Y. Yamasaki, Int. J. Pharmaceutics 10, 1, 1982;
- (18) E.D.T. Atkins, I.A. Nieduszynski and A.A. Horner, Biochem. J. 143, 251, 1974;
- (19) S.P. Perlin, Fed. Proc. 36, 101, 1977;
- (20) T. Barzu, P. Mohlo, J.L.M.L. Petitou, J.P. Caen, Biochem. Biophys. Acta 845, 196, 1985;
- (21) G. Grayson, W.W. Li, P.A.D'Amore and J. Folkman, Invest. Ophthamol.Vis. Sci. 29, 49a, 1988;

RECEIVED January 25, 1989

Chapter 4

Crystallography and Site-Directed Mutagenesis of Two Isomerases

Thomas C. Alber¹, Robert C. Davenport, Jr.², Gregory K. Farber,
D. Ann Giammona³, Arthur M. Glasfeld, William D. Horrocks⁴,
Masaharu Kanaoka, Elias Lolis, Gregory A. Petsko⁵,
Dagmar Ringe, and Gerard Tiraby⁶

Department of Chemistry, Massachusetts Institute of Technology,
Cambridge, MA 02139

The Ferrari of Enzymes vs. the Fiat of Enzymes in a Drag Race for Protein Engineering

Suppose you want to travel from Stuttgart to Munich on the Autobahn. The distance is about 200 km, the road is excellent and there are no speed limits. The journey could be made in one hour if one were driving a Ferrari Testarossa, the fastest production automobile in the world. Its top speed of over 180 mph allows one to cruise comfortably at 125 mph, which is over 200 km/hr. In addition, the Ferrari is beautiful: it has a chassis designed by the great Italian carrozzeria Sergio Pinninfarina, and its 12 cylinder engine is the product of decades of development from the original superb designs of Enzo Ferrari himself.

Of course, if you can't afford a Ferrari (one costs about as much as some medium-field NMR spectrometers), you could drive a Fiat. Some of the better Fiats were also designed by the Pinninfarina organization, and since Fiat owns Ferrari now anyway, one might hope that some of the Ferrari engineering would rub off. But you get what you pay for. A Fiat Spyder costs 1/10th of what a Ferrari costs, it has a four-cylinder engine, and its top speed is under 100 mph. The trip from Stuttgart to Munich would take twice as long.

Now suppose you want to get from an aldehyde to a ketone. That is a race-course called isomerization (Figure 1), and it is the simplest reaction in all of chemistry. One proton moves from

¹Current address: Departments of Biochemistry and Chemistry, University of Utah, Salt Lake City, UT 84112

²Current address: Department of Biology, Massachusetts Institute of Technology, Cambridge, MA 02139

³Current address: Bolt, Beranek, and Newman, Cambridge, MA 02138

⁴Current address: Department of Chemistry, Pennsylvania State University, University Park, PA 16802

⁵Corresponding author

⁶Current address: Laboratoire de Microbiologie et Génétique Appliquées, Université Paul-Sabatier, Toulouse 31062, France

0097-6156/89/0392-0034\$06.00/0
© 1989 American Chemical Society

one carbon atom to the adjacent one, a distance of 1.5 Å. You can travel that distance via the enzyme triose phosphate isomerase (Figure 2), and you will cover it in about 1/10,000th of a second. Or you can travel it via the enzyme glucose isomerase (Figure 3), and it will take you more than a second.

Triose phosphate isomerase is a Ferrari, glucose isomerase is not. Just as one can understand the difference between a Ferrari and a Fiat in terms of their designs, it should be possible to understand the difference between triose phosphate isomerase (TIM) and glucose isomerase (GI) in terms of their structures and chemical mechanisms. We have set out to do exactly that, using the techniques of protein engineering. We have applied X-ray crystallography and site-directed mutagenesis to both enzymes and have discovered some of the reasons why their catalytic rates are so different. This has in turn led us to ask the question whether we might be able to alter GI so that it approaches the speed of TIM.

Glucose isomerase is one of the most important industrial enzymes. All of the high-fructose corn syrup used to sweeten soft-drinks, candy-bars, and most other foods is made using glucose isomerase. A reengineered GI that had the catalytic rate of TIM would not only be interesting, it might be very profitable. In any case, the fact that there are two enzymes that run the same course with vastly different speeds provides the enzymologist with a splendid opportunity to understand the origins of the catalytic potency of enzymes.

The First Lap: The Kinetic Parameters

Triose phosphate isomerase enzyme catalyses interconversion of the 3-carbon triose phosphate dihydroxyacetone phosphate (DHAP) and D-glyceraldehyde-3-phosphate (D-GAP). The reaction is just the transfer of the pro-R hydrogen from carbon 1 of DHAP stereospecifically to carbon 2 to form the D-isomer of GAP (Figure 2). Although the equilibrium constant on the enzyme is not known, K_{eq} for the overall reaction is 300 to 1 in favour of DHAP. The large magnitude of this number arises from the combination of an apparent K_{eq} of 22 with a hydration equilibrium of 29 for the hydrated and unhydrated forms of D-GAP (Trentham *et al.*, 1969); only the unhydrated forms of the triose phosphates are substrates for or even bind to the isomerase (Webb *et al.*, 1977).

The simplicity of the TIM reaction allowed Albery and Knowles and their coworkers to determine the complete free energy profile of the catalytic process (summarized in Albery and Knowles, 1976a). These data showed that the highest free energy transition state was that for the diffusion-limited bimolecular association of GAP with the enzyme.

The free energy profile showed that TIM has reached evolutionary perfection as a catalyst (for details see Albery and Knowles, 1976b). In addition, the availability of the complete free energy profile for the TIM-catalysed reaction meant that the mechanism could be understood in great detail. In particular, if a mutant made by site-directed mutagenesis caused a major change in

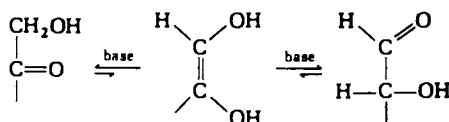


Figure 1. The isomerization of a ketone to an aldehyde. The reaction in aqueous solution is base-catalysed and is thought to proceed through a cis-enediol intermediate.

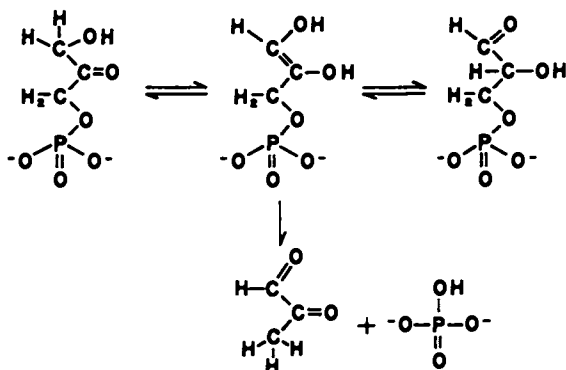


Figure 2. The isomerization reaction catalysed by triosephosphate isomerase. The enzyme takes the ketone dihydroxyacetone phosphate to the aldehyde D-glyceraldehyde-3-phosphate. Evidence for an enediol intermediate comes in part from the side-reaction that also occurs: the enzyme produces methyl glyoxal and inorganic phosphate.

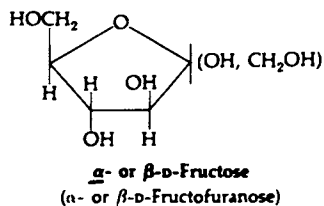
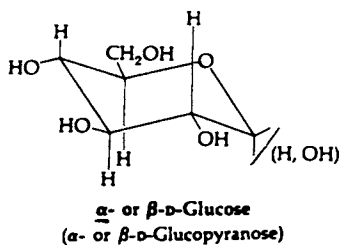


Figure 3. The reaction catalysed by glucose isomerase. The enzyme takes the ketone fructose to the aldehyde glucose. The sugars exist in ring forms in solution, and there are two anomers for each. There is good evidence that glucose isomerase only acts on the alpha anomers.

binding or in the rate of catalysis, the free energy profile of that mutant could be determined, and the specific microscopic step(s) that were altered by the mutation could be identified.

Richard (1984) has determined that TIM accelerates the rate of GAP to DHAP isomerization by almost 10 orders of magnitude over the rate enhancement provided by a simple base catalyst such as the acetate ion. Moreover, as indicated by the free energy profile, the enzymatic reaction rate is very fast in physical-chemical terms. k_{cat}/K_m (the pseudo first-order rate constant for the reaction of enzyme with substrate) in the thermodynamically favourable direction GAP to DHAP is $400,000,000 \text{ M}^{-1}\text{s}^{-1}$, which is close to the expected diffusion-controlled limit. A Ferrari indeed!

Glucose isomerase is also known in the biochemical literature as xylose isomerase, and there is some evidence that xylose is the physiological substrate. Nevertheless, we are concerned in this paper with its action on glucose, and so those are the kinetic values we shall report. (Even though the enzyme is more efficient with xylose, the numbers are not very different from those for glucose; it is like the difference in running your Fiat on high-test vs. regular gasoline. It is still a Fiat.) The reaction is the transformation of the alpha-anomer of glucose into the alpha-anomer of fructose; there is NMR evidence that the beta-anomers, even though predominant in solution, do not bind to the enzyme.

The turnover number for glucose at optimum pH is about 1 per second, and the substrate is not very tightly bound. k_{cat}/K_m is over 6 orders of magnitude lower than that for TIM, far from the diffusion-controlled limit. Unlike TIM, the catalytic rate of GI is not governed by a purely physical step. Chemistry is rate-determining.

There are two complications with this comparison. Glucose isomerase requires a divalent metal ion for catalysis, whereas TIM uses no metals or cofactors. The physiological metal for GI is thought to be magnesium. The second complication arises from the different structural characteristics of the two substrates. DHAP and GAP are open-chain sugars and have charged phosphate groups available for binding, while glucose and fructose, which lack these convenient "handles", exist chiefly in the closed form. Yet, isomerization requires that the ring be open, so GI actually has a more complex problem to face than it would appear on first analysis.

The Second Lap: The Assumed Basic Chemical Mechanism

Elegant isotope labelling studies by Rose and coworkers (Rieder and Rose, 1959; Rose, 1962) established the general mechanistic features of the TIM reaction. Proton transfer is mediated by a single enzymatic base, and the reaction proceeds via an intermediate that is either a *cis* enediol phosphate (Figure 2) or one of the two possible symmetrical enediolates. The evidence for enzyme-mediated proton transfer is the catalysis by the enzyme of loss of radioactive label from substrate to solvent water, or of exchange-in of label from deuterated or tritiated water to

substrate. Chemical labelling by Offord, Waley, Knowles, and Hartmann (e.g., Waley *et al.*, 1970) has identified the base as the side-chain carboxylate of glutamic acid 165.

Knowles has pointed out that the pKa of the transferred hydrogen could be lowered by polarization of the adjacent carbonyl group (Webb and Knowles, 1974). Electron withdrawal to the oxygen atom would weaken the carbon-hydrogen bond and promote enolization. Two possible polarization mechanisms suggest themselves: hydrogen bonding to the carbonyl oxygen by a neutral donor, and electrostatic interaction by a cation, which may or may not also directly hydrogen-bond. Here at once a role for the magnesium ion in glucose isomerase suggests itself: the positive charge on the metal could act as an electrophile and facilitate base attack at C1 of the substrate. Use of highly directional coordination to a metal cation has the advantage of providing electrostatic stabilization for incipient negative charge development on the carbonyl oxygen, which is expected to occur in the endiolate-like transition state. These considerations apply whichever direction the reaction runs. And indeed, for TIM, there is direct evidence for polarization of the substrate carbonyl from infra red spectroscopy (Belasco and Knowles, 1980), although the relevant electrophile in the TIM case must be an amino acid.

There is only one problem with this scenario: it may be wrong for glucose isomerase. When the critical experiment of looking for exchange-in of radioactivity from solvent to product is done for this enzyme, no exchange is seen (Rose, 1981). The same holds for exchange-out of label from substrate into water: it does not occur for this enzyme. Thus, there is no direct evidence for the participation of an enzymic base, or for the existence of an enediol-like intermediate.

The Third Lap: The Structures of the Enzymes

Triose phosphate isomerase is a homodimer with an extensive, mostly hydrophobic subunit interface. Monomers have a strikingly symmetrical beta/alpha folding pattern that has come to be termed the "TIM barrel". The core of the monomer consists of eight strands of parallel twisted beta-pleated sheet, wrapped around the surface of an imaginary cylinder. Each strand is connected to the next, in the expected right-handed cross-over manner (Richardson, 1981), by one (or occasionally two) alpha helical segment. To a first approximation, the structure can be represented as (beta, alpha) x 8 (Figure 4). The connections between sheet and helix are not smooth, and short segments of polypeptide normally bridge the two regular secondary structure elements. In some cases, these segments are classical beta-turns, but often they are irregular in conformation and are simply termed "loops". Two of them are quite long (>7 residues) and deserve special attention. Residues 72 to 79 protrude from the surface of the monomer but are completely buried in the dimer; they form an interdigitating loop that leaves one monomer, forms extensive contacts with a pocket on the other monomer, and then returns (Figure 4). Although this loop does not generate all of the intersubunit contacts, it does form

most of them. The other long loop is comprised of residues 168 to 177. This loop sticks out into the solvent. Curiously, the amino acid sequence of this loop is highly conserved throughout the evolutionary history of the enzyme, from bacteria to people. Yet, the apex of the loop is about 10 Å from the active site glutamate 165 and is even farther from the subunit interface, the only other two regions of high amino acid sequence conservation in TIM (Alber and Kawasaki, 1982), so it is hard to see immediately what its function is.

The active site of TIM is a pocket containing Glu 165. This pocket is located near the centre of the circular-like structure shown in Figure 4, at the C-terminal end of the beta-sheet cylinder, the end where all of the alpha helical segments begin. Hol *et al.* (1978) have pointed out that the dipole moment of the peptide bond gives rise to an appreciable macro dipole for an alpha helix. The positive end of the helix dipole is the amino terminal end, so the TIM active site is at the focus of the positive electrostatic potential produced by the helices.

More than a dozen enzymes have now been found to have domains that possess the characteristic TIM-barrel. Some of the others are pyruvate kinase, KDPG aldolase, glycolate oxidase, Taka amylase, muconate lactonizing enzyme, ribulose *bis*-phosphate carboxylase oxygenase, tryptophan synthase alpha subunit (C. Hyde, personal communication), enolase, muscle aldolase, flavocytochrome b₂, trimethylamine dehydrogenase, alpha amylase, and the two components of the bifunctional enzyme phosphoribosyl-anthranilate isomerase/indole-3-glycerolphosphate synthase. The TIM fold is the most common structural motif in biochemistry, at least so far. And glucose isomerase has it too (Figure 5). The GI polypeptide chain fold is strikingly similar to that of TIM, with two exceptions. The loop from residues 168-177 is missing in GI, and the intersubunit loop has been replaced by a long C-terminal domain that wraps around an adjacent subunit to form a dimer. Thus, the monomer of GI is bigger than that of TIM (40,000 MW), and the dimer interface is completely different. Glucose isomerase has a much larger intersubunit contact region; in fact, it seems to be the largest hydrophobic monomer-monomer interface yet observed. The active site of GI is a deep pocket containing histidine 219, glutamic acid 180, and aspartic acid 286. Any of these residues could serve as the catalytic base in an enediol-type mechanism, although one might expect that at least one of the two carboxylates would be needed to bind the metal. Unfortunately, the crystal structure of the native enzyme at pH 7 does not reveal which one, for no metal ion is observed, even in the presence of high concentrations of cobalt or magnesium. In the absence of substrate, the cation is not tightly bound by *Streptomyces olivochromogenes* GI.

The Fourth Lap: The Structures of the Enzyme-Substrate Complexes

The wonderful thing about both GI and TIM, from a structural enzymologist's point of view, is that for these enzymes it is actually possible to determine the structure of the productive

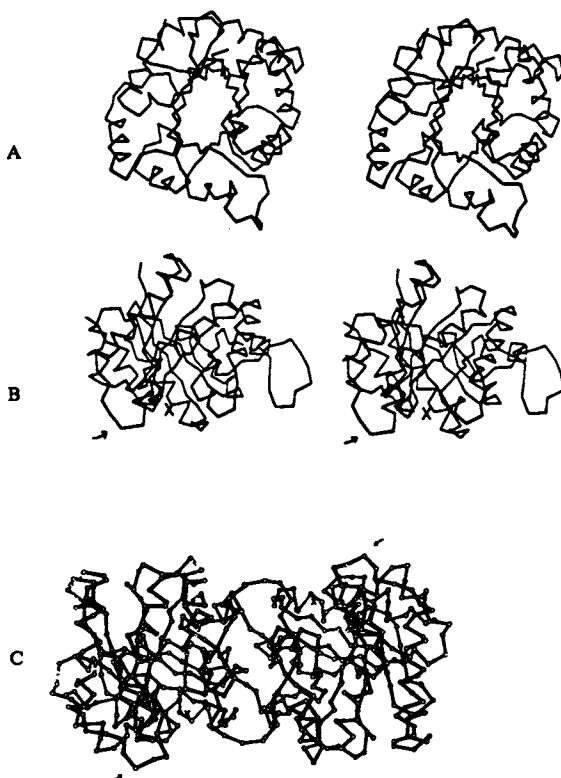


Figure 4. The structure of triose phosphate isomerase. A) Stereo view of one monomer down the axis of the eight-stranded alpha-beta barrel. B) Stereo view orthogonal to the first view. C) A view of one dimer looking down the two-fold axis relating each subunit. In both B) and C) the loop that moves when substrate binds is indicated by an arrow.



Figure 5. The structure of glucose isomerase. This is a stereo view of one subunit down the axis of the eight-stranded alpha-beta barrel.

enzyme-substrate complex by X-ray crystallography. That is not possible for most enzymes. For a hydrolase, for example, an attempt to do the crystal structure of a Michaelis complex at room temperature by conventional crystallography would be futile: substrate could be diffused into the solvent-filled channels in the crystal, but it would rapidly be hydrolysed to products, which would diffuse away (unless product binding was tight). Averaged over the time required for data collection (days to a week or more) the occupancy of the ES complex would be negligible. But TIM and GI catalyse a simple single-substrate/single-product equilibration: if substrate is soaked into the crystal, it will be converted to product, but product is just the substrate for the back reaction. So the crystalline enzyme system will settle to equilibrium, and as long as the substrate concentration in the mother liquor around the crystal is kept in excess of K_m , the thermodynamically-favoured complex will dominate what is observed in the crystal. The free energy profile of Alber and Knowles (1976a) indicates that, for TIM, the predominant form will be the enzyme-DHAP complex. We do not have these data for the GI reaction, so we must expect that at equilibrium we could see an equally-occupied mixture of E-glucose and E-fructose. Whether the resulting averaged structure could be interpretable will depend on the resolution of the data as well as the similarity of the two complexes conformationally. We prepared this complex (TIM-DHAP) by diffusing 10 mM DHAP into a crystal of TIM mounted in a flow cell (Petsko, 1985) on the diffractometer at -15°C . Data were collected to 3.5 Å resolution and a difference electron density map was calculated using native amplitudes and phases (Alber *et al.*, 1981). The map showed the substrate bound in the pocket containing Glu 165. The phosphate group, clearly identified by its high electron density, lay nearest the solvent. However, most dramatic was a large difference density feature indicating a conformational change in the conserved loop, residues 168-177. This loop had moved over 6 Å through space to fold down like a giant flap or lid onto the phosphate end of the substrate, thus closing off the active site (Figure 4).

This conformational change on substrate binding is consistent with the fact that product release is rate-limiting for TIM: the loop must move back out of the way to allow GAP to escape from the active site pocket. If there is a disorder-to-order transition as well, it may contribute directly to catalysis by raising the free energy of the enzyme-substrate complex (Alber, 1981). We have explored the role of the flexible loop by site-directed mutagenesis. The yeast TPI gene was cloned and sequenced by Alber and Kawasaki (1982), and has been expressed in *E. coli* (Petsko *et al.*, 1984; Davenport, 1985). Site-directed mutagenesis was carried out by the two-primer oligonucleotide method of Zoller and Smith (1983) using single-stranded bacteriophage M13 as a vector. We elected to change Thr 172, which is the side-chain in the loop nearest the contact point between the loop and the phosphate group of the substrate, to aspartic acid on the assumption that charge repulsion between the Asp carboxylate and substrate phosphate would prevent closure of the loop. We also deleted the central five

residues of the loop genetically so that there would no longer be a flap to close over the substrate. We expected that both of these mutants of TIM would still catalyze isomerization but show increased methyl glyoxal production. Preliminary kinetic analysis of both mutants from crude *E. coli* extract shows that k_{cat}/K_m for the direction GAP to DHAP is reduced by approximately tenfold over that for the wild-type enzyme. Assuming that closure has indeed been prevented, the loop would appear to play a role in orienting as well as binding the substrate. We have not yet quantitated methyl glyoxal production for either mutant.

DHAP is bound in an extended conformation. No positively-charged residues make contact with the phosphate; it is held in place by hydrogen bonds from several glycine-containing loops, particularly 209-212 and 232-234. Main-chain hydrogen bonding to phosphate is a common mode of binding in proteins, especially those that do not carry out chemistry on the phosphate group (for an example, see Smith *et al.*, 1983). We presume that the negative charge on the phosphate is compensated by the positive helix dipoles that are oriented towards the active site. The catalytic sub-site consists of Glu 165, Cys 126, His 95, Ser 96, Glu 97, Asn 10, and Lys 12. Only Glu 165 and Cys 126 are on the side of the substrate where proton transfer occurs. The remainder of the residues interact with the substrate (or each other) on the carbonyl side of the sugar. The carboxylate group of Glu 165 is perfectly positioned for nucleophilic abstraction of the pro-R proton from C1 of DHAP and subsequent direct transfer to C-2. To test the importance of the position of this residue, Straus, *et al.* (1985) have carried out site-directed mutagenesis of the cloned gene for chicken TIM, and changed Glu 165 to Asp. The fundamental kinetic parameters k_{cat} and K_m have been determined in both directions for this mutant, as has the complete free energy profile (Raines *et al.*, 1986). K_m is only slightly affected, but k_{cat} is reduced by several orders of magnitude in both the forward and reverse directions. The free energy profile for the mutant shows that only the transition-state free energies have been seriously altered. Glu 165 to Asp substitution has slowed each of the enolization steps by a factor of about one thousand. We undertook to calculate the structure of the mutant enzyme in its complex with DHAP. Our starting point was the coordinate set for wild-type yeast TIM with substrate bound. The method of structure prediction was the minimum perturbation approach developed by Karplus and coworkers (Shih *et al.*, 1985). We replaced Glu 165 by Asp in the ES complex, using computer graphics to position the aspartate side-chain. We then cranked the two side-chain torsion angles of the new Asp 165 through all possible values in increments, keeping the rest of the protein fixed. At each point in the torsion angle scan, the interaction potential energy between Asp 165 and the surrounding protein atoms was computed. The resulting energy map was inspected for low energy regions and each of these low energy structures was then subjected to full energy minimization, with all atoms in a 7 Å sphere about the alpha carbon of the mutant residue allowed to move freely, while atoms outside this sphere were restrained with harmonic restraints. An adapted-basis Newton

Raphson minimizer was used. A variation of this procedure has been used with success by Snow and Amzel (1986) to model immunoglobulin variable regions.

The minimum perturbation approach yielded two minima separated by large energy barriers. One minimum energy structure places the side-chain carboxylate oxygens of Asp 165 over 5 Å from the nearest substrate atom, an impossible position for catalysis. The other structure, which is the lowest energy structure found in the calculation, has one carboxylate oxygen 2.9 Å from C1 of DHAP, just as observed in the wild-type TIM-DHAP crystal structure. But although the distance of Asp 165 to the substrate in this model is the same as the distance of the oxygen of Glu 165 to DHAP in the wild-type ES complex, the orientation of the carboxylate group is quite different in the mutant. Replacement of glu by asp is not a structurally conservative mutation: it moves the bulky carboxylate group closer to the surface of the protein. In the TIM active site, this movement causes the carboxylate to collide with the backbone of the protein around Gly 209. To relieve this steric crowding the carboxylate must rotate (this is the minimum energy position found), and when it does it can only reach the substrate in a conformation in which the outer (anti) orbital of the oxygen atom acts as the proton acceptor (Figure 6). In the wild-type TIM-DHAP structure, where the longer side-chain of glutamate pushes the carboxylate beyond the 209 loop, the syn orbital (the orbital on the same side of the C-O bond as the C=O bond) is the proton acceptor. Gandour (1981) has pointed out that the anti orbital is 10,000-fold less basic than the syn orbital. If that equilibrium difference is used in the Bronsted formula together with a beta of about 0.7, a rate reduction of 1,000-fold for proton transfer is calculated for the mutant enzyme. This is the same value as observed experimentally.

Although these calculations do not establish that the difference in orbital usage is responsible for the reduced activity of the Asp 165 mutant, they do provide a testable hypothesis. The three-dimensional structure of the mutant enzyme, complexed with substrate, will indicate whether the anti orbital is in fact the only one available for proton transfer.

There are three residues that are in contact with the carbonyl and hydroxyl oxygen atoms of the triose phosphates. One of these, which is uncharged and may be purely involved in substrate binding, is Asn 10. Mutation of this residue to valine or alanine would be of interest. The other two residues may have more complex roles. Lys 12 is positively charged at neutral pH and is close to the C2 oxygen of the substrate. We speculate that its role may be to stabilize the transition state by charge-charge interaction. A mutant TIM with glutamine replacing the lysine has been made but not yet characterized: in crude cell extract it shows little or no TIM activity. The positive charge on Lys 12 will also affect the oxygen at C1, since electrostatic interactions remain strong at reasonably long distances, and the dielectric of the active site will be very low when the flexible loop is in the closed position, so there should be little screening. His 95 is the most complex of the putative electrophiles. It is hydrogen-bonded to the C1

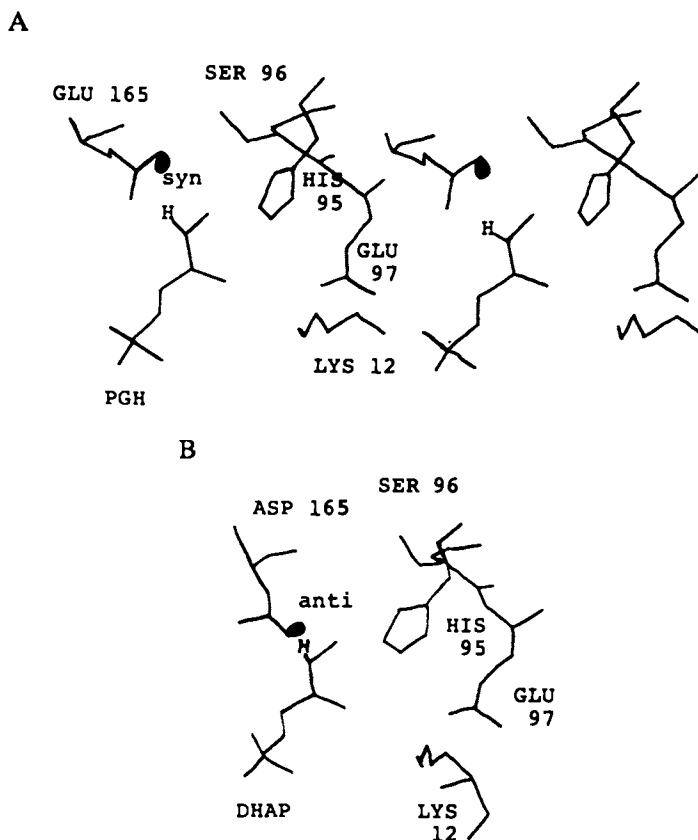


Figure 6. A) The active site of TIM in the crystallographically determined enzyme-substrate complex. Some of the important catalytic residues are indicated. Note that the active-site base, Glu 165, is positioned to use its more basic syn orbital for proton abstraction. B) The active site of TIM mutant E165D in the model-built enzyme-substrate complex. Note that the active-site base, Asp 165, is positioned to use its less basic anti orbital for proton abstraction.

substrate oxygen through its epsilon NH. If it has the normal histidine pKa of about 6, it could function as an acid, protonating the substrate carbonyl to form the *cis*-enediol intermediate (if His 95 does not do this, the proton needed to form the enediol may come from water, or the intermediate may always be the charged enediolate). The crystal structure is ambiguous on this point. Protein crystallography cannot ordinarily detect protons, so the ionization state of the histidine must be inferred from its environment and interactions. In the refined native crystal structures of yeast and chicken TIM, His 95 appears to be hydrogen-bonded through its delta nitrogen to the main-chain -NH of residue 97 at the beginning of a short, irregular alpha helix. Since the backbone amide must be protonated, the structure suggests that the delta nitrogen of the histidine is unprotonated. Therefore, the epsilon nitrogen must carry the proton, and the histidine, by this analysis, is neutral. If it is, its two possible roles are as an acid (though this is unlikely as on deprotonation the histidine would become anionic) or, more likely, purely as an electrophile. Electrophilic catalysis could be accomplished solely by the neutral histidine hydrogen-bonding to the substrate oxygen at C1, but it is also possible that the histidine could act as a relay for the positive dipole of the short irregular helix. In that case, it would also have a through-space electrostatic role.

We have investigated the function of this residue by replacing it with a side-chain that is uncharged and incapable of functioning as an acid, namely, glutamine (Davenport, 1985; Nickbarg *et al.*, 1988). Glutamine is a better choice than asparagine because it retains hydrogen bonding at a position comparable to that of the epsilon nitrogen. If only hydrogen bonding to the substrate were important, the glutamine mutant should be fully active. If acid behavior is essential for catalysis, glutamine 95 would inactivate the enzyme. If a through-space electrostatic affect is occurring at this position, the mutant TIM might have reduced activity.

His 95 to Gln TIM is an active enzyme. Kinetic measurements indicate that K_m is unchanged, but k_{cat} in both directions is reduced by a factor of about 200. This observation is in keeping with the hypothesis that His 95 is not essential as an acid but does act to stabilize the transition state electrostatically. Support for this view comes from inhibition studies of the mutant enzyme: simple competitive inhibitors are bound equally tightly by wild-type TIM and the H95Q mutant, but the transition-state analog inhibitor PGH binds to the mutant over 50-fold less well than to the wild-type enzyme (Nickbarg *et al.*, 1988). Unfortunately, label exchange-in and exchange-out experiments, carried out by Elliot Nickbarg and Jeremy Knowles at Harvard to determine the free-energy profile of this mutant, show that it has undergone a subtle change in mechanism. The data are complex, but the best interpretation of them seems to be that, in the mutant enzyme, Glu 165 abstracts the proton from C1 and then protonates the C2 carbonyl oxygen to form the enediol intermediate (Nickbarg *et al.*, 1988). It then abstracts a proton from the C1 hydroxyl and delivers it to the C2 carbon to form product! These data could be interpreted to indicate that there must be direct proton donation to the substrate oxygen to

form the intermediate, and that His 95 normally fills that role. Alternatively, there could have been a conformational change in the mutant that allowed this two-base pathway to become favoured for steric reasons. Mutating His 95 has proven that an acidic residue is not necessary at that position, but it has not settled the question of the actual protonation state and role of His 95 in the normal enzyme. There is a caveat for all protein engineering in this result: it is dangerous to assume that simple mutations leave the catalytic mechanism unchanged.

Our findings on TIM, though incomplete, are consistent with the following picture:

1. The TIM-catalysed isomerization of DHAP to GAP proceeds via base-catalysed proton abstraction and formation of an enzyme-bound enediol or diolate intermediate. The organic chemistry analog of this reaction is the Lobry de Bruyn-Alberda van Ekenstein transformation, exemplified by the production of fructose when glucose is heated in base.
2. Desolvation of the active site maximizes all electrostatic effects by reducing the effective dielectric.
3. Glu 165 acts as the catalytic base. Steric desolvation of the active site increases the pKa of Glu 165 when substrate binds. The structure of the enzyme orients the carboxylate group so that proton abstraction is carried out by the more basic syn orbital.
4. The likely catalytic electrophiles are Asn 10, Lys 12 and His 95.
5. Acid catalysis by His 95 is not essential for isomerization.
6. Rather than a unique electrophile for each substrate oxygen, the enzyme seems to provide a positive electrostatic potential by means of a combination of side-chains and alpha helix dipoles. Thus, it is more accurate to speak of a catalytic surface than a specific site for electrophilic catalysis.
7. Substrate specificity is chiefly provided by helical dipole and backbone hydrogen bonding to the phosphate group.
8. The active site of triose phosphate isomerase is complementary, in both stereochemistry and charge configuration, to the transition state of the reaction it catalyses. This fact, combined with very efficient general base catalysis, is largely responsible for the high efficiency of TIM.

Glucose isomerase has not yet been investigated in anything like the same detail. In particular, the results from molecular biology are just beginning to come in. However, structural studies have been carried out on several enzyme-substrate complexes, and

although their results are still only at medium resolution, the preliminary indications are that the GI mechanism is much more complex.

Since GI is a single-substrate/single-product enzyme, the structure of the GI-glucose-Mg adduct can be observed directly. There are two alternative experimental methods: just soaking the crystal in substrate solutions prior to mounting and data collection, or continuously flowing substrate and metal over the crystal. The former is an equilibrium experiment, but the latter is a kinetic one. Continuous flow of glucose might be expected to reveal the structure of the species that accumulates prior to the rate-determining step of the reaction. Unfortunately, since the reaction has not been dissected mechanistically, we have no idea what that step is.

The crystal structure of the GI-glucose-Mg complex under continuous flow conditions has been determined at 3 Å resolution. The position of the bound metal atom has been confirmed by a separate experiment in which the heavier cation manganese was substituted for magnesium. The enzyme-substrate complex is a glucose-metal-enzyme bridged system, with both protein and sugar providing ligands to the magnesium atom. This result explains why magnesium binds so weakly in the absence of substrate. The active site glutamate and aspartate residues are both coordinated to the metal, making them unavailable to serve as the catalytic base. Glucose is bound in a compact manner, although at 3 Å resolution it is impossible to determine if the ring has been opened. Histidine 286 is not positioned to function as the base in proton abstraction: it appears to be on the wrong side of the sugar. There are no other residues in the vicinity that can serve to abstract the proton, and no electrophilic groups positioned for polarization of the oxygens.

The mystery deepened when we examined the structure of the enzyme-glucose complex in the absence of metals. The enzyme is known to be catalytically inactive under these conditions. This experiment was done in an equilibrium fashion, that is, by soaking the demetallized GI crystal in a solution of glucose and then mounting it in a sealed quartz capillary tube for data collection. The 3 Å resolution structure of the complex revealed that the sugar ring had been opened and the substrate was bound in a fully-extended conformation. This result seemed to confirm an earlier observation by one of us (G.K.F.), together with Mary F. Roberts of Boston College, that the enzyme was able to catalyse the opening of the ring. There was still no obvious candidate for a proton-transfer base in this new conformation.

The mechanistic picture most consistent with these preliminary data is a multi-step sequence in which sugar and metal bind to the enzyme with the sugar in a closed, ring form coordinated to magnesium via its C1 and C2 oxygen atoms. An enzymic base, probably the imidazole side-chain of His 286, then catalyses the

opening of the ring. Subsequent steps are less clear structurally, but it is possible that a large rearrangement of the sugar then takes place, with an extended sugar conformation then binding, with metal, in the active site. In this scheme, the rate-limiting step is probably ring opening, as that would explain why the closed form was observed in the flow-cell experiment.

How is the actual isomerization catalysed? Failure to observe exchange-in or exchange-out of label, combined with the lack of an obvious basic amino acid side-chain in the right position, forces us to consider the possibility that the mechanism is fundamentally different from that of TIM. To return to the possibly overworked automotive analogy, the difference in top speed between the Ferrari and the Fiat is chiefly due to the differences in their engines, but both are still internal combustion engines of the same general principles. The mechanistic differences between GI and TIM appear to be more fundamental than that. It is almost as though one looked under the hood of one of the automobiles and saw, not an internal combustion engine at all, but a pair of squirrels in a cage. A race between such a car and a Ferrari would be unsporting indeed. TIM and GI may differ in a similarly radical way: the isomerization step of GI may not be a base-catalysed proton transfer via an enediol. It may be unfair to compare the speed of the two enzymes because GI may not be doing the same chemistry after all.

What chemistry is it doing? There is one other obvious mechanism for interconversion of a ketone and an aldehyde, a hydride transfer pathway. Such a mechanism would not lead to any exchange, since there is no hydride in solution to exchange with. Direct hydride transfer from C1 to C2 would require no enzymic base and would produce no intermediate. Direct hydride transfer would explain the requirement for a metal ion: in addition to providing binding for the sugar, the metal would polarize the sugar oxygen atoms and, in so doing, help generate the hydride ion. This mechanism would fit all of the observed data for GI. And it would be almost without enzymatic precedent.

There are, however, numerous organic precedents. The Cannizzaro reaction, in which two equivalents of a nonenolizable aldehyde such as benzaldehyde are reacted with hydroxide to form a primary alcohol and the salt of a carboxylic acid, is thought to involve hydride transfer to one aldehyde carbonyl from the carbonyl-addition product of the other aldehyde and hydroxide. The Leuckart reaction, formation of a tertiary amine from formic acid, a primary amine and either a ketone or an aldehyde, seems to proceed via hydride transfer from formate to an iminium ion. And the Meerwein-Ponndorf-Verley-Oppenauer reaction, the reversible transfer of hydrogen between ketones and secondary alcohols in the presence of excess aluminum isopropoxide, is almost certainly a hydride-transfer reaction. This latter process is of particular interest to us because it requires a metal, just as GI does. The aluminum acts as a Lewis acid, coordinating the carbonyl oxygen and

bringing the hydride donor (the carbon atom attached to the hydroxide of the alcohol) adjacent to it by simultaneously coordinating that oxygen as well. The magnesium or manganese in GI could be playing an identical role in an intramolecular hydride transfer. The mechanism of GI may have always been different from that of TIM because of the necessity of finding a way to bind a sugar correctly. The substrates for TIM have convenient handles: the phosphate group. TIM can use the phosphate to bind its substrates tightly and then do chemistry on a different part of the molecule. Glucose and fructose have no handles; the enzyme must use every available portion of the sugar to hold it in the active site, including the portion of the sugar where the isomerization is to take place. Once a metal ion was used to grab the C1 and C2 oxygen atoms, the chemistry of the reaction may have been unavoidable. A hydride transfer path was the lowest free-energy route to product with the strong Lewis acid attached to the substrate.

Structure can never prove mechanism. There is no direct evidence that GI uses a hydride transfer mechanism, and we do not wish to assert that it does. Our results, however, do suggest that alternatives to the traditional enediol mechanism should be considered for this enzyme, and that careful mechanistic studies should be carried out to evaluate the possibility that a hydride transfer could be involved. Until such studies have been completed, we believe that the race should be postponed. If the rate-determining step for GI really is ring-opening, it would be unsporting to match it against TIM, which faces no such problem. And it may also be impossible ever to engineer the TIM mechanism into GI, if the requirement of a metal atom to bind the sugar mandates a different mechanism for proton transfer. Nevertheless, comparison of these two enzymes has led to greater understanding, and appreciation, for both. A Fiat is not a Ferrari, but it is still a beautiful machine.

Literature Cited

1. Alagona, G.; C. Ghio; Kollman, P.A. J. Mol. Biol. 1986, 191, 23.
2. Alber, T. Ph.D. Thesis, Massachusetts Institute of Technology, Cambridge, 1981.
3. Alber, T.; Kawasaki, G. J. Molec. Appl. Gen. 1982, 1, 419.
4. Alber, T.; Banner, D.W.; Bloomer, A.C.; Petsko, G.A.; Phillips, D.C.; Rivers, P.S.; Wilson, I.A. Phil. Trans. Roy. Soc. Lond. 1981, B 293, 159.
5. Albery, W.J.; Knowles, J.R. Biochemistry 1976a, 15, 5627.
6. Albery, W.J.; Knowles, J.R. Biochemistry 1976b, 15, 5631.
7. Belasco, J.G.; Knowles, J.R. Biochemistry 1980, 19, 472.
8. Campbell, I.D.; Jones, R.B.; Kiener, P.A.; Waley, S.G. Biochem. J. 1979, 179, 607.
9. Casal, J.I.; Ahern, T.J.; Davenport, Jr., R.C.; Petsko, G.A.; Klibanov, A.M. Biochemistry 1987, 26, 1258.
10. Collins, K.D. J. Biol. Chem. 1974, 249, 136.

11. Davenport, Jr., R.C. Ph.D. Thesis, Massachusetts Institute of Technology, Cambridge, 1985.
12. Farber, G.K.; Petsko, G.A.; Ringe, D. Protein Engineering 1987, 1, 459-466.
13. Gandour, R.D. Bioorganic Chem. 1981, 10, 169.
14. Hol, W.J.G.; Van Duijnen, P.T.; Berendsen, H.J. Nature, Lond. 1978, 273, 443.
15. Nickbarg, E.B.; Davenport, Jr., R.C.; Petsko, G.A.; Knowles, J.R. Biochemistry 1988, 27, 5948.
16. Petsko, G.A. Methods Enzym. 1985, 114, 141.
17. Petsko, G.A.; Davenport, Jr., R.C.; Frankel, D.; RajBhandary, U.L. Biochem. Soc. Trans. 1984, 12, 229.
18. Raines, R.T.; Straus, D.R.; Gilbert, W.; Knowles, J.R. Phil. Trans. Roy. Soc. Lond. 1986, A 317, 371.
19. Richard, J.P. J. Am. Chem. Soc. 1984, 106, 4926.
20. Richardson, J.S. Adv. Prot. Chem. 1981, 34, 168.
21. Rieder, S.V.; Rose, I.A. J. Biol. Chem. 1959, 234, 1007.
22. Rose, I.A. Brookhaven Symp. Biol. 1962, 15, 293.
23. Rose, I.A. Phil. Trans. Roy. Soc. Lond. 1981, B 293, 131.
24. Rose, I.A. Methods Enzymol. 1982, 87, 84.
25. Shih, H.H.-L.; Brady, J.; Karplus, M. Proc. Nat. Acad. Sci. USA 1985, 82, 1967.
26. Smith, W.W.; Pattridge, K.A.; Ludwig, M.L.; Petsko, G.A.; Tsernoglou, D.; Tanaka, M.; Yasunobu, K.T. J. Mol. Biol. 1983, 165, 737.
27. Snow, M.E.; Amzel, L.H. Proteins 1986, 1, 267.
28. Straus, D.; Raines, R.T.; Kawashima, E.; Knowles, J.R.; Gilbert, W. Proc. Nat. Acad. Sci. USA 1985, 82, 2272.
29. Trentham, D.R.; McMurray, C.H.; Pogson, C.I. Biochem. J. 1969, 114, 19.
30. Waley, S.G.; Miller, J.C.; Rose, I.A.; O'Connell, E.L. Nature, Lond. 1970, 227, 181.
31. Webb, M.R.; Knowles, J.R. Biochem. J. 1974, 141, 589.
32. Webb, M.R.; Standing, D.N.; Knowles, J.R. Biochemistry 1977, 16, 2738.
33. Wolfenden, R.G. Nature, Lond. 1969, 223, 704.
34. Zoller, M.J.; Smith, M. Methods Enzymol. 1983, 100, 468.

RECEIVED January 3, 1989

Chapter 5

Computer-Automated Sequence Evaluation of Peptides

Application to the Study of Snake Venom Toxicity

Gilles Klopman and Ruben E. Venegas

Department of Chemistry, Case Western Reserve University,
Cleveland, OH 44106

A modified version of the Computer Automated Structure Evaluation (CASE) program has been successfully applied to the study of the neurotoxic and cytotoxic activity of the snake venom toxins. The program identified the sites that seem to be the most relevant to the activity of these two classes of peptides. The knowledge of the three dimensional structure of these peptides together with the relevant fragments selected by the CASE program helped to clarify the differences between the activity of each type of toxin.

Traditional Quantitative Structure-Activity studies are pretty much limited to the study of the biological activity of relatively small Organic Molecules. We have introduced, some time ago, the CASE program, a Computer Automated Structure Evaluation program that can be used to identify molecular fragments directly responsible for the biological activity of such organic molecules (1-10). With this paper, we wish to introduce an expanded version of CASE, capable to identify the relation between peptide sequences and biological activity. The expectation is that such a program could help delineate the activity of peptides and provide a better understanding of the receptor site's geometry. For this initial study we have selected a data base consisting of snake venom toxins (11,12), for which extensive studies have been made and whose tertiary structure has been well established (13).

Snake venom toxins are usually classified into three categories: short neurotoxins, long neurotoxins and cytotoxins. Short neurotoxins contain 60-62 amino acid residues and 4 disulfide bridges. Long neurotoxins have 60-62 amino acid residues and 5 disulfide bridges. Cytotoxins also contain 60-61 amino acid residues and 4 disulfide bridges. It is known that short and long neurotoxins act on postsynaptic nicotinic cholinergic receptors (13), but the mode of action of cytotoxins is unclear.

0097-6156/89/0392-0052\$06.00/0
• 1989 American Chemical Society

Elucidation of the active site of toxins would be of enormous importance for the understanding of both the mechanism of action of the toxins and of the structural organization of the receptor. A considerable amount of work has been done to that effect; this includes the study of many snake venom's sequences (11) and their three dimensional structures (14,15). The toxicity and binding of chemically modified toxins (11,16,17) have also been reported as well as that of smaller peptides with residual toxicity (18,19). In spite of all this work, the specific regions and the minimum number of functional amino acids needed to bind to the receptor and to produce toxicity have not been entirely clarified. Nevertheless, a number of conclusions have been reached from previous studies. Thus, from a comparison of neurotoxin sequences with that of similarly structured proteins but without toxic activity, the residues Trp-25, Arg-33, and Gly-34 (numeration according to Karlsson, ref. 11) were thought to be necessary for neurotoxicity (11). From chemical modifications studies (11,16), it was found that Trp-25, Asp-27, Arg-33, Gly-34, and Lys-49 seemed to be essential. X-ray studies of two neurotoxins showed that a few pairs of amino acids appeared to mimic the structure of acetylcholine (20). Finally, it was also observed that the four disulfide bridges appear to play an important part in maintaining the active conformation of the toxins and that complete reduction (21) or oxidation (22) terminate toxicity while denaturants such as urea have little or no effect on the toxicity of non-reduced toxin.

From a comparison of the primary structure of the neurotoxins, Karlsson (11) and Ryden et al. (12) observed that certain invariant amino acid positions in the structural chain are important for the general folding of the molecule, while others are important for the neurotoxic activity. The former are called structurally invariant residues, whereas the later are called functionally invariant residues.

Most previous studies are based on the assumption that the toxicity of snake toxins is induced by a narrowly defined active region. As a consequence, single amino acid residues were chemically modified and the effects of the modification assayed by *in vivo* toxicity tests (11,14,18). However, it was found that the derivatives modified at all those positions believed to be important still have significant activity. Instead, as has been previously shown by Karlsson (11), there is a gradual decrease of, but never a complete reduction in toxicity (affinity of binding).

A detailed analysis of these results seem to indicate that unlike most of the enzymes, there is not a single amino acid residue or small region in the toxin structure that is essential for biological function. Instead, the structure-function relationships of this important group of biologically active polypeptides may be governed by more global principles of organization.

Methodology

The CASE methodology has been modified to be usable for the evaluation of the amino acid sequences required for activity. The procedure calls for fragmentation of the peptide chain in fragments of 3 to 10 constituent units. These formerly consisted of heavy

atoms with their hydrogens and, in the new context, are made up by small sequences of linked amino acids. For this purpose the molecular entry program (23), formerly KLN, has been modified so that each letter of the alphabet now represents an amino acid (see Table I). Each of these amino acid is only permitted one neighbor if it exists at the beginning or end of a chain and two neighbors if it exists within the bulk of the peptide. Furthermore, fragment inversion is not permitted anymore since, in contrast to ordinary molecules, peptide termini are not interchangeable. Once the fragments have been identified and collected along with a numerical representation of the biological activity of the peptides, the CASE analysis begins. Fragments coming from active peptides are labeled activating, while fragments arising from biologically inactive peptides are labeled as deactivating.

Table I. IUPAC Coding System*

Letter	Abbreviation	Amino Acid
A	Ala	ALANINE
R	Arg	ARGININE
N	Asn	ASPARAGINE
D	Asp	ASPARTIC ACID
B	Asx	ASPARTIC ACID/ASPARAGINE
C	Cys	CYSTEINE
Z	Glx	GLUTAMIC ACID/GLUTAMINE
Q	Gln	GLUTAMINE
E	Glu	GLUTAMIC ACID
G	Gly	GLYCINE
H	His	HISTIDINE
I	Ile	ISOLEUCINE
L	Leu	LEUCINE
K	Lys	LYSINE
M	Met	METHIONINE
F	Phe	PHENYLALANINE
P	Pro	PROLINE
S	Ser	SERINE
T	Thr	THREONINE
W	Trp	TRYPTOPHAN
Y	Tyr	TYROSINE
V	Val	VALINE

* The symbols used for amino acids are those recommended by the IUPAC-IUB Commission on Biochemical Nomenclature, as published in J. Biol. Chem. 1972, 247, 977.

The fragmentation of the peptide data base generates thousands of fragments consisting of short amino acid sequences. In order to establish which fragments are relevant to activity, a binomial distribution is assumed and any significant deviation from a random distribution of a fragment among the active and inactive categories indicates its possible contribution to the biological activity. At

this point of the procedure the program is capable to distinguish between active and inactive toxins on the basis of the presence or absence of these fragments. Additionally, the program selects a subset of molecular fragments to be considered for multivariate linear regression. First, the program searches for a fragment which can effectively discriminate between active and inactive peptides. Subsequent fragments are then chosen to account for the remaining variance. The program executes a forward stepwise regression analysis on these independent variables to derive a quantitative estimate of each peptide's activity. The F partial statistic (95% confidence level) is applied to assure statistical validity of the incorporated variables. The measure of the activating/inactivating contribution made to the overall biological activity by the fragments is represented by the magnitude of the regression coefficients.

Once the analysis is completed, the program has the capability to evaluate the probability that unknown compounds have activity and to anticipate the extend of this activity.

Results

Short Neurotoxins. The 58 snake venom short neurotoxins submitted to analysis are presented in Table II. This data base, which contains 27 inactive and 30 active toxins, was built from data reported by Karlsson (11) and Dufton et al. (12).

F_I : S S Q	F_{II} : D H R G
F_{III} : Synergistic presence of fragments T T K and R G T I I E R G C G C P	
F_{IV} : W S D	F_V : C P T V K
F_{VI} : S C Y K K	F_{VII} : W R D
F_{VIII} : C N L	

Figure 1. The most important fragments selected by the CASE program from the short neurotoxins data base.

After the training set was entered in the computer, the program generated all the fragments believed to be related to the observed activities of each toxin. In this case, 20 fragments (10 inactivating and 10 activating) were selected as potential descriptors of the experimentally observed toxicity. Based on these, a stepwise regression analysis was performed. The activity of the toxins were represented as 0 indicating no activity, 1, indicating marginal activity and 2, substantial activity. Eight descriptors were selected to be of particular significance to the actual toxicity of the short neurotoxins. They are shown in Figure 1; the following Quantitative Structure Activity Relationship (QSAR) was generated:

Table II. The actual and predicted value of the short toxins submitted to the CASE program

Neurotoxins	Actual*	Calc.*
1 NAJA HAJE ANNULIFERA: CM-10	-	-
2 NAJA HAJE ANNULIFERA: CM-12	-	-
3 DENDROASPIS JAMESONI KAIMOSE: S5C10	-	-
4 DENDROASPIS JAMESONI KAIMOSE: S4C1	-	-
5 DENDROASPIS JAMESONI KAIMOSE: S4C4	-	-
6 DENDROASPIS JAMESONI KAIMOSE: S4CB	-	-
7 DENDROASPIS ANGUSTICEPS: C10S2C2	-	-
8 DENDROASPIS ANGUSTICEPS: C13S1C1	-	-
9 DENDROASPIS POLYLEPSIS: C	-	-
10 DENDROASPIS POLYLEPSIS: FS2	-	-
11 OPHIOPHAGUS HANNAH: DE-1	-	-
12 NAJA HAJE HAJE: CM-2	-	-
13 DENDROASPIS JAMISONI KAIMOSE: S2C4	-	-
14 DENDROASPIS ANGUSTICEPS: C8S2	-	-
15 DENDROASPIS ANGUSTICEPS: C9S3	-	-
16 NAJA MELANOLEUCA: S4C11	-	-
17 NAJA HAJE ANNULIFERA: CM-13B	-	-
18 NAJA HAJE HAJE: CM-11	-	-
19 NAJA NIVEA: CM-10	-	-
20 NAJA NAJA SIAMENSIS (KAOUTHIA): CM-9A	-	-
21 HEMACHATUS HEMACHATES: CM-1B	-	-
22 NAJA HAJE ANNULIFERA: CM-2A	-	-
23 NAJA HAJE ANNULIFERA: CM-3	-	-
24 DENDROASPIS VIRIDIS: TOXIN TA2	-	-
25 DENDROASPIS VIRIDIS: TOXIN 4.9.6	-	-
26 HEMACHATUS HAEMACHES: TOXIN 9B	-	-
27 DENDROASPIS ANGUSTICEPS: TOXIN TA1(F-VII)	-	-
28 NAJA NIVEA: B, (BETA)	++	++
29 NAJA MOSSAMBICA MOSSAMBICA: I	++	++
30 NAJA MOSSAMBICA MOSSAMBICA: III	++	++
31 NAJA HAJE HAJE: CM-10A	++	++
32 NAJA HAJE HAJE: CM-6	++	++
33 NAJA HAJE ANNULIFERA: A, (ALPHA)	++	++
34 NAJA HAJE ANNULIFERA: CM-14	++	++
35 NAJA MELANOLEUCA: D	++	++
36 NAJA NIGRICOLLIS: A, (ALPHA)	++	+++
37 NAJA NAJA ATRA: COBROTOXIN	++	+++
38 NAJA NAJA OXIANA: II	++	++
39 HEMACHATUS HEMACHATES: II	++	+++
40 HEMACHATUS HEMACHATES: IV	++	++
41 DENDROASPIS VIRIDIS: 4.11.3	++	++
42 DENDROASPIS JAMESON: VN'I	++	++
43 DENDROASPIS POLYLEPIS	++	++
44 LATICAUDA SEMIFASCIATA: ERABUTOXIN A	++	++
45 LATICAUDA SEMIFASCIATA: ERABUTOXIN B	++	++
46 LATICAUDA SEMIFASCIATA: ERABUTOXIN C	++	++
47 LATICAUDA LATICAUDA: LATICOTOXIN A	++	++
48 LATICAUDA LATICAUDA: LATICOTOXIN A'	++	++
49 LATICAUDA COLUBRINA: II	++	++
50 LATICAUDA SCHISTOSA: 5	++	++
51 ENHYDRINA SCHISTOSA: 4	++	++
52 AIPYSURUS LAEVIS: A	++	+
53 AIPYSURUS LAEVIS: B	++	++
54 AIPYSURUS LAEVIS: C	++	+
55 HYDROPHIS CYANOCINCTUS: HYDROPHITOXIN A	++	++
56 HYDROPHIS ORNATUS: 75A	++	++
57 ASTROTIA STOKESII: A	++	++
58 ACANTHOPIS ANTARCTICUS: C	++	++

* - indicates inactivity, + indicates marginal activity
 ++, substantial activity and +++, extremely high activity.

$$\begin{aligned} \text{Activity} = & 0.240 + 0.637 F_I + 0.586 F_{II} + 0.266 F_{III} \\ & + 0.750 F_{IV} + 0.358 F_V + 0.533 F_{VI} \\ & + 0.917 F_{VII} - 0.543 F_{VIII} \end{aligned} \quad (1)$$

Fragments I to VII are activating whereas Fragment VIII is deactivating. The F-test for regression is satisfied at the 0.05 confidence limit; $F(8,49,0.05)=201.79$, with a correlation coefficient r^2 of 0.97 and a standard deviation of residuals of 0.217. The correlation is significant since the F-test is substantially better than required by our criteria to eliminate fortuitous correlations (24).

It can be seen from Table II that the predictions (using Equation 1) were quite satisfactory. All the inactive neurotoxins are accounted for correctly. Among the actives, two were predicted to be marginally active (52 and 54) and two extremely active (36 and 39). It has been observed that these two toxins (36 and 39) are indeed very potent (20).

We also submitted 6 short toxins that were found in the literature (25) after the training data base had been entered to the computer. Table III shows the results of the prediction for these neurotoxins; 4 out of the 6 compounds were correctly predicted to be active. The other two were predicted to be marginally active. To us, this indicates satisfactory predictive capability.

Table III. The actual and predicted values \star of the test compounds using Equation 1

Neurotoxins	Actual	Calculated
1 D.j.kaimosae Toxin Vn-II	++	++
2 L.colubrina c	++	+
3 L.colubrina d	++	+
4 L.laticaudata c	++	++
5 L.crockeri c	++	++
6 Hcyan Hyd B	++	++

\star See footnote in Table II.

Cytotoxins. The 58 snake venom cytotoxins submitted to analysis are shown in Table IV. The data base, containing 35 inactive and 23 active toxins, was also build with data from the articles of Karlsson (11) and Dufton et al. (12). The same procedure as described for the short toxins was performed. 15 fragment were selected as potential descriptors of the toxicity of the cytotoxins and the stepwise regression analysis selected only 3 fragments as descriptors of their activity. The three fragments are shown in Figure 2. The following QSAR equation was generated:

$$\text{Activity} = 0.296 + 1.231 F_I + 1.088 F_{II} - 1.029 F_{III} \quad (2)$$

Table IV. The actual and calculated values of the Cytotoxins submitted for analysis

	Cytotoxins	Actual	Calc.
1	NAJA MELANOLEUCA: V ³	-	+
2	NAJA HAJE ANNULIFERA: CM-13A	-	+
3	HEMACHATUS HEMACHATES: 9B	-	-
4	HEMACHATUS HEMACHATES: 9BB	-	-
5	HEMACHATUS HEMACHATES: 11	-	-
6	HEMACHATUS HEMACHATES: 11A	-	-
7	HEMACHATUS HEMACHATES: 12A	-	-
8	NAJA NAJA: CM-XI	-	-
9	NAJA NAJA IIA	-	-
10	NAJA NAJA ATRA : CARDIOTOXIN	-	-
11	NAJA MELANOLEUCA : V ²	-	-
12	NAJA MELANOLEUCA : 3.22	-	-
13	HEMACHATUS HEMACHATES: 12B	-	-
14	DENDROASPIS JAMESONI KAIMOSE: S2C4	-	-
15	DENDROASPIS ANGUSTICEPS: C8S2	-	-
16	NAJA HAJE HAJE: CM-2	-	-
17	DENDROASPIS ANGUSTICEPS: C9S3	-	-
18	NAJA NIVEA : CM-10	-	-
19	NAJA NAJA SIAMENSIS: CM-9A	-	-
20	HEMACHATUS HEMACHATES: CM-1B	-	-
21	HEMACHATUS HEMACHATES: CM-2B	-	-
22	HEMACHATUS HEMACHATES: CM-1C	-	-
23	HEMACHATUS HEMACHATES: CM-12B	-	-
24	NAJA HAJE ANNULIFERA: CM-2A	-	-
25	ACANTHOPIS ANTARCTICUS: P2	-	-
26	ACANTHOPIS ANTARCTICUS: P3	-	-
27	ACANTHOPIS ANTARCTICUS: P5	-	-
28	ACANTHOPIS ANTARCTICUS: P6	-	-
29	PELAMIS PLATURUS: P6	-	-
30	PELAMIS PLATURUS: S07	-	-
31	DENDROASPIS VIRIDIS: 4.11.3	-	-
32	DENDROASPIS JAMESONI: VNII	-	-
33	DENDROASPIS POLYLEPIS: ALPHA	-	-
34	NAJA HAJE ANNULIFERA: CM-13B	-	-
35	NAJA HAJE HAJE CM-11	-	-
36	NAJA NAJA NAJA: II COBRAMINE B	++	++
37	NAJA NAJA OXIANA	++	++
38	NAJA NAJA ATRA: II	++	++
39	NAJA NAJA NAJA: I COBRAMINE A	++	++
40	NAJA MELANOLEUCA: VII1	++	++
41	NAJA NAJA ATRA: I	++	++
42	NAJA HAJE ANNULIFERA: CM-4A	++	++
43	NAJA HAJE ANNULIFERA: CM-2A	++	++
44	NAJA HAJE ANNULIFERA: VII1	++	+
45	NAJA NIVEA: VII1	++	+
46	NAJA NIVEA: VII3	++	++
47	NAJA HAJE ANNULIFERA: CM-8	++	++
48	NAJA HAJE ANNULIFERA: CM-8A	++	++
49	NAJA HAJE ANNULIFERA: VII2	++	++
50	NAJA NIVEA: VII2	++	++
51	NAJA HAJE HAJE: CM-10B	++	++
52	NAJA NIGRICOLLIS: CARDIOTOXIN	++	++
53	NAJA MOSSAMBICA MOSSAMBICA: VII2	++	++
54	NAJA MOSSAMBICA MOSSAMBICA: VII3	++	++
55	HEMACHATUS HEMACHATES: 12B	++	+
56	NAJA HAJE ANNULIFERA: CM-13B	++	+
57	NAJA MELANOLEUCA: 3.20	++	+
58	NAJA MELANOLEUCA: CYTOTOXIN 2	++	+

* See footnote in Table II.

The correlation coefficient r^2 of 0.90 and a standard deviation of residuals of 0.479, together with a F-test value of $F(3,54,0.05) = 154.56$ seem to indicate that the equation is highly significant.

F_I : P V K R G C I D V C P K F_{II} : C C N F_{III} : G C G

Figure 2. The fragments selected by the CASE program from the Cytotoxins data base.

The predictions, using Equation 2, are displayed in Table IV. The results show that 17 out of the 23 active and 33 of the 35 inactive cytotoxins are predicted correctly. The remaining 6 actives and 2 inactives are predicted to have marginal activity. Thus, almost 90% of the variation of the data base can be explained with Equation 2.

Discussion

Short Neurotoxins. Figure 1 shows the fragments that were selected by the program for the QSAR equation. Figure 3 shows the primary structure of some of the snake venoms. In these, we have underlined the fragments that were selected by the QSAR equation as significant to activity.

RICYNHLGTKPPTTECTQEDSCYKNIWRNITEDNIRRGGCFTPRGDMPPGYCCESDKCNL
MICHNQSSQRPTIKTCPGETNCKYKKRWR <u>DHRG</u> TIIERGCGCPSVKKGVIYCKTKDKNCR
MECHNQSSQP <u>PTTK</u> TCPCGETNCKYKKQWSD <u>HRTIIERGCGC</u> PSVKKGVKINCCCTTDRCNN
LECHNQSSQPPTTKSCPGDTNCKYKRW <u>RDHRG</u> TIIERGCG <u>CPTVK</u> PGINLKCCTTDRCNN
MTCCNQSSQPKTTTNC <u>AESSCYKKT</u> WSD <u>HRT</u> RIERGCGCPQVKKGIKLECCHTNECNN

Figure 3. Examples of the relative positions of the most important fragments selected by the CASE program in some short neurotoxins.

Fragment I, SSQ, corresponding to the Ser-Ser-Gln amino acid sequence, is present in almost all the snake venoms except those from the snake of the family Elapinae (mambas). Fragment II, DHRG (Asp-His-Arg-Gly), contains two of the functionally invariant amino acids as defined by Karlsson. These are Arg and Gly. According to the QSAR equation, these are the two most important fragments. Fragment III represents the synergistic presence of the fragments TTK (Thr-Thr-Lys), and RGTIIERGCGCP (Arg-Gly-Thr-Ile-Ile-Arg-Gly-Cys-Gly-Pro). This descriptor is the least potent, according to the QSAR equation (Equation 1); its coefficient is very small. It should be noted that the RGTIIERGCGCP fragment contains two of the

functionally invariant (Arg-Gly) and four of the structurally invariant (Gly-Cys, Gly-Cys) amino acids. Finally, it appears that fragments 7 and 8 (WRD; Trp-Arg-Asp and WSD; Trp-Ser-Asp) are similar and occupy similar locations in the peptide sequences. Thus we conclude that Arg and Ser are interchangeable in this position without any significant activity change.

It is interesting to realize that many of these fragments occupy the same positions that Osthoff et al. (26) identified as surface accessible/inaccessible residues. In fact, five out of the six activating fragments (I-V) contain surface accessible residues only. On the other hand, the inactivating fragment (IV) has an surface inaccessible residue. Fragment VI seems to be the only exception, it contains a mixture of surface accessible and inaccessible residues.

The consideration of the relative location of the fragments within the three dimensional structure of the peptide provide some additional insight into the mechanism of action of these peptides. Figure 4 shows the 3-dimensional structure of a typical short toxin (12). It is based on the crystal structure of the short neurotoxin erabutoxin b. We have indicated the positions of the fragments relevant to activity with solid lines.

The first and most important conclusion comes from the observation that the two most important fragments(SSQ and DHRG) are located at the extremities of loops 1 and 2 and that they face each other controlling the entrance to the channel between them. The other fragment (WSD/WRD) is connected to the DHRG fragment and completes the outer loop of the toxin. These three fragments clearly delineate a primary interaction site with the receptor. There is a secondary region, apparently less important, but not necessary less significant, that needs to be considered as well. It is the region where the CPTVK fragment is located, i.e. in the third loop.

One may speculate that the outer region, corresponding to the fragments SSQ, DHRG, WSD/WRD is required in order for the peptide to be able to attach to the receptor, while the inner region, consisting of the CPTVK fragment could be linked to the toxic activity. This is supported by the fact that the QSAR equation (Equation 1) requires a minimum of three activating fragments in order to yield an actual activity value of 1.9 or larger and accept a peptide as active.

Cytotoxins. Figure 2 shows the fragments selected by the QSAR equation for the activity of the cytotoxins. It can be seen that the most important fragment related to the biological activity of the cytotoxins is much larger than those identified as relevant to the activity of the short neurotoxins. A consideration of the tertiary structure of these cytotoxins is even more revealing as to the difference between their activity and that of the short toxins.

Figure 5 displays the backbone of a cytotoxin showing the normal location of these fragments. The three dimensional structure is extrapolated from the crystal structure of the short neurotoxin, erabutoxin b (12). As in the case of the short neurotoxins, we have drawn the different fragments with solid lines.

It can easily be seen that the extremities of loops 1 and 2, which appeared to be so important in the case of the short

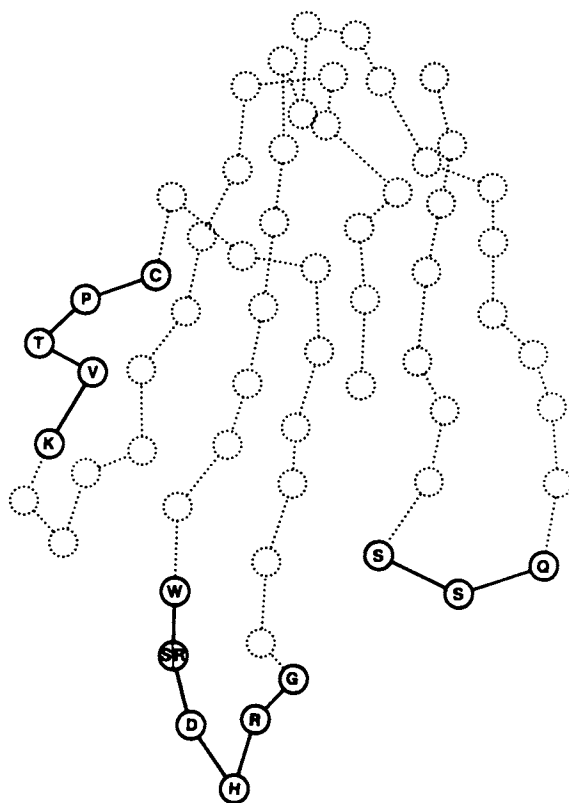


Figure 4. A typical backbone of a short neurotoxin. The most important fragments selected by the CASE program have been indicated with solid lines.

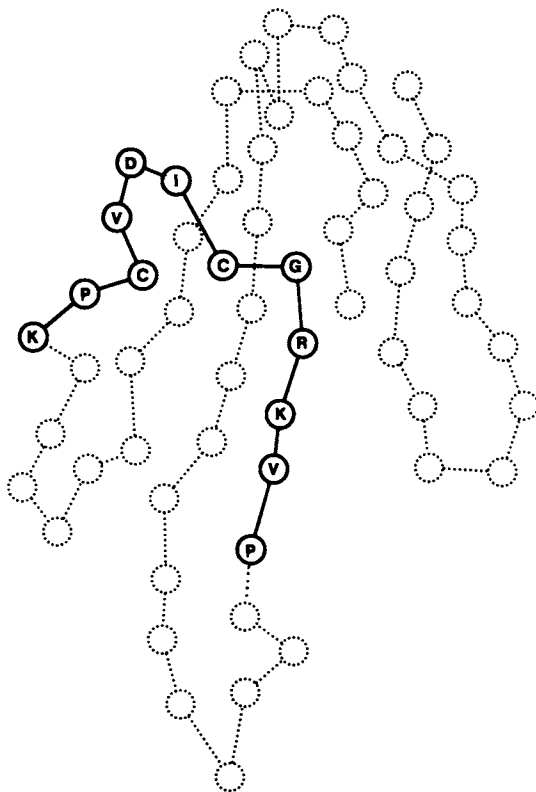


Figure 5. A typical backbone of a cytotoxin. The most important fragments selected by the CASE program have been indicated with solid lines.

neurotoxins, are not relevant anymore, thus suggesting that different receptors are involved. It is now found that all the relevant fragments are concentrated in the secondary region between loops 2 and 3. Thus, while the folding of the cytotoxins is very similar to that of the short neurotoxins, it is clear that the site of activity is completely different and different strategies should be used to either inhibit or simulate the activities of these two classes of structurally related snake venom components.

Conclusions

The CASE analysis was able to identify the relevant sites of activity of two series of peptides. From an evaluation of the location of the relevant fragments, one can conclude that even though both types of toxins have similar three dimensional structure, the sites of neurotoxicity and cytotoxicity activity are completely different and occur at totally different regions of the peptides.

These conclusions were made possible by the combined knowledge of relevant fragments and the three dimensional structure of the peptide. In the absence of a three dimensional structure, the program would hardly be able to recognize the relative location of relevant fragments in widely different peptides. This will strongly limit the use of the CASE program in attempts to identify active peptides of unknown three dimensional structure. On the other hand, in those cases where the tertiary structure of the peptides is known and constant, as it is here, the CASE analysis can help identify relevant regions and gain insight into the nature of the receptor.

Acknowledgment

We wish to thank the Environmental Protection Agency and the Office of Naval Research through its Selected Research Opportunities Program (NO014-85-K-0090) for support this work.

Literature Cited

1. Klopman, G. and Rosenkranz, H. Mut. Res. 1984, 126, 227.
2. Klopman, G. and Contreras, R. Mol. Pharmacol. 1985, 27, 86.
3. Klopman, G., Kalos, A., and Rosenkranz H. Mol. Toxic. 1987, 1, 61.
4. Klopman, G. and Macina, O. J. Theor. Biol. 1985, 113, 637.
5. Klopman, G. and Frierson, M., and Rosenkranz, H. Environ. Mutagen. 1985, 7, 625.
6. Klopman, G. and Venegas, R. Acta Pharm. Jugosl. 1986, 36, 189.
7. Klopman, G. and Venegas, R. Pure & Appl. Chem. 1988, 60, 265.
8. Klopman, G., Contreras, R. and Waters, M. Mut. Res. 1985, 147, 343.
9. Klopman, G., Dimayuga, M. Mol. Pharmacol. 1988, 34, 218.
10. Klopman, G. J. Am. Chem. Soc. 1984, 106, 7315.
11. Karlsson, E. In Handbook of Experimental Pharmacology; Lee, C.Y. Ed.; Springer-Verlag: Berlin, Heidelberg, 1979; Vol. 52, pp. 159-212.
12. Dufton, M. and Hider, R. Crit. Rev. Biochem. 1981, 24, 113.

13. Ryden, L., Gabel, D. and Eaker, D. J. Peptide Protein Res. 1973, 5, 261.
14. Tsernoglou, D. and Petsko, G. FEBS Lett. 1976, 68, 1.
15. Low, B., Preston, H., Sato, A., Rosen, L., Searl, J., Rudko, A., and Richardson, J. Proc. Natl. Acad. Sci., USA. 1976, 73, 2991.
16. Walkinshaw, M., Saenger, W., and Maelicke, A. Proc. Natl. Acad. Sci. U.S.A. 1980, 77, 2400.
17. Menez, A. Pharmac. Ther. 1986, 30, 91.
18. Tu, A. Annu. Rev. Biochem. 1973, 42, 235.
19. Juillerat, M., Schwendimann, B., Hauert, J., Fulpius, B., and Bargetzi, J. J. Biol. Chem. 1982, 257, 2901.
20. Low, B. In Handbook of Experimental Pharmacology; Lee, C.Y. Ed.; Springer-Verlag: Berlin, Heidelberg, 1979; Vol. 52, pp. 213-257
21. Yang, C. Biochim. Biophys. Acta 1967, 359, 242.
22. Yang, C. Toxicon 1965, 3, 19.
23. Klopman, G. and McGonigal, M. J. Chem. Inf. Comput. Sci., 1981, 21, 48.
24. Klopman, G. and Kalos, A. J. Comp. Chem., 1985, 6, 492.
25. Endo, T., Nakanishi, M., Furukawa, S., Joubert, F., Tamiya, N. and Hayashi, K. Biochemistry. 1986, 23, 395.
26. Osthoff, G., Louw, A., and Reinecke, C. Toxicon. 1988, 26, 475.

RECEIVED November 14, 1988

Chapter 6

Application of Simulation and Theory to Biocatalysis and Biomimetics

Adel M. Naylor and William A. Goddard III

Arthur Amos Noyes Laboratory of Chemical Physics, California
Institute of Technology, Pasadena, CA 91125

Examples are given for the role of simulation and theory in biocatalysis and biomimetics. Simulations on the novel Starburst Dendrimer polymers are used to suggest a design for encapsulating and delivering dopamine to the kidney for cardiovascular therapies. For Dihydrofolate Reductase (DHFR), the simulations (i) indicate why a particular mutation (Phe-31 to Tyr-31) causes a significant change in the catalytic rate, (ii) explain the high degree of kinetic similarity between two dissimilar forms of DHFR, and (iii) suggest that the stable form of the enzyme/substrate complex is *not* the reactive one.

A goal of our research efforts is to develop the theoretical tools useful in designing artificial biocatalytic systems for the production of fuels and chemical feedstocks. In the long term, one would envision the development of biocatalysts that could convert methane into more valuable (or more transportable) fuels or to convert syngas ($\text{CO} + \text{H}_2$) into various fuels and feedstocks. In the short term, we are focusing on systems capable of selective oxygenations or reductions. We would hope to develop artificial systems with the selectivity of cytochrome P-450 enzymes that play a role in selective oxidation of long chain alkanes and selective epoxidation of alkenes (1). Although selective, the various cytochrome P-450 enzymes involve complex assemblies (cofactors, co-enzymes) that would be difficult to reproduce and control in an artificial system (see Figure 1). Thus, we would hope to incorporate catalytic control procedures as effective as those in P-450, yet delete the excess baggage special to biological systems (e.g., cofactor, bulk protein necessary to elicit stability and to create substrate binding pockets, etc.)

To that end we have focused our research on two aspects of this complex problem: (i) the design of artificial systems that possess precision sites capable of selectively encapsulating and delivering smaller molecules, and (ii) understanding the detailed structural and chemical aspects of enzyme active

0097-6156/89/0392-0065\$06.75/0

© 1989 American Chemical Society

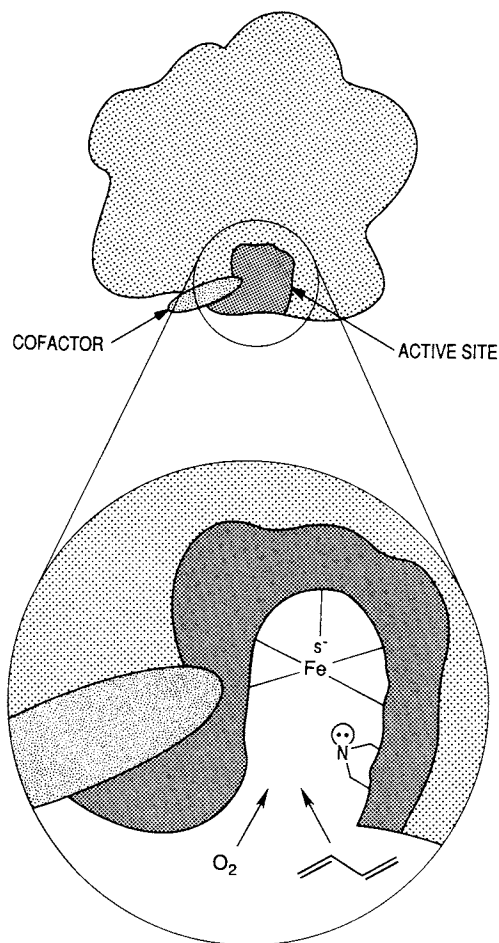


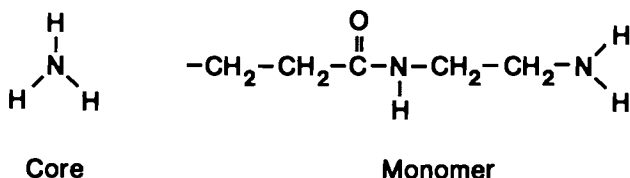
Figure 1. Schematic representation of cytochrome P-450 indicating the excess baggage carried by many biological catalysts.

sites involved in and affecting the important catalytic processes, i.e., substrate binding, product release, rate of catalysis.

Starburst Dendrimers: Molecular Encapsulation

A recent synthetic development has led to a new class of polymers called "starburst dendrimers" (2) that provide the opportunity for design of precise encapsulation strategies. These novel materials (i) start with an initiator unit (termed the "core") that possesses multiple sites for monomer condensation and (ii) use monomer subunits terminating in functional groups that allow for regularized growth and multiple branching at the next generation. With the appropriate use of protecting groups and synthetic strategies, each generation of monomer condensation can be completed before embarking on a new one. Because of the unique chemical requirements for dendrimer formation, these polymers grow in a systematic manner, producing materials with a well-defined number of monomer subunits and a quantized number of terminal groups (Figure 2). With precise topology and chemical properties suitable for the encapsulation of specific target molecules that could be delivered to particular organs (by recognition of surface molecules), one could, in principle, change the monomer from generation to generation, developing onion-like molecules where every layer of the onion has a different chemical composition, thickness, or number of branching sites. Thus, one can imagine designing and synthesizing complex polymer structures where (i) internal layers are suitable for encapsulation of the desired molecule, (ii) outer layers are suitable for recognizing binding sites on the organ to which the target molecule is to be delivered, and (iii) intermediate layers protect the target molecule in the blood stream but release them (a) upon binding of the outer layer to recognition sites, (b) upon radiation with external light or charged particles or (c) upon change in acidity or solvent associated with the target organ.

β - Alanine Dendrimers. To illustrate this application, consider the β -alanine dendrimers where the core unit is ammonia (with three condensation sites) and the monomer unit is an amino amide (with two branch sites) as depicted below.



Experimentally it has been possible to develop complete dendrimers up through the tenth generation. However, no experimental structural data are available (these materials are fractal and do not crystallize). We have been carrying out molecular dynamics simulations on these β -alanine dendrimers up through generation 9 (3) using the molecular simulation facilities of POLY-GRAF (from Biodesign, Inc., Pasadena, CA 91101). These investigations indicate a dramatic change in the overall structural properties for the β -alanine systems as these polymers grow past generation 4. The early generation dendrimers

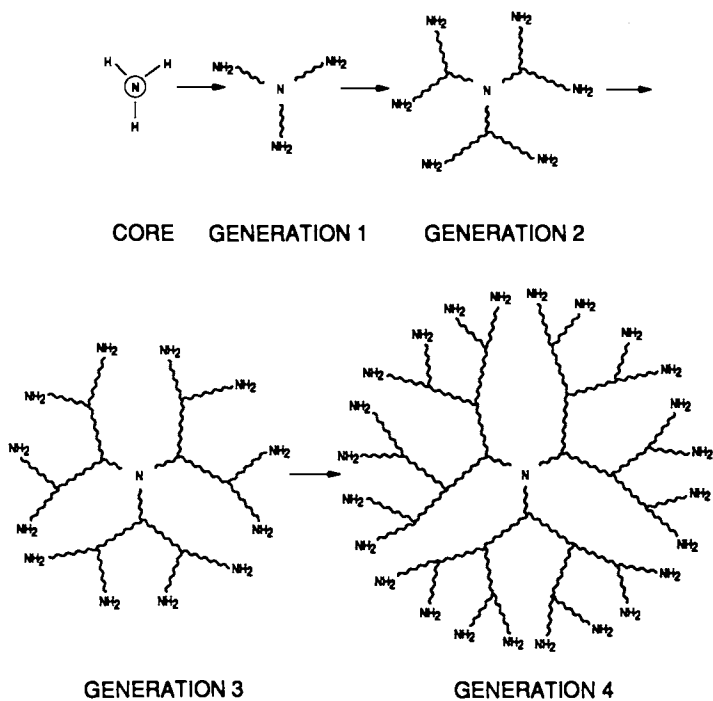
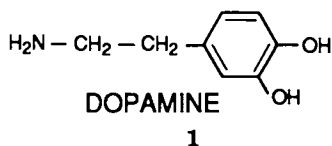


Figure 2. Cascade growth pattern for the β -alanine type dendrimers from the core ammonia unit up to generation 4.

(generations 1 through 3) possess very open and well-extended structures. These structures are hemispherical disks (with the core nitrogen responsible for the curvature) but there is no real inside to the polymer. This topology for the early generation systems is strikingly different from earlier proposals (4), but these hemispheric structures provide a simple interpretation of observed nuclear magnetic resonance relaxation times (Naylor, A. M.; Goddard III, W. A.; Keifer, G. E.; Tomalia, D. A. *J. Am. Chem. Soc.*, in press 1988).

We find a distinct change in structural properties for those polymers above generation 5. The overall structure of the polymers is more sphere-like, with ample internal hollows connected by channels that run the length of the polymer assembly. These interior cavities should be suitable for sequestering guest molecules. Thus, in Figure 3, which limns a generation 6 dendrimer, we find an overall spherical structure containing a channel running through the interior of the polymer from one side to the other! To better illustrate the space available in the interior, we show in Figure 4 the solvent-accessible surface for the polymer (generation 6). [The solvent-accessible surface is constructed using the approach developed by Michael Connolly (University of California, San Diego) and is based on the definitions for molecular surfaces proffered by Frederic Richards (5). The molecular surfaces are composed of dots located in terms of a probe sphere (radius = 1.4 Å for water) rolling along the van der Waals spheres of the outer (accessible) atoms of the polymer.] Here we have used graphical slabbing to remove from view the front and rear portions of the image. The channels and cavities in this structure are representative of those found in the higher generation β -alanine dendrimers.

Dopamine – Sequestered Dendrimers. As an illustration of the dimensions of these channels and of how dendrimers might be used to sequester small molecules, we have used the molecular simulation capabilities of POLYGRAF to predict the optimum conformations for several dopamine 1 molecules

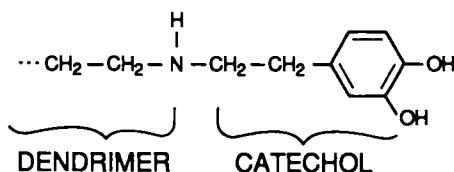


inside this starburst polymeric matrix. Dopamine was chosen because it is a good candidate for effective sequestration in a β -alanine type dendrimer. Its size and shape are suitable for the cavities and channels found to exist in the higher generation β -alanine systems. From a chemical standpoint, dopamine possesses both the hydrogen bond donor and acceptor sites needed for favorable binding interactions to the polymer's carbonyl, amide, and amino substituents. We estimate that a generation 6 polymer should be capable of holding 15-20 molecules of dopamine. Figure 5 illustrates a dopamine/dendrimer complex with examples of the conformations adopted by the sequestered molecules and the polymeric material.

Pharmacologically, the ability (i) to selectively deliver dopamine to peripheral kidney receptors without eliciting complications due to the presence of dopamine receptors in the central nervous system (CNS) and (ii) to maintain a supply of nonmetabolized dopamine would be advantageous in cardiovascular hypertension therapy (8). The additional issues presented by this type of application include the dimensions of the dendrimer encapsulated dopamine and the targetting of the unit to the appropriate dopamine receptor sites.

The dimensions of the higher generation β -alanine dendrimers (see Figure 6 with the minimum diameter plotted as a function of generation) are such that these dopamine/dendrimer complexes would not readily cross the CNS blood-brain barrier.

In order to ensure the delivery to kidney dopamine receptors, we suggest modifying the terminal amine sites of the polymer with catechol fragments, as shown in 2



2

This leads to surface features resembling dopamine and may lead to selective binding at dopamine receptor sites (Figure 7). The polymer encapsulation matrix should protect the catecholamine from rapid metabolic inactivation.

These studies provide structural models that should be useful for analyzing the dopamine/dendrimer systems. The next step is to test the effectiveness of these modified materials for encapsulation of dopamine (and related materials) and to determine how effectively they are delivered to the kidney centers. As such experiments proceed, continuing simulation will be useful in providing a quantitative framework for understanding various results.

We expect that the judicious selection of a core unit, internal monomer subunits, and terminal monomer fragments will allow the design of dendrimers to complex with specific guest molecules and to deliver them to specific sites. It will, of course, be essential to develop synthetic schemes that allow for chemical control and fidelity.

Dihydrofolate Reductase: Roles of Precise Structure in Catalysis

In designing new catalysts, it is essential to understand how the character of the active site (including cofactor) controls catalytic activity since one will want to modify this active site or cofactor. As a prototype for such studies, we have carried out a series of molecular simulations on the Dihydrofolate Reductase (DHFR) system.

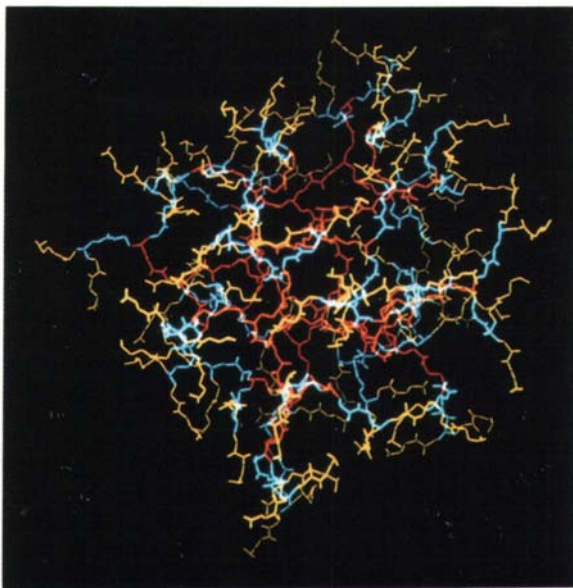


Figure 3. A representative structure for a generation 6 β -alanine dendrimer where generations 1 to 4 are colored red, generation 5 is shown in light blue, and generation 6 is yellow. .



Figure 4. A view of a generation 6 dendrimer with its solvent-accessible surface displayed and clipped to reveal the nature of the internal cavities and channels found in the higher generation β -alanine dendrimers.

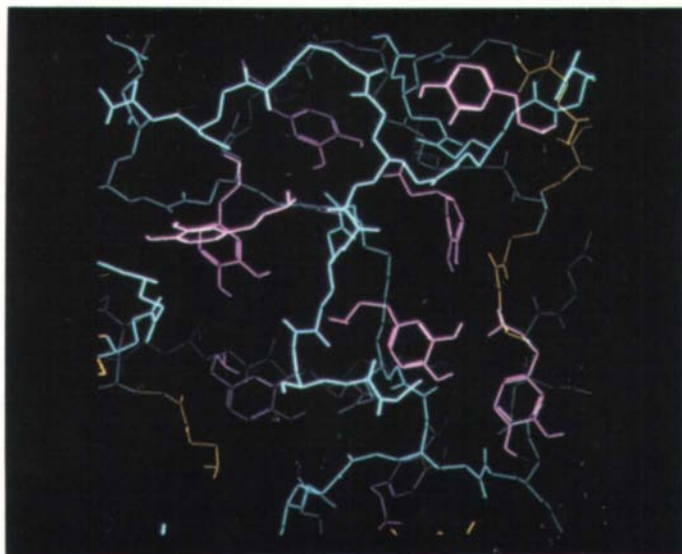


Figure 5. A view of various dopamine molecules (magenta) bound in the inner regions of a β -alanine dendrimer (generations 1 through 5 in light blue; generation 6 in yellow).

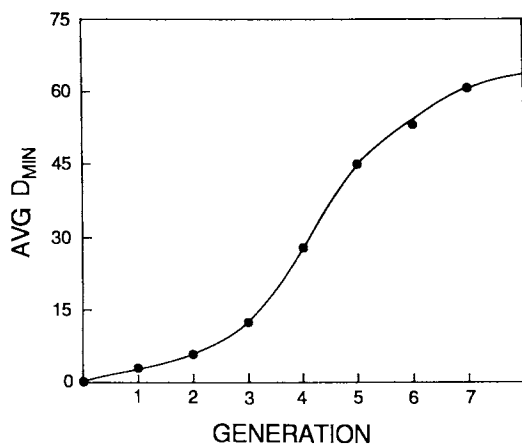
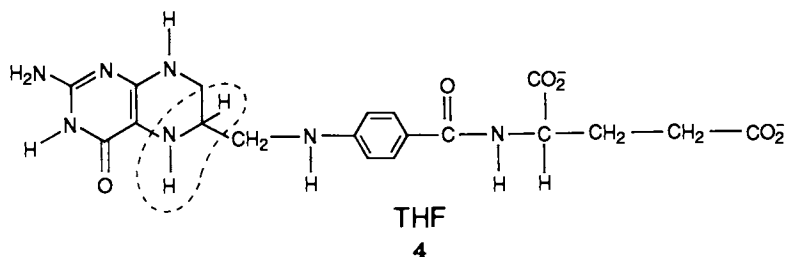
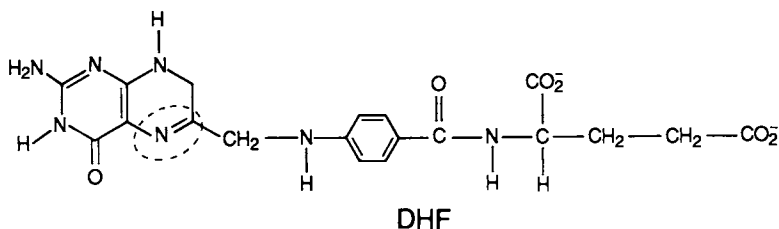


Figure 6. A plot of the β -alanine dendrimers "short" diameter (see text) as a function of generation. These diameters were calculated from our molecular simulations and based on the average of the smallest principal moment of inertia.

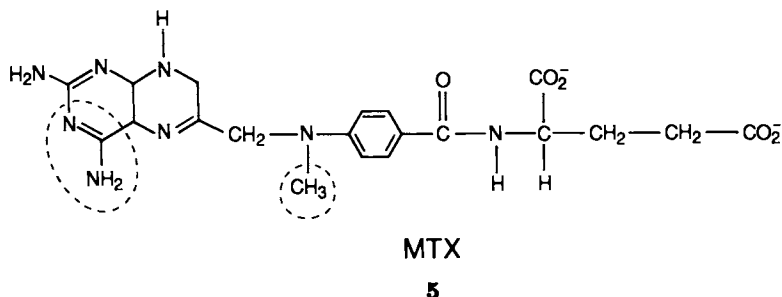
Introduction and Rationale. DHFR is an ideal system to study for a number of reasons. The catalytic properties of DHFR are such that under normal physiologic conditions and with the NADPH cofactor bound, 7,8-dihydrofolate (DHF) is reduced to 5,6,7,8-tetrahydrofolate (THF) (7). Thus DHFR plays an important role in cell metabolism by maintaining a supply of THF. THF is used by the cell as both a cofactor and in substrate quantities in the synthesis of deoxythymidine. By inhibiting the production of THF, deoxythymidine synthesis is curtailed, nucleic acid replication comes to a halt, and cell proliferation ceases. It is this biochemical cascade which supplies the pharmacological and chemotherapeutic applications of inhibitors to DHFR.

The abundant experimental data on DHFR provide both inspiration and detailed checks upon theoretical studies. The crystal structures of DHFR from two bacterial sources have been resolved, reported, and coordinates made available through the Brookhaven Data Base (8-10). The kinetic profiles of the enzyme under various conditions and, hence, mechanistic details have been determined (11,12). The recombinant DNA protocols for the successful study of site-directed mutants of DHFR have been reported (13-17).

DHF **3** is composed of (from left to right, below) a pterin ring, a bridging methylene unit, p-aminobenzoate, and a glutamate fragment.



It is the N5-C6 double bond (circled, above) of 7,8-DHF that is reduced to 5,6,7,8-THF (4) by DHFR. Methotrexate (MTX), an important chemotherapy and anti-bacterial agent, is chemically quite similar to DHF (differences are circled).



MTX 5 contains the same benzylglutamate fragment as DHF (but with a methylated amine) and a pteridine ring with an amino substitution at position 4. Indeed, we find similar binding sites for MTX and DHF on DHFR.

The crystal structure of the *E. coli* DHFR/MTX binary complex (9) reveals that the inhibitor binds in the active site in a kinked fashion (Figure 8). Asp-27 forms a salt-bridge to the bound pteridine ring while Phe-31 allows for the bend in the bound inhibitor. The remainder of the active site cavity surrounding the pterin ring is composed of amino acid residues that create a very hydrophobic environment.

Before embarking on designing improvements into the catalytic sequence, it is useful to know the detailed kinetics of the system. A profile of the steady-state kinetics of the *E. coli* form of DHFR was recently reported by Fierke, Johnson, and Benkovic (12). This study used stopped flow fluorescence and absorbance spectroscopies to measure the rates of ligand association and dissociation and the binding constants of key intermediates in the catalytic sequence, as diagrammed in Figure 9. This study revealed that the catalytic step, i.e., the N5-C6 double bond reduction, proceeds at a steady-state rate of 950 sec^{-1} , whereas the rate of THF product release was only 12.5 sec^{-1} , making it the rate-limiting step. Hence, any design modifications to increase the turnover of this system should focus first upon increasing the product off-rate.

A Synthetic Mutant : Phe - 31 \rightarrow Tyr - 31. We now turn to using molecular simulation methods to examine some areas of the biocatalytic properties of DHFR that are not easily investigated experimentally. The general methods used for our studies incorporate computer graphics, molecular force fields, energy minimization, and molecular dynamics. BIOGRAF (from Biodesign, Inc., Pasadena, CA 91101) was the molecular simulation package used for these investigations. The AMBER force field was used for the calculations (18).

As an illustration of the use of simulations, we consider the effect on rate of a site mutation of DHFR. Benkovic *et al.* used recombinant-DNA techniques to synthesize the protein where Phe-31 was transformed into Tyr-31 (14). Preliminary experimental studies indicated a change in the pK_a of Asp-27 in this mutant form of the enzyme. Molecular simulations were run on both the wild-type enzyme and the Tyr-31 mutant to assess the structural changes produced by such a modification.

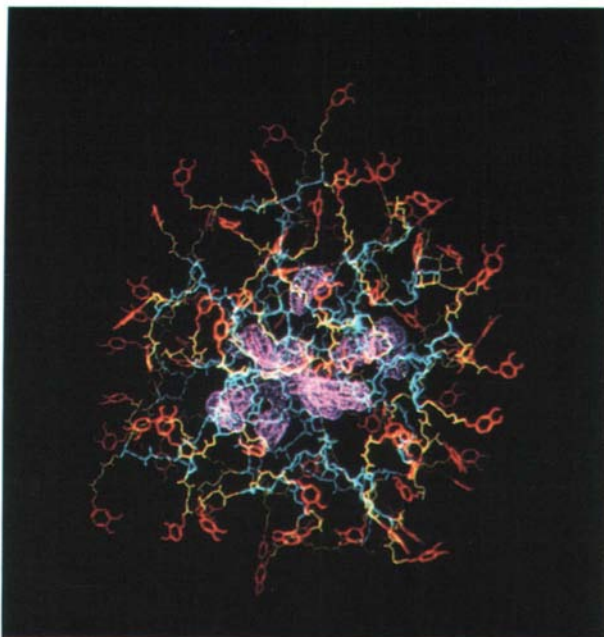


Figure 7. A catechol-modified, dopamine-loaded β -alanine dendrimer where the dopamines are displayed in magenta, generations 1 through 5 in light blue, generation 6 in yellow, and the catechol cap in red.

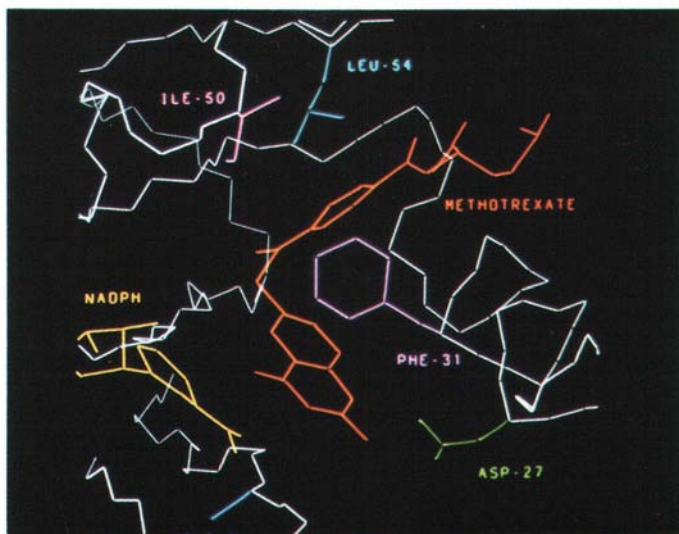


Figure 8. The active site of *E. coli* DHFR with MTX and NADPH bound.

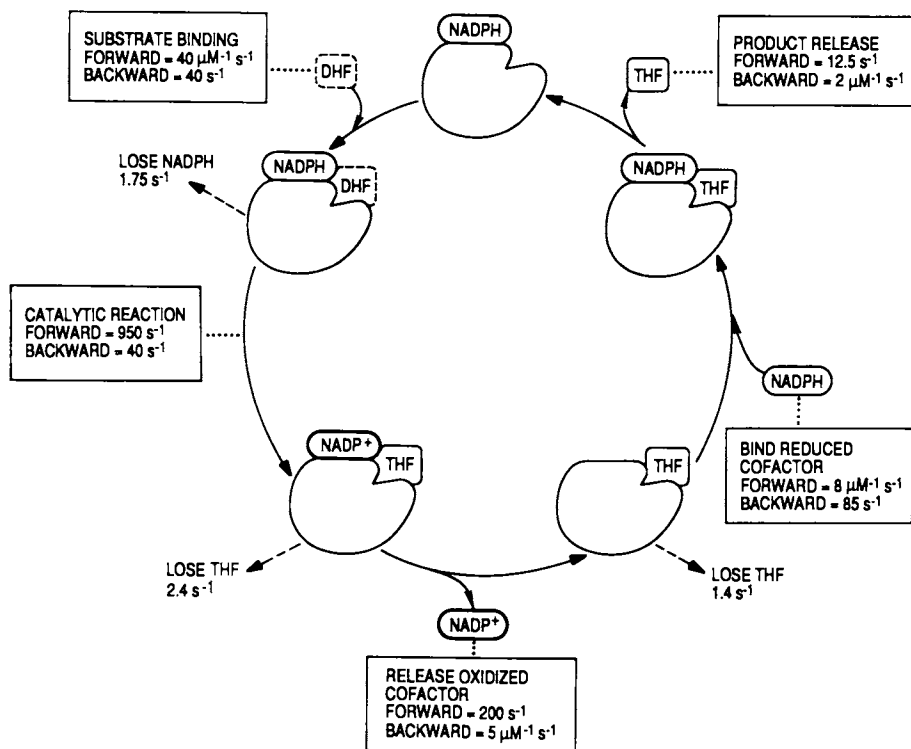


Figure 9. Steady-state kinetic cycle for the reduction of 7,8-DHF to 5,6,7,8-THF via DHFR.

The starting structure for our wild-type protein complex was based upon the crystallographic data, where the *L. casei* NADPH coordinates were used to model the cofactor into the *E. coli* system. To create the Tyr-31 mutant, the replace facility of BIOGRAF was used. For both series of simulations, a 10 Å solvent shell (containing experimental plus supplemental waters) surrounded the protein complexes. Counter ions were positioned near charged amino acid side chains to achieve electroneutral systems. The structures were then equilibrated via a sequence of molecular dynamics and energy minimization calculations.

Our calculations show that the pteridine ring is relatively undisturbed by the introduction of the Tyr hydroxyl group, yet the benz-glutamate portion of the bound substrate (or inhibitor) is markedly displaced (see Figure 10). We find that the mutant -OH group produces a 'bump' on the surface of the hydrophobic pocket near the benzyl group that disrupts the binding of the benz-glutamate fragment. This suggests that the product off-rate from the DHFR/NADPH/THF complex should be affected markedly by this substitution. Kinetic studies have verified that the product off-rate for the Tyr-31 form of *E. coli* DHFR is 50 times faster than that of wild-type protein (14)!

Natural Mutants: *E. coli* and *L. casei*. Consider now the question of how different one can make the active site *without* affecting the chemistry. The overall amino acid sequence homology between the *E. coli* and *L. casei* forms of DHFR is only 27%. However, as shown in Figure 11, a Gibbs free energy comparison of the steady-state data for the *E. coli* and the *L. casei* proteins shows that the reaction kinetics for these two forms of the enzyme are remarkably similar (19). In fact (using the ternary DHFR/NADPH/DHF complex as the energy reference), the energy differences between the two are, at every step, within 1 kcal/mol! Using the x-ray crystal structures and reorienting them so that the MTX of both complexes are superimposed (by docking one structure with respect to the other), we see that the conformation of MTX bound to the *E. coli* DHFR is very similar to that of MTX in the *L. casei* ternary crystal complex. The orientations of both the pteridine and the benzyl rings are identical for the two complexes and the backbone atoms of the glutamate substituent also align quite nicely. The discrepancy in these two forms of bound MTX occurs at the C- δ carboxylate group of the glutamate fragment, a position far removed from the catalytic site. A glance at the two different enzymes reveals that this difference in conformation is due to the positions of positively charged amino acid side chains on opposite sides of the opening for the active site (Arg-52 for the *E. coli* form and His-28 for the *L. casei* complex).

The results of docking the *L. casei* structure to the *E. coli* show that the overall folds for these two proteins are quite similar. Regions of secondary structural elements, i.e., α -helices and β -sheets, are conserved, while insertions and deletions in the amino acid sequences occur in loop regions located about the exterior regions of the enzyme. The structural domains of the DHF and NADPH binding sites are maintained. In the comparison of the DHF substrate

binding pockets, one finds that nature, in some instances, substitutes like for like by using

- (1) different aromatic side chains [as Trp-30 (*E. coli* \equiv *Ec*) \rightarrow Tyr-29 (*L. casei* \equiv *Lc*), Tyr-100 (*Ec*) \rightarrow Phe-103 (*Lc*), and Phe-153 (*Ec*) \rightarrow Tyr-155 (*Lc*) indicate] or
- (2) different aliphatic side chains [as Ile-5 (*Ec*) \rightarrow Leu-4 (*Lc*), Leu-36 (*Ec*) \rightarrow Val-35 (*Lc*), and Leu-112 (*Ec*) \rightarrow Val-115 (*Lc*) demonstrate].

But there also are examples where aliphatic is substituted for aromatic (and vice versa) as with Ile-50 (*Ec*) \rightarrow Phe-49 (*Lc*) and Tyr-111 (*Ec*) \rightarrow Leu-114 (*Lc*). Similar substitution patterns are found in the NADPH cofactor binding site, where, in addition to those types described above, charged residues are maintained [i.e., His-45 (*Ec*) \rightarrow Arg-44 (*Lc*) and Lys-76 (*Ec*) \rightarrow His-77 (*Lc*)].

Using these superimposed structures with the MTX (from both crystal structures) and the NADPH (from the *L. casei* complex) as guides, the active site regions are identified for both enzymes. Here we define the active site to be those amino acids containing any atom within 7 Å of either of the bound substrates. Analyses of the residues in the active site region determine that the amino acid sequence homology in this portion of the protein is 35% (see Table I).

The two docked active site regions (with MTX bound) are shown in Figure 12. Examination of the docked active sites reveals that there are three general types of amino acid residues involved in the construction of the active site surface:

- (1) amino acid residues conserved between the two bacterial forms of DHFR, e.g., Phe-31 (*Ec*) and Phe-30 (*Lc*);
- (2) amino acid residues that differ between the two sequences and contribute chemically different side chains to the construction of the active site, e.g., Ile-50 (*Ec*) and Phe-49 (*Lc*); and
- (3) amino acid residues that differ between the two sequences but contribute only chemically homologous main chain atoms to the construction of the active site, e.g., Ala-6 (*Ec*) and Trp-5 (*Lc*).

Thus, by modifying the definition of homology to also include those residues in the active site supplying only backbone atoms, one obtains a generalized 'chemical homology' of the active site. Indeed, the 'chemical homology' between the *E. coli* and the *L. casei* substrate binding pockets becomes 60% (19)!

A comparison of the solvent accessible surfaces [as described above; (5)] for these segments of the protein further substantiates these remarkable structural similarities. The surface areas mapped out for these regions agree within 93%. The solvent accessible surfaces for the MTX pteridine and the NADPH nicotinamide rings are essentially interchangeable for the two different sequences, as illustrated in Figure 13.

Hence, we see that nature creates essentially identical reactive surfaces for these bacterial DHFR systems from different amino acid building blocks (19) (Benkovic, S. J.; Adams, J. A.; Fierke, C. A.; Naylor, A. M. Pteridines, in press 1988). The components necessary for DHFR's ability to catalytically reduce the N5-C6 double bond of 7,8-DHF to 5,6,7,8-THF are conserved. The carboxylate group that supplies a proton to the pterin ring is present in both the *E. coli* and

Table I. Comparison^a of DHFR Active Site Residues from *E. coli* and *L. casei*

Residue ^b	4	5	6	7	8	9	10	...	13	14	15	16	17	18
<i>E. coli</i>	L	i	A	A	L	A	V	...	V	i	G	M	e	n
<i>L. casei</i>	F	l	W	A	Q	N	R	...	L	l	G	K	d	g
	19	20	21	22	23	24	25	26	27	28	29	30	31	32
	a	m	P	W	n	L	P	A	D	L	a	w	F	k
	h	l	P	W	h	L	P	D	D	L	h	y	F	r
	33	34	35	36	...	42	43	44	45	46	47	48	49	50
	r	n	T	l	...	m	G	R	h	T	W	E	S	i
	a	q	T	v	...	v	G	R	r	T	Y	E	S	f
	51		52	53	54	55	56	57	...	61	62	63	64	65
	g	...	R	P	L	P	G	R	...	i	L	s	s	Q
	p	k	R	P	L	P	E	R	...	v	L	t	h	Q
	66	67	68	...	74	75	76	77	78	79	...	93	94	95
	p	G	t	...	w	V	K	S	V	D	...	V	I	G
	e	D	y	...	v	V	H	D	V	A	...	I	A	G
	96	97	98	99	100	101	102	103	...	111	112	113	114	115
	G	G	r	v	y	E	q	F	...	y	l	T	H	i
	G	A	q	i	f	T	a	F	...	l	v	T	R	l
	122	123	124	125	...	153								
	D	T	H	f	...	f								
	D	T	K	m	...	y								

^a Bold upper case indicates homologous, lower case indicates nonhomologous, and nonbold upper case indicates backbone chemical homology, as described in the text.

^b Numbered for the *E. coli* form.

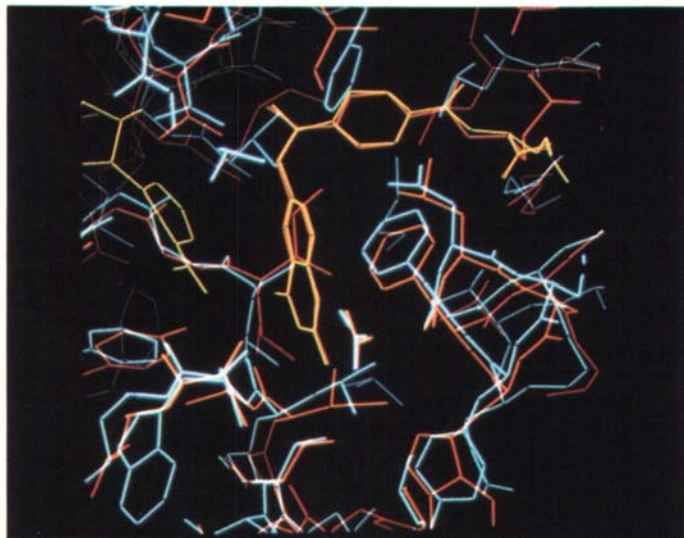


Figure 12. A comparison of the docked *E. coli* (red MTX and enzyme) and *L. casei* (yellow MTX and NADPH; blue enzyme) active sites. The conserved Phe's are shown to the right of the pteridine rings. The substituted side chains [Ile-50 (*Ec*) and Phe-49 (*Lc*)] appear in the 12 o'clock position above the benzyl ring. The chemically homologous main chain contributors [Ala-6 (*Ec*) and Trp-5 (*Lc*)] are shown in the 7 o'clock position.

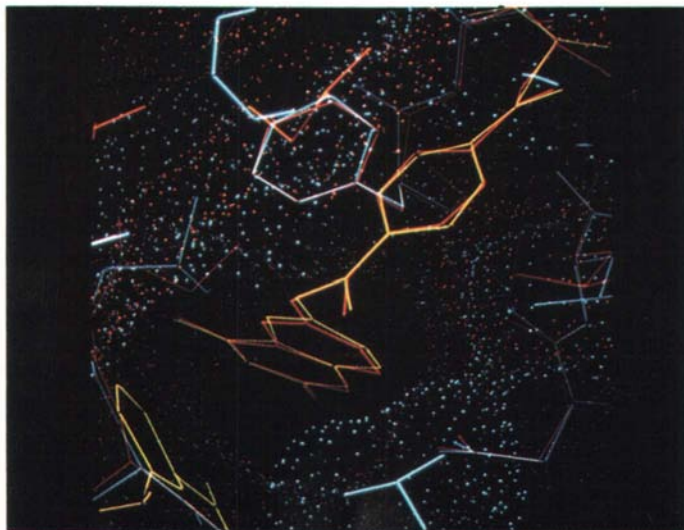


Figure 13. Dotted surface comparison showing the congruence of the *E. coli* (red) and *L. casei* (blue) active sites.

the *L. casei* sites as an Asp side chain. The hydrophobic pocket that surrounds the reactive pteridine moiety and prevents the aqueous environment from disturbing the catalytic process is formed by varied amino acids but maps out the same surface area and hydrophobic character. The hydride donating NADPH nicotinamide ring is positioned adjacent to the reactive center even though the NADPH binding sites are composed of different amino acid sequences.

Conformation of Bound Inhibitor. Another area under investigation focuses on the conformation(s) of the substrate and an inhibitor (MTX) bound to DHFR. The form of the DHFR/MTX complex is known from the crystallographic studies of Kraut *et al.* (8-10). However, the orientation of the bound pterin ring in the reactive DHFR/DHF is known to differ dramatically from the MTX crystal structure (20). Basically, these differences arise because there are two possible orientations of the pterin ring in the active site; one is flipped by 180° with respect to the other. Isotope labelling experiments on THF show that the reactive DHF must be bound in the conformation flipped from that observed by x-ray for MTX. In order to understand these differences, we ran simulation studies on altered forms of bound MTX and DHF to investigate the structural and energetic properties of these systems.

The starting structures for our binary DHFR/MTX calculations were based upon the crystallographic data. For the experimental form of bound MTX we used the coordinates as they were reported. For the pteridine-flipped form of bound MTX, termed MTX-flipped, we rotated about the C6-C9 and C9-N10 bonds of MTX to produce a starting conformation with the pteridine ring positioned in the active site but with its face flipped 180° (Figure 14). To be consistent with experiment, the bound MTX inhibitor was protonated at N1 (21). For both systems we used the experimentally determined solvent plus additional water to create a 10 Å solvent shell around the enzyme-inhibitor complex. Electroneutral systems were achieved by positioning the appropriately charged counter ions near to cationic and anionic side chains. The entire solvated protein and inhibitor systems were then equilibrated with a sequence of molecular dynamics and energy minimization calculations (using BIOGRAF and the AMBER force field).

These simulations indicate that the active site of DHFR can accommodate both forms of the bound MTX. After equilibration of both the experimental and the flipped forms, the carboxylate group of Asp-27 is found to be involved in a salt bridge with the pteridine ring of the inhibitor. The hydrophobic pocket surrounding the pterin ring has adjusted adequately to either conformation of the bound MTX. The energetic profiles indicate that the experimentally observed form of MTX bound to DHFR is ~3 kcal/mol lower in energy than the flipped form of the bound inhibitor.

Conformation of Bound Substrate. Now the question of the conformation of bound DHF substrate was addressed. Simulations were run on DHFR/DHF/NADPH ternary complexes to investigate both the structural and energetic requirements associated with the reactive and nonreactive forms of DHF (see Figure 14). As above, the crystallographic information available for

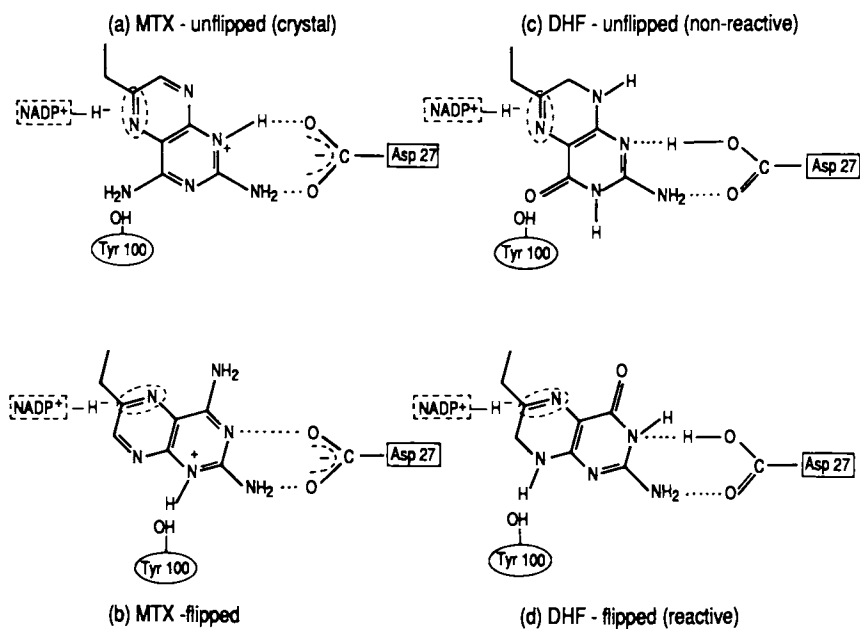


Figure 14. The orientations of the MTX and DHF pteridine rings in the active site of DHFR.

the *E. coli* binary and *L. casei* ternary complexes (with MTX) was used to generate starting structures for the molecular simulations. The coordinates for the *E. coli* bound NADPH were modeled based upon those from the *L. casei* ternary complex. The DHF units were positioned based upon the coordinates of the MTX. For these simulations, the carboxylate group of Asp-27 was protonated while the pterin ring of the substrate was not protonated at the N1 position. Again, solvent and counterions were included and all atoms of the structures were relaxed and equilibrated during the calculations.

The simulations indicate that there are two favorable conformations of bound DHF in the active site of DHFR, each analogous to the favorable conformations of MTX. The amino acid side chains that create the hydrophobic portion of the active site reposition themselves to allow for either form of the pteridine ring. In the reactive orientation (termed DHF-flipped), the Asp-27 COOH prongs the C4 oxygen and the N3 sites. In the nonreactive conformation (termed DHF-unflipped), the carboxylate group straddles the N1 and the N8 positions. The energetic results of the simulations find *the unflipped nonreactive form* (analogous to the x-ray form in MTX) of the pteridine ring *lower in energy than the reactive form* by ~ 4 kcal/mol! This result seems to contradict experiment since no radio-labeled product resulting from DHF reduction accommodates this orientation of bound substrate.

Closer examination of the active site regions reveals that the reducible C-N bond of the pterin ring differs substantially with respect to the positions of the NADPH nicotinamide rings. In the low energy nonreactive state, the NADPH C'4 site is 4.1 Å from the carbon of the pteridine N5-C6 double bond, while in the higher energy reactive form, this interatomic distance is reduced to only 3.2 Å! The shorter distance for hydride transfer during catalysis favors the reactive conformation even though the energetics slightly favor the nonreactive form of bound DHF. This information clearly suggests a kinetic mechanism for the control of DHF reduction to THF via DHFR. Figure 15 depicts the relationship between the NADPH nicotinamide ring and the reactive DHF substrate.

Wu and Houk have used *ab initio* calculations to propose a mechanism for hydride transfer to the methyl iminium cation (22). Their results indicate that H^- transfer proceeds via a *syn* transition state structure with a C-H-C angle of 150-160° and a C-C interatomic distance of 2.6 Å (see Figure 16). What we find for the reactive form of bound DHF and NADPH in an equilibrated ground state is a pseudo-*syn* orientation of the reacting ring systems, a C-H-C angle of 155°, and an equilibrium distance of 3.2 Å between the two carbon centers (19). In contrast to the nonreactive conformer of DHF, simulations suggest that the equilibrium distance between the two reacting carbons is 4.1 Å. The key difference in character is the orientation of the pterin and nicotinamide rings. In the productive conformation, the two-ring systems adopt positions that allow for H^- transfer from the nicotinamide center to C6, while this relationship is not accommodated by the nonreactive bound conformation of DHF.

In order to address the reaction rates of these species, we could monitor the C-C distance as a function of time. Taking the probability distribution of C-C

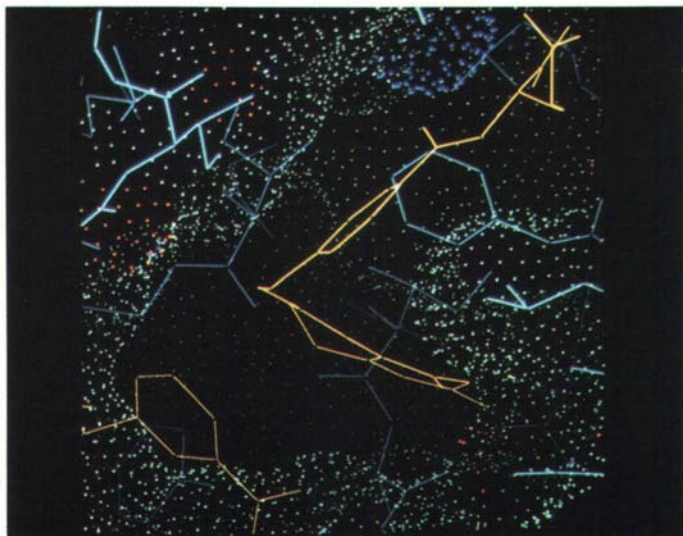


Figure 15. The catalytic pocket of DHFR showing the relationship between the NADPH nicotinamide ring (left) and the reactive DHF pteridine ring (right).

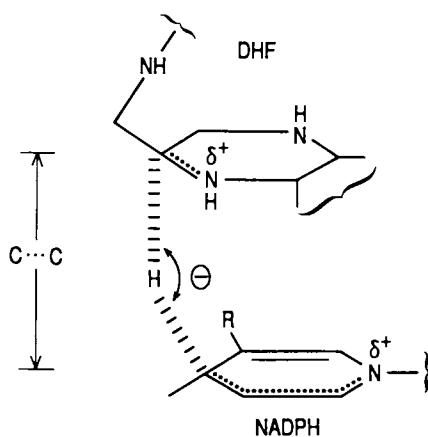


Figure 16. Proposed model for hydride transfer from NADPH to DHF (adapted from ref. 19). θ is the angle between the C4' of NADP⁺, the H⁻ being transferred, and C6 of DHF.

with the reaction rate as a function of C-C distance, one should be able to predict relative reaction rates. However, qualitatively the large differences in equilibrium position certainly suggest a significant difference in rate. A test of this prediction would be to use NMR NOE experiments to examine conformation. We predict that over 90% of the bound complexes are the *nonreactive* forms.

Summary

We have examined several systems chosen to illustrate the current role of theory and simulation in biomimetics and biocatalysis. It should be clear that the theory is not done in a vacuum (so to speak) but rather that the theory becomes interesting only for systems amenable to experimental analysis. However, the examples illustrate how the theory can provide new insights and deeper understanding of the experiments. As experience with such simulations accumulates and as predictions are made on more and more complex systems amenable to experiment, it will become increasingly feasible to use the theory on unknown systems. As the predictions on such unknown systems are tested with experiment and as the reliability of the predictions increases, these techniques will become true design tools for development of new biological systems.

Acknowledgments

This work was funded by a grant from the Department of Energy, Energy Conversion and Utilization Technologies. The DOE-ECUT program funded this work with the hope that development of simulation techniques would eventually have an impact on development of new, industrially useful processes for biotechnology and biocatalysis. We especially wish to acknowledge the foresight of Drs. Jim Eberhardt, Minoo Dastoor, and Jovan Moacanin in encouraging these efforts. The equipment used was also funded by the ONR/DARPA (Contract No. N00014-86-K-0735) and by a grant from the Division of Materials Research, Materials Research Groups, of the National Science Foundation (Grant No. DMR84-21119). We thank Professor Stephen J. Benkovic of the Pennsylvania State University and Dr. Donald A. Tomalia of The Dow Chemical Company for numerous helpful discussions and for materials in advance of publication.

Literature Cited

1. Cytochrome P - 450: Structure, Mechanism, and Biochemistry; Ortiz de Montecellano, P. R., Ed.; Plenum Press: New York, 1986.
2. Tomalia, D. A.; Baker, H.; Dewald, J.; Hall, M.; Kallas, G.; Martin, S.; Roeck, J.; Ryder, J.; Smith, P. Macromolecules 1986, **19**, 2466-2468.
3. Naylor, A. M.; Goddard III, W. A. Polymer Preprints 1988, **29**, 215-216.
4. Tomalia, D. A.; Hall, M.; Hedstrand, D. M. J. Am. Chem. Soc. 1987, **109**, 1601-1603.
5. Richards, F. Ann. Rev. Biophys. Bioeng. 1977, **6**, 151-176.
6. Keabian, J. W.; Agui, T.; van Oene, J. C.; Shigematsu, K.; Saavedra, J. M. Trends in Pharmacological Sciences 1986, **96-99**.
7. Greedy, J. E. Adv. Pharmacol. Chemother. 1980, **17**, 37-102.

8. Matthews, D. A.; Alden, R. A.; Bolin, J. T.; Filman, D. J.; Freer, S. T.; Hamlin, R.; Hol, W. T. J.; Kisliuk, R. L.; Pastore, E. J.; Plante, L. T.; Xuong, N.; Kraut, J. J. Biol. Chem. 1978, **253**, 6946-6954.
9. Bolin, J. T.; Filman, D. J.; Matthews, D. A.; Hamlin, R. C.; Kraut, J. J. Biol. Chem. 1982, **257**, 13650-13662.
10. Filman, D. J.; Bolin, J. T.; Matthews, D. A.; Kraut, J. J. Biol. Chem. 1982, **257**, 13663-13672.
11. Stone, S. R.; Morrison, J. F. Biochemistry 1984, **23**, 2753-2758.
12. Fierke, C. A.; Johnson, K. A.; Benkovic, S. J. Biochemistry 1987, **26**, 4085-4092.
13. Villafranca, J. E.; Howell, E. E.; Voet, D. H.; Strobel, M. S.; Ogden, R. C.; Abelson, J. N.; Kraut, J. Science 1983, **222**, 782-788.
14. Chen, J.-T.; Mayer, R. J.; Fierke, C. A.; Benkovic, S. J. J. Cellular Biochem. 1985, **29**, 73-82.
15. Howell, E. E.; Villafranca, J. E.; Warren, M. S.; Oatley, S. J.; Kraut, J. Science 1986, **231**, 1123-1128.
16. Taira, K.; Chen, J.-T.; Fierke, C. A.; Benkovic, S. J. Bull. Chem. Soc. Jpn. 1987, **60**, 3025-3030.
17. Mayer, R. J.; Chen, J.-T.; Taira, K.; Fierke, C. A.; Benkovic, S. J. Proc. Natl. Acad. Sci. U.S.A. 1986, **83**, 7718-7720.
18. Weiner, S. J.; Kollman, P. A.; Case, D. A.; Singh, U. C.; Ghio, C.; Alagona, G.; Profeta, Jr., S.; Weiner, P. J. Am. Chem. Soc. 1984, **106**, 765-784.
19. Benkovic, S. J.; Fierke, C. A.; Naylor, A. M. Science 1988, **239**, 1105-1110.
20. Charlton, P. A.; Young, D. W.; Birdsall, B.; Feeney, J.; Roberts, G. C. K. J. Chem. Soc., Chem. Commun. 1979, 922-924.
21. Cocco, L.; Temple, Jr., C.; Montgomery, J. A.; London, R. E.; Blakley, R. L. Biochem. Biophys. Res. Commun. 1981, **100**, 413-419.
22. Wu, Y.-D.; Houk, K.N. J. Am. Chem. Soc. 1987, **109**, 2226-2227.

RECEIVED November 4, 1988

Chapter 7

Enzymatic Reactions in Reversed Micelles at Low Solubilized Water Concentrations

J. W. Shield, H. D. Ferguson, K. K. Gleason, and T. A. Hatton

Department of Chemical Engineering, Massachusetts Institute of Technology, Cambridge, MA 02139

α -Chymotrypsin has been used as a model enzyme to investigate dipeptide synthesis, hydrolysis kinetics, and substrate localization, in reversed micelles composed of cationic surfactants. Synthesis of the dipeptide *N*-benzoxycarbonyl-L-tyrosine glycylamide has been demonstrated with a non-optimized yield of 75%. Hydrolysis of a synthetic substrate, *N*-glutaryl-L-phenylalanine *p*-nitroanilide, is greatly enhanced in reversed micelles versus in aqueous solution, and does not demonstrate typical enzyme saturation kinetics. Reaction kinetics of a similar substrate, *N*-benzoyl-L-tyrosine *p*-nitroanilide, are not enhanced and do show enzyme saturation behavior. NMR free induction decay and spin-lattice relaxation measurements suggest that these differences are a result of different interactions of the substrates with the surfactant interface.

There are many potential advantages associated with conducting enzyme-catalyzed reactions in organic solvents, as opposed to traditional aqueous reaction media (1-2). A major benefit is the greater solubility and consequently higher concentrations some reactants and products have in an organic solvent. Secondly, the reaction equilibria for enzymatic reactions involving water can be manipulated to favor product synthesis in the low water environment of an organic solution; the low water environment also minimizes undesired hydrolysis side reactions. When substrate or product inhibition is a significant limitation, organic solvents can be used to partition the inhibiting molecule away from the enzyme. Furthermore, substrate specificity of enzymes can be different in organic solutions and can potentially be controlled by the choice of solvents.

Reversed micelles represent one technique of utilizing enzymes in organic solvents (3-5). Reversed micelles are thermodynamically stable, spherical, nanometer scale aggregates of amphiphilic

0097-6156/89/0392-0090\$06.00/0

© 1989 American Chemical Society

molecules solubilizing aqueous droplets in an organic solvent continuum. The hydrophilic head groups of the surfactant molecules surround the aqueous droplet or "water pool", while the hydrophobic surfactant tails protrude into the organic medium enveloping the micelle (Figure 1). Enzymes can be solubilized within the reversed micelle with retention of their catalytic activity. The parameter ω_0 , defined as the ratio of the water concentration to the surfactant concentration, is an indication of the size of the reversed micelles.

This paper has two primary objectives. The first is to report on the use of an enzyme-containing reversed micellar medium for organic synthesis: specifically the formation of a model dipeptide. The feasibility of peptide synthesis in reversed micelles has been previously demonstrated (6). Small peptides are used in a variety of applications, such as artificial sweeteners, pesticides and pharmaceuticals. Since peptide bonds between an aromatic amino acid and a hydrophilic amino acid are of considerable interest (for instance in peptide analgesics), the synthesis of a tyrosine-glycine dipeptide was chosen for the model reaction.

The second objective is to examine the influence of reversed micellar solution parameters, including the interaction of substrates with the surfactant interface, on observed initial rate kinetics. This is of interest because a number of reports have indicated that enzymes in reversed micellar solutions exhibit an enhanced reactivity, or "super-activity" (7-9). As a model system, the hydrolysis reactions of synthetic substrates of α -chymotrypsin were studied in a reversed micellar solution. Nuclear magnetic resonance was used to examine the interactions between these substrates and the micellar environment.

Experimental

Materials. *N*-benzoxycarbonyl-L-tyrosine glycinamide (Z-Tyr-Gly-NH₂) and *N*-benzoxycarbonyl-L-tyrosine hexyl ester (Z-Tyr-OHx) were purchased from Bachem, Switzerland. *N*-benzoxycarbonyl-L-tyrosine methyl ester (Z-Tyr-OMe) was purchased from Chemical Dynamics, S. Plainfield, NJ. Glycinamide (Gly-NH₂), *N*-glutaryl-L-phenylalanine *p*-nitroanilide (GPANA) and *N*-benzoyl-L-tyrosine *p*-nitroanilide (BTPNA), bovine pancreatic α -chymotrypsin, and enzyme grade tris buffer were all obtained from Sigma, St. Louis, MO. Dodecyltrimethyl ammonium bromide (DTAB), also from Sigma, was recrystallized from diethyl ether and methanol. *n*-Hexanol and cetyltrimethyl ammonium bromide (CTAB) were from Fluka, Switzerland. *n*-Octane was from Aldrich, Milwaukee, WI. Analytical grade chloroform and *n*-heptane were from Mallinckrodt, Paris, KY and analytical grade methanol was from J.T. Baker, Phillipsburg, NJ. Deionized water was used throughout. Deuterated water, methanol, chloroform and octane from Aldrich were used as solvents in the NMR work.

Methods. Z-Tyr-Gly-NH₂ was synthesized from Z-Tyr-OMe and Gly-NH₂ in reversed micellar solutions containing 0.15 M DTAB as the surfactant in a 1:5 volume mixture of *n*-hexanol and *n*-octane. Hexanol acts as a cosurfactant and aids in solubilizing the Z-Tyr-OMe. Initial rate kinetic studies employed the hydrolysis of the synthetic substrates GPANA and BTPNA in reversed micelles of CTAB in a

1:1 volume mixture of chloroform and n-heptane. Owing to the limited commercial availability of deuterated n-heptane, deuterated n-octane was substituted in the NMR work. A control experiment showed that there was no effect on the observed reaction kinetics due to this substitution in the bulk organic continuum. Reversed micellar solutions were made by slow addition of 0.2 M tris pH=9.0 aqueous buffer to a dispersion of the CTAB surfactant in the organic solvent. Substrate solutions were made by adding the substrate directly to the reversed micellar solutions.

α -Chymotrypsin dissolved in 0.2 M tris buffer, pH=9.0, was injected into the substrate-containing reversed micellar organic solution to initiate the above reactions. Enzyme solutions were prepared fresh, stored on ice and used within four hours of preparation. Gentle agitation after addition of the aqueous α -chymotrypsin solution would produce an optically-transparent solution. For the dipeptide synthesis, 0.2 ml aliquots of the reaction mixture were periodically removed and the reaction stopped by the addition of 2 ml of methanol. Analysis was conducted on a Perkin-Elmer Series 4 HPLC using a C-18 column (Serva, Westbury, NY) and a gradient 0.1 M acetic acid/methanol elution scheme. Commercially available Z-Tyr-Gly-NH₂ and Z-Tyr-OHx were used as standards.

Initial reaction rates were discerned spectrophotometrically at 410 nm by measuring the evolution of the chromophoric *p*-nitroaniline on a recording Perkin Elmer Lambda 3B spectrophotometer. Extinction coefficients were determined for every surfactant concentration and ω_0 ; they varied from 4000 to 6000 ABS-M⁻¹-cm⁻¹. Reaction mixtures and the spectrophotometer cell holder were maintained at 25°C.

Proton chemical shift values were obtained on a homebuilt 500 MHz nuclear magnetic spectrometer at a resolution of 0.003 ppm; spin-lattice relaxation times (T₁'s) were determined using 1 to 4 repetitions of the standard inversion recovery 180°- τ -90° pulse sequence for eight τ values between 0.1 and 8 seconds. The T₁ values ranged from 2 to 5 seconds with a standard deviation of ± 0.06 seconds. A delay of 30 seconds was used between repetitions to ensure that the protons had returned to equilibrium. To remove paramagnetic oxygen, samples were degassed by freezing, evacuating the head space and thawing for three cycles.

Owing to the limited aqueous solubility of GPANA and BTPNA, it was necessary to use water-miscible organic solvents to increase the substrate solubility in these solutions. For the initial reaction rate studies, GPANA was dissolved in 10% by volume methanol and BTPNA was dissolved in 20% by volume acetone. For the NMR studies, GPANA was dissolved in 10% by volume deuterated methanol and BTPNA was dissolved in 60% by volume deuterated methanol.

Results and Discussion

Dipeptide Formation. Figure 2 presents the time course of the dipeptide formation reaction. The limiting reactant, Z-Tyr-OMe, is depleted rapidly, being converted via nucleophilic attack of the glycinamide to the desired dipeptide product, Z-Tyr-Gly-NH₂; via trans-esterification to a transient intermediate, Z-Tyr-OHx; and via hydrolysis to the undesired side product Z-Tyr-OH. Dipeptide yield, based on the more expensive amino acid substrate, Z-Tyr-OMe, is 75% after 30 minutes using an enzyme concentration of 1 μ M. Both the

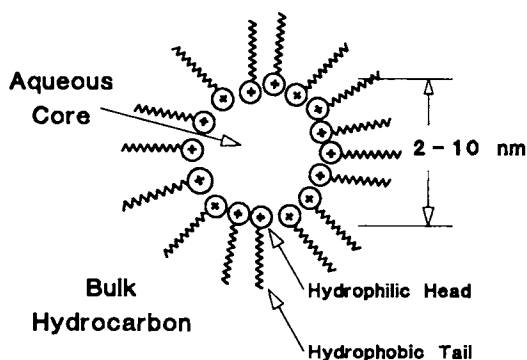


Figure 1. Schematic representation of a CTAB reversed micelle.

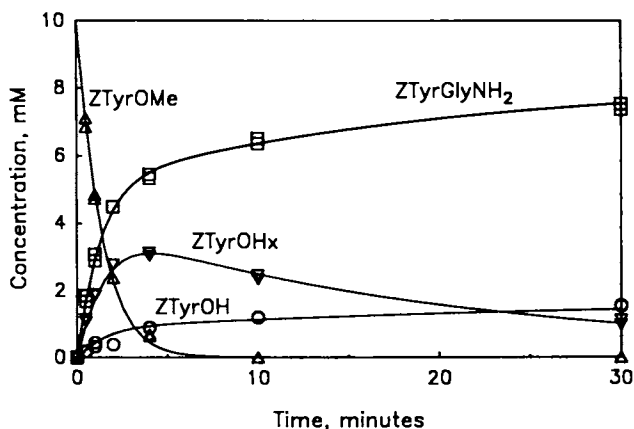


Figure 2. Time course of the dipeptide synthesis of Z-Tyr-Gly-NH₂. Initial concentrations were [Z-Tyr-OMe] = 10 mM, [Gly-NH₂] = 15mM. [DTAB] = 0.15 M in 1:5 n-hexanol and n-octane. $\omega_0 = 6.5$

yield and productivity obtained are comparable to similar reactions in other media (10).

Dipeptide formation in the reversed micellar medium is influenced by the localization and concentration of the various species in the reaction medium (Figure 3). α -Chymotrypsin is a hydrophilic protein and resides within the water pool of the reversed micelle. Glycinamide is a polar molecule and as such partitions into the reversed micellar water pools. Consequently, in the immediate environment of the enzyme, there is a locally high glycinamide concentration (ca. 0.8 M), accelerating the rate of dipeptide formation. The dipeptide product that is formed is hydrophobic and will partition away from the water pool, isolating it from back reaction and thus forcing the equilibrium towards synthesis.

The well-characterized mechanism of α -chymotrypsin-catalyzed hydrolysis of esters can be expanded to encompass transesterification and peptide bond synthesis. Such a kinetic model has been developed using the reaction scheme outlined in Figure 4. The highly reactive methyl ester substrate, Z-Tyr-OMe, is assumed to degrade irreversibly, while the desired dipeptide product and the acid byproduct form irreversibly. The third product, Z-Tyr-OHx, is a transient intermediate; thus the model provides for both its formation and subsequent degradation to either the dipeptide product or the free acid. Both esters are assumed to be in equilibrium with their Michaelis complexes, Z-Tyr-OMe-enzyme and Z-Tyr-OHx-enzyme, respectively. Best fit kinetic constants were found and are used to generate the concentration profiles shown in Figure 2. These kinetic constants qualitatively and often quantitatively describe the time course of the reaction conducted under a variety of other reaction conditions, including different hexanol, glycinamide, enzyme, and water concentrations (Ferguson, H. D., unpublished data.).

Kinetics of Model Substrates. In an effort to better understand enzymatic kinetics within reversed micelles, α -chymotrypsin hydrolysis of a model substrate, GPANA, was studied in CTAB reversed micelles. The hydrolysis kinetics of substrates by α -chymotrypsin is described by the Michaelis-Menten formulation

$$\text{rate} = \frac{d[P]}{dt} = \frac{k_{\text{cat}}[E][S]}{K_M + [S]} \quad (1)$$

In a reversed micellar system containing solubilized enzyme molecules, it is assumed that catalytically active enzyme molecules are only found within the reversed micelles. Furthermore there is no more than one enzyme molecule per reversed micelle, since the enzyme concentration is sufficiently small compared to the concentration of reversed micelles.

When considering enzyme kinetics in a reversed micellar system it is critical to recognize that there are two volumes upon which to base concentration dependent constants and variables, the total or observed reaction volume and the micellar or aqueous water pool volume (11). Additionally, the partitioning of the substrate between the bulk organic solvent mixture and the reversed micelles

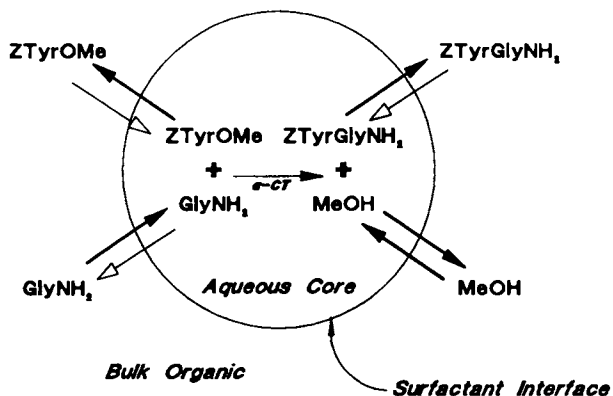


Figure 3. Schematic representation of the partitioning of reactants and products in Z-Tyr-Gly-NH₂ synthesis within reversed micelles. Filled arrows indicate direction of preferential partitioning.

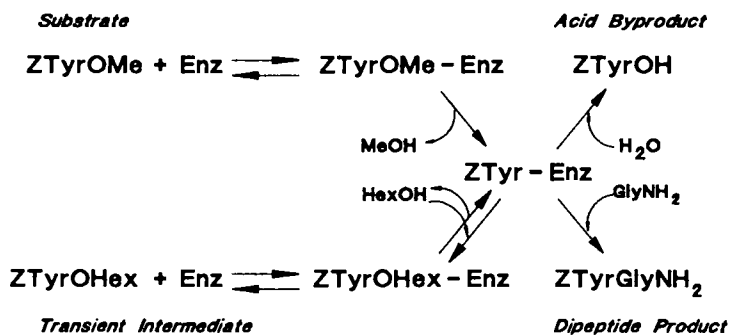


Figure 4. Reaction mechanism for Z-Tyr-Gly-NH₂ synthesis in DTAB, n-octane/n-hexanol reversed micelles.

is important. It can be characterized by a partition coefficient, P_S , defined as

$$P_S = \frac{[S]_{\text{micelles}}}{[S]_{\text{bulk organic}}} \quad (2)$$

If the substrate is preferentially soluble in the reversed micelles ($P_S \gg 1$), a comparison of the kinetic parameters observed for the overall system and the kinetic parameters intrinsic to the reversed micellar reaction medium gives

$$k_{\text{cat,observed}} = k_{\text{cat,micelle}} \quad (3)$$

and

$$K_{M,\text{observed}} = \phi \cdot K_{M,\text{micelle}} \quad (4)$$

where ϕ is the micelle volume fraction, and is directly proportional to both the micelle size and to the number of micelles. The parameter ω_0 is an indication of the micelle size, while the overall surfactant concentration is indicative of the number of micelles. Therefore, ϕ can be represented as

$$\phi = \text{Constant} \cdot \omega_0 \cdot [\text{Surfactant}] \quad (5)$$

The K_M dependence on ϕ has been shown for trypsin and *N*-benzoyl-D,L-arginine *p*-nitroanilide, but only when ω_0 was held constant (12).

The rate of α -chymotrypsin-catalyzed hydrolysis as a function of overall GPANA concentration in CTAB reversed micelles and in aqueous solution are shown in Figure 5. It is apparent that the reaction rate in the reversed micellar solution is on the order of 50 times more rapid than in the aqueous system. Furthermore, in the reversed micellar system there is no indication of enzyme saturation as the reaction is first order in substrate concentration. As enzyme saturation kinetics are not observed, it is impossible to differentiate between the parameters k_{cat} and K_M . Instead a second order bimolecular rate constant for both the micelle interior (k_{micelle}) and for what is experimentally observed (k_{observed}) is defined.

$$k_{\text{micelle}} = \frac{k_{\text{cat,micelle}}}{K_{M,\text{micelle}}} \quad \text{and} \quad k_{\text{observed}} = \frac{k_{\text{cat,observed}}}{K_{M,\text{observed}}} \quad (6)$$

In the case where $P_S \gg 1$, or the substrate is associated with the micelles not with the bulk organic solvent, Equations 3 and 4 become

$$k_{\text{observed}} = \frac{1}{\phi} \cdot k_{\text{micelle}} \quad (7)$$

Thus, if the intrinsic constant, k_{micelle} , is independent of the volume fraction of micelles, ϕ , k_{observed} should be a linear function of $1/\phi$. Table I gives maximum solubility data for GPANA and BTPNA indicating that these substrates are associated with the

reversed micelles and, consequently, should obey Equation 7. Results for GPANA in which ϕ was varied by changing the surfactant concentration, holding ω_0 constant, show that this is indeed the case (Figure 6). The increase in the rate constant observed with decreasing ϕ is due to the reversed micelles ability to concentrate the hydrophilic substrate within the reversed micelles. However, when ϕ is varied by changing ω_0 , holding the surfactant concentration constant, k_{observed} is no longer proportional to $1/\phi$, but instead increases beyond what is predicted as ω_0 is decreased (Figure 6). Therefore, other phenomenon, in addition to the concentration of substrate within the reversed micelles, must account for this rate enhancement at low ω_0 .

A second synthetic substrate, BTPNA, was investigated to clarify if this rate enhancement in CTAB reversed micelles is observed for all substrates (Figure 7). Two major differences are observed: first, that there is no reaction rate enhancement in reversed micelles versus an aqueous based system, and second, that saturation kinetics are observed.

The observation that different substrates behave differently, and that there is an dependence on ω_0 beyond that of ϕ , present the possibility that the specific localization of the substrate within the reversed micelle plays a role in determining the kinetics.

Table I. Maximum solubility of substrates

Solution	GPANA	BTPNA
Aqueous	$< 1 \times 10^{-3}$ M	$< 1 \times 10^{-3}$ M
1:1 chloroform/heptane	2×10^{-5} M	$< 2 \times 10^{-5}$ M
Reversed micellar		
0.1 M CTAB	2.5×10^{-3} M	8×10^{-3} M
$\omega_0 = 3$		

Substrate Localization. To determine how the substrate molecules are associated with the surfactant interface layer, chemical shifts and spin-lattice relaxation rates for substrate molecule protons in reversed micellar and in aqueous solutions were measured. Both substrate molecules, GPANA and BTPNA, have three subunits: the phenylalanine or tyrosine aromatic ring, the *p*-nitro anilide, and the acyl group. Because each subunit has non-overlapping NMR spectral assignments, and assuming proton-proton dipolar coupling between the subunits is weak due to motional averaging, the spin-lattice relaxation behavior of protons on each of the three subunits can be considered separately. In fact, the relaxation rate, R , ($R=1/T_1$) for GPANA protons in aqueous solution varies from 0.29 to 1.39 s^{-1} , supporting this assumption. In addition, the *p*-nitro anilide protons of both GPANA and BTPNA in aqueous solution have $R=0.30 \pm 0.05 \text{ s}^{-1}$, demonstrating little change upon chemical substitution of the other two subunits. A faster spin-lattice relaxation rate of a given proton is indicative of increased rotational and translational motions occurring at the NMR frequency (500 MHz). Such an increase results when higher frequency motions are re-

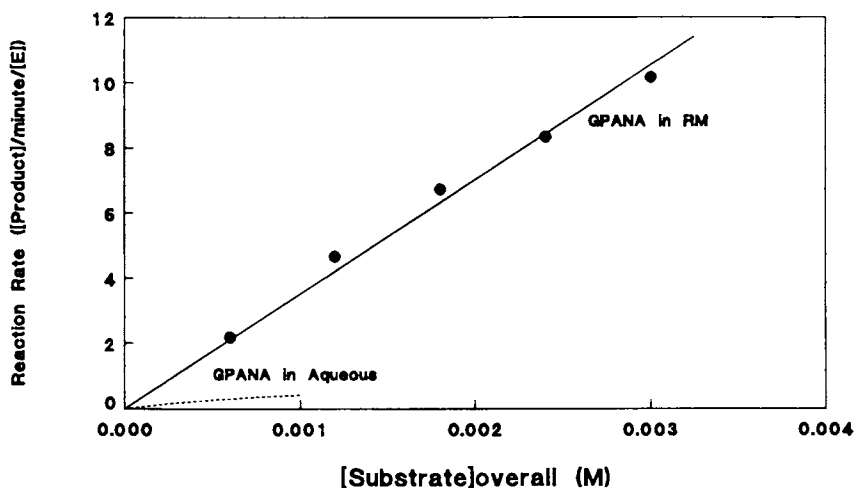


Figure 5. Comparison of GPANA hydrolysis rates in aqueous solution and CTAB reversed micelles. $[\text{CTAB}] = 0.1 \text{ M}$ $\omega_0 = 3$

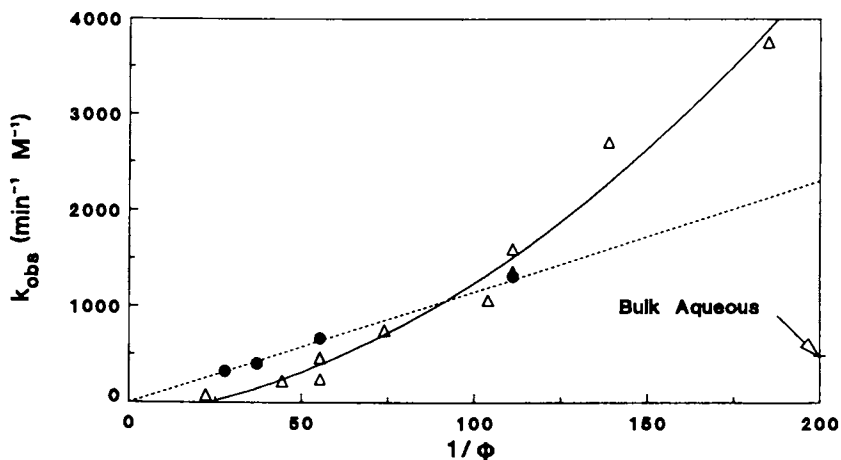


Figure 6. Second order bimolecular rate constant for the hydrolysis of GPANA by α -chymotrypsin in CTAB reversed micelles as a function of $1/\phi$. ϕ = volume fraction of reversed micelles.
 (●) $\omega_0 = 3$, $[\text{CTAB}] = .1, .2, .3, .4 \text{ M}$
 (Δ) $[\text{CTAB}] = .1 \text{ M}$, $w_0 = 3, 4, 5, 5.4, 7, 10, 12, 25$

stricted or new modes of low frequency motions are introduced. Restricted motion is the more probable effect in reversed micelles since the dimensions of the aqueous pool and the substrate are comparable and the largest increase in R occurs at the smallest ω_0 . Also, since R changes differently for the various subunits, the concerted motion of the micelles is not the dominant effect.

The chemical shifts (δ s) of substrate protons are different in reversed micellar media compared to aqueous solution. The chemical shift is a complex function of the environment around a proton, influenced by the solvent type, external electrostatic forces and the internal electronic structure of the molecule. A change in the chemical shift for substrate protons between an aqueous and reversed micellar solution is an indication of a change in the local electronic environment.

Table II details the changes in the chemical shift for protons on the three subunits of the substrate molecules for two different micelle sizes. The proton numbers refer to the identifications made in Figure 8. Table III shows the ratio of relaxation rates in reversed micelles to the relaxation rates in an aqueous system. These values have a standard deviation of ± 0.05 units.

The protons on GPANA associated with the phenylalanine benzene ring (numbers 1 and 2) and those on BTPNA associated with the acyl group (numbers 5, and 6) have little or no change in their available motions in a reversed micellar environment versus in aqueous solution. Furthermore, these protons undergo small changes in their chemical shifts, indicating a minimal alteration in their local electronic environment. Thus the reversed micellar environment of these protons is similar to an aqueous environment, suggesting that these two subunits are in the water pool of the micelle.

In contrast, those protons on the other subunits of the substrate molecules do experience hinderance in the reversed micelles and undergo significant changes in their electronic environment. The *p*-nitro anilide protons (numbers 3 and 4) on both substrates have increased relaxation rates and proton 4 undergoes a large downfield chemical shift. Similar effects are seen in the GPANA protons associated with the acyl group composed of the glutaric acid (numbers 5 and 6) and in the BTPNA protons located near the hydroxyl on the tyrosine benzene ring (numbers 1 and 2).

Table II. Differences in Chemical Shifts
 $\delta_{\text{Reversed Micelles}} - \delta_{\text{Aqueous}}$

Substrate Subunit	Proton Number	GPANA		BTPNA	
		$\delta_{\omega_0=5} - \delta_{\text{Aq}}$	$\delta_{\omega_0=10} - \delta_{\text{Aq}}$	$\delta_{\omega_0=5} - \delta_{\text{Aq}}$	$\delta_{\omega_0=10} - \delta_{\text{Aq}}$
amino acid	1	0.061	0.067	0.271	0.254
side group	2	0.273	0.252	0.242	0.222
<i>p</i> -nitro anilide	3	0.172	0.169	0.125	0.125
	4	0.650	0.630	0.484	0.464
acyl group	5	0.285	0.273	0.048	0.086
	6	0.428	0.298	-0.021	-0.027

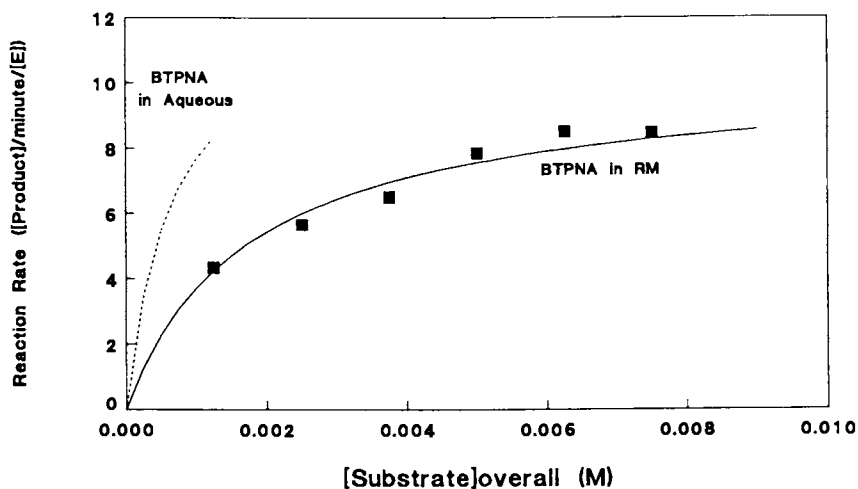


Figure 7. Comparison of BTPNA hydrolysis rates in aqueous solution and CTAB reversed micelles. [CTAB] = 0.1 M $\omega_0=3$

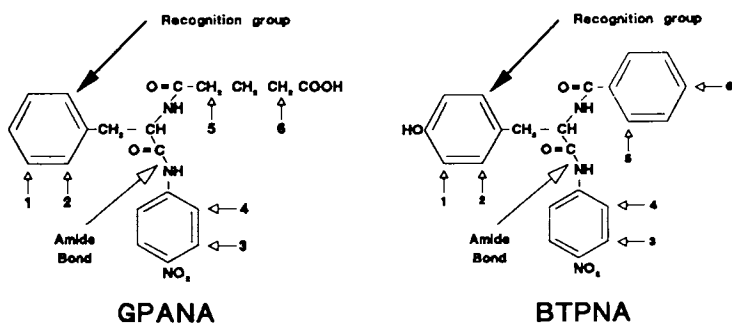


Figure 8. Synthetic substrates GPANA and BTPNA. Open arrows indicate amide bond hydrolyzed by α -chymotrypsin. Solid arrows indicate hydrophobic recognition groups. Numbers refer to protons examined by NMR.

Table III. Ratios of Relaxation Rates

Substrate Subunit	Proton Number	GPANA		BTPNA	
		$\frac{R_{\omega_0=5}}{R_{Aq}}$	$\frac{R_{\omega_0=10}}{R_{Aq}}$	$\frac{R_{\omega_0=5}}{R_{Aq}}$	$\frac{R_{\omega_0=10}}{R_{Aq}}$
amino acid	1	1.04	1.00	2.14	1.83
side group	2	1.10	1.08	1.66	1.59
p-nitro	3	1.48	1.38	1.48	1.60
anilide	4	1.49	1.37	1.46	1.43
acyl	5	1.47	1.47	1.18	1.15
group	6	1.61	1.56	1.13	0.99

Consequently, these four subunits may be associated with the positively charged surfactant layer hindering their motion and inducing a downfield chemical shift. These substrate moieties could interact with the positively charged head groups of the surfactant, because the carboxylic acid carries a negative charge, the oxygens of the nitro group carry a fractional negative charge and the hydroxyl group is polar (Figure 9).

The configuration of the substrate within the reversed micelle may have significant implications for enzyme kinetics. In nature, α -chymotrypsin only hydrolyzes the peptide bond of polypeptides on the carboxylic acid end of aromatic amino acid residues. This selectivity arises because the aromatic portion of the amino acid fits into a recognition site next to the reactive site on the enzyme. The comparable amide bond on the synthetic substrates is noted with the open arrow in Figure 8. The aromatic ring that fits into the recognition site for GPANA and BTPNA comes from the amino acid side group in phenylalanine and tyrosine and are noted with solid arrows in Figure 8.

Can the localization of the substrate molecule within the reversed micellar environment explain why there are differences in reaction rate enhancement for different substrates? For the substrate GPANA there is a significant rate enhancement, more so than would be expected from a simple kinetic treatment due to concentration of the substrates in the reversed micelles. A similar substrate, BTPNA, does not show a rate enhancement; instead, the observed rate in reversed micelles is less than in an aqueous solution. For GPANA, the molecule interacts with the surfactant layer, in a manner exposing the recognition moiety and the amide bond to the center of the micelle, where the bond can be more easily recognized and hydrolyzed by the enzyme catalyst. For BTPNA, the recognition portion of the molecule interacts with the surfactant layer making it more difficult for the enzyme to hydrolyze the amide bond. It appears that the positioning and localization of substrate molecules within the reversed micelle has a profound effect on reaction rates. Further understanding of the factors influencing these effects would facilitate the design of enzyme-containing

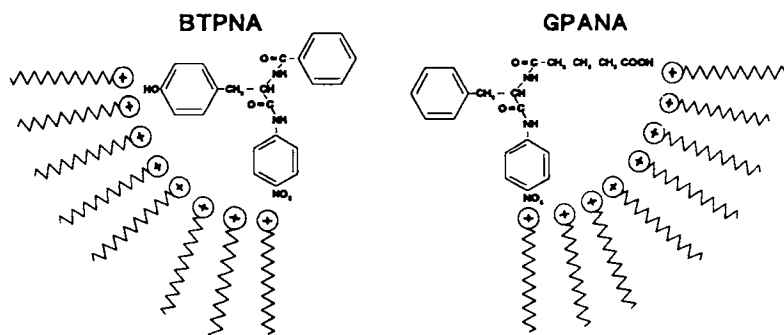


Figure 9. Schematic representation of interaction between GPANA and BTPNA with surfactant head groups within cationic reversed micelles.

reversed micellar systems having the optimal selectivity and productivity for the reaction of interest.

Conclusions

Reversed micellar systems have certain attributes which can be exploited when considering enzymatically-based synthesis reactions. These systems can solubilize hydrophilic and hydrophobic reactants and, if the reactants interact with the surfactant layer, higher concentrations can be obtained than is possible in either an aqueous or an organic environment. Partitioning of reactants between the bulk organic portion of a reversed micellar solution and the micellar core can result in localized high concentrations of polar reactants. This can be used to promote desired reactions, such as the synthesis of dipeptides.

Observed reaction kinetics for some enzyme substrate systems solubilized within a reversed micellar solution are enhanced relative to those observed in aqueous solution. This enhancement can be due to simple concentration of the reactants within the micelles, but can also be influenced by the localization and orientation of the substrates being used.

Acknowledgments

The high field NMR experiments were performed at the NMR Facility for Biomolecular Research located at the F. Bitter National Magnet Laboratory, M.I.T. The NMR Facility is supported by Grant No. RR00995 from the Division of Research Resources of the NIH and by the National Science Foundation under Contract No. C-670.

This work was supported by Dow Chemical, an NSF Graduate Fellowship to H.D.F., and an NSF Presidential Young Investigator Award to T.A.H.

Literature Cited

1. Martinek, K.; Semenov, A. N. Russ Chem Rev 1981, **50**, 718-734
2. Klibanov, A. M. Chemtech, June 1986, 354-359
3. Martinek, K.; Levashov, A. V.; Klyachko, N.; Khmel'nitski, Y. L.; Berezin, I. V. Eur. J. Biochem. 1986, **155**, 453-468
4. Shield, J. W.; Ferguson, H. D.; Bommarius, A. S.; Hatton, T. A. I&EC Fund. 1986, **25**, 603-612
5. Luisi, P. L.; Giomini, M.; Pileni, M. P.; Robinson, B. H. Biochim et Biophys Acta 1988, **947**, 209-246
6. Lüthi, P.; Luisi, P. L. JACS 1984, **106**, 7285-7286
7. Martinek, K.; Levashov, A. V.; Khmel'nitsky, Yu. L.; Klyachko, N. L.; Berezin, I. V. Science 1982, **218**, 889-891
8. Barbaric, S.; Luisi, P. L. JACS 1981, **103**, 4239-44
9. Fletcher, P. D. I.; Rees, G. D.; Robinson, B. H.; Freedman, R. B. Biochim et Biophys Acta 1985, **832**, 204-214
10. Morihara, K.; Tatsushi, O. Biochem J. 1977, **163**, 531-542
11. Bonner, F. J.; Wolf, R.; Luisi, P. L. J. Solid-Phase Biochem 1980, **5**, 255-268
12. Martinek, K.; Levashov, A. V.; Klyachko, N. L.; Pantin, V. I.; Berezin, I. V. Biochim et Biophys Acta 1981, **657**, 277-294

RECEIVED November 4, 1988

Chapter 8

Enzyme Structure and Function in Water-Restricted Environments

Electron Paramagnetic Resonance Studies in Organic Solvents and Reverse Micelles

Douglas S. Clark, Louise Creagh, Paul Skerker,
Mark Guinn, John Prausnitz, and Harvey Blanch

Department of Chemical Engineering, University of California,
Berkeley, CA 94720

Structure-function relationships were investigated for two water-restricted enzyme systems: immobilized horse liver alcohol dehydrogenase (LADH) in organic solvents containing varying amounts of water, and tryptophanase in reverse micelles of different water contents. Electron paramagnetic resonance (EPR) spectroscopy and spin-labelling techniques were used to probe the effects of low water content on enzyme structure. The oxidation of cinnamyl alcohol to cinnamaldehyde using LADH was studied in various organic solvents. The activity of the enzyme increased dramatically as small amounts of water were added to each solvent; however, the increase in activity could not be attributed to a loosening up of the active-site conformation. Tryptophan was produced from indole and serine using tryptophanase in reverse micelles. The enzyme became less flexible and the water became more rigid as reverse micelle size decreased.

Recent research has demonstrated that enzymes can function in various low-water environments (1-4), and that the properties of enzymes can be favorably modified by nonaqueous solvents (5-7). Increased substrate solubility, reversal of hydrolytic reactions, and improved thermostability are among the practical advantages afforded by nonaqueous solvents. However, the role of water in enzymatic reactions at low water concentrations is not generally understood, and there is some uncertainty regarding how much the conformation of a protein changes as solvent water is removed (8,9). Nonaqueous solvent systems therefore represent important media in which to examine enzyme structure and function at the molecular level. Such studies will prove valuable for the application of enzymes in low-

0097-6156/89/0392-0104\$06.00/0

• 1989 American Chemical Society

water environments and should also provide fundamental insights into enzymatic reaction mechanisms and structure-function relationships.

This paper describes preliminary results from studies of two water-restricted enzyme systems: immobilized horse liver alcohol dehydrogenase (LADH) in organic solvents containing various amounts of water, and tryptophanase in reverse micelles of different water contents. In each case, electron paramagnetic resonance (EPR) spectroscopy and spin labelling techniques were used to probe the effects of low water concentrations on enzyme structure. Advantages of EPR and spin labelling include their versatility (a wide range of spin labels can be purchased or synthesized and EPR spectroscopy can easily be applied to multiphase samples) and sensitivity to changes in the microstructure and internal dynamics of proteins. Moreover, the motion of spin labels can be quantified with the aid of computer simulations (10,11).

Immobilized LADH in Organic Solvents

Methods. LADH (Sigma Chemical Co.) was immobilized to controlled-pore aminopropyl glass (Sigma, 75-100 Å nominal pore size) activated with glutaraldehyde at pH 7.5. The activated glass (750 mg) was rotated end over end in 30 ml of enzyme solution (25 mg LADH, 5 mg NAD⁺ in 0.01 M phosphate buffer, pH 7.5) at room temperature for 3 hr. The immobilized enzyme was then washed with 500 ml of the phosphate buffer, and lyophilized from 5 ml of buffer containing 3 mg NAD⁺. Immobilized LADH was assayed at room temperature in a variety of organic solvents containing 10 mM cinnamyl alcohol and 10 mM octanal (all organic solvents were dried initially over molecular sieves). Vials containing 10 mg of the immobilized enzyme in 4 ml of the reaction mixture were rotated at 60 rev/min, and 0.2 ml samples were withdrawn periodically. The samples were analyzed by HPLC (Hewlett Packard model HP-1090) and the formation of cinnamaldehyde was monitored at 300 nm. The thermal stability of immobilized enzyme in different solvents was determined by measuring the activity remaining after incubation in the solvent for 30 min at 80°C.

For EPR measurements, LADH was spin labeled with 4-(2-Iodoacetamido)-TEMPO (abbreviated as SL-1 and obtained from Aldrich Chemical Co.) prior to immobilization as described in reference 12. All spectra were collected at room temperature on a Bruker ER200D-SRC EPR spectrometer using a microwave power of 15.9 mW, a modulation amplitude of 1.0 G, and a scan range of 100 G.

Results and Discussion. To examine the behavior of LADH in different organic solvents containing various amounts of water, the oxidation of cinnamyl alcohol to cinnamaldehyde was studied (cinnamyl alcohol oxidation by LADH in organic solvents was first reported by Deetz and Rozzell (13)). Reaction rates were measured in nearly anhydrous organic solvents and in solvents containing from 0.1 to 10% added water. The water content in the nearly anhydrous solvents ranged from 0.01 to 0.02%, as measured by Karl-Fischer titration. All rate data were obtained with enzyme immobilized to controlled pore glass and lyophilized from aqueous phosphate buffer of pH 7.5. Immobilized

enzyme was used to prevent aggregation of the enzyme in the organics, which could lower the concentration of active enzyme and/or increase the likelihood of mass transfer limitations influencing the measured reaction rates.

The enzyme's activity in several nearly anhydrous solvents increased from total absence in acetonitrile to a maximum of 11 nmols (min-g support)⁻¹ in hexane, and in general the activity increased as the water solubility in the solvent decreased. This trend is believed to result from more extensive stripping of the essential hydration layer from the enzyme molecule by a more hydrophilic solvent like acetonitrile than by a less hydrophilic solvent like hexane (1). Furthermore, the activity of the enzyme increased dramatically as small amounts of water were added to each solvent. For example, the activity of immobilized LADH increased from 6.3 to 83 nmols (min-g support)⁻¹ when the water concentration in butyl acetate was increased from about 0.02% to 1.0%. It is of interest at this point to investigate more closely the role of water in these reactions and to examine the conformation of LADH in each of these solvent systems.

To this end, the spin labeling technique was used to probe the active site structure of LADH in various solvent systems. The spin label, SL-1, alkylated cysteine 46 (12), an amino acid in the active site of LADH that normally serves as a ligand to the catalytic zinc ion. LADH is a dimer, and each monomeric subunit contains one firmly-bound catalytic zinc ion. The position of enzyme-bound SL-1 was estimated by the spin label-spin probe technique (14,15). Cobalt (II) was employed as the spin probe, and the catalytic zinc in the enzyme's active site was replaced by Co²⁺ according to the procedure of Sytkowski and Vallee (16). The EPR spectrum of enzyme-bound SL-1 was then measured before and after replacement of the active-site zinc by cobalt; from the decrease in spectral amplitude the average nitroxide-metal distance was determined to be $4.8 \pm 1.5 \text{ \AA}$ (17).

Shown in Figure 1 are the EPR spectra of spin-labeled LADH recorded in various solvents ranging from water to nearly anhydrous hexane, along with the spectrum of the completely dry, lyophilized enzyme. Also included are values of log P, a quantitative measure of the solvent's hydrophobicity (18), and the mean rotational correlation times (τ_R) of the spin label determined from spectral simulations (10,11). Since the EPR spectra are very sensitive to the spin label's motional dynamics and to the conformation of the surrounding protein (in general, spectra become broader and more asymmetric as the mean rotational correlation time of the spin label slows from about 10^{-10} to 10^{-7} sec), the spectra in Figure 1 indicate that the enzyme's active-site conformation became more rigid as the solvent became more hydrophobic. Indeed, the EPR spectrum of spin-labeled enzyme in hexane is virtually identical to the spectrum of lyophilized enzyme in the absence of solvent. However, increased rigidity appears to have had at most a secondary influence on the enzyme's activity. For example, the spectrum in anhydrous acetonitrile shows the greatest flexibility of all the organic-solvent spectra yet the enzyme had no activity in anhydrous acetonitrile. On the other hand, the spectrum in hexane reflects the

most rigid conformation yet hexane afforded the highest activity of all the organic solvents.

Moreover, adding small amounts of water to the solvent had no apparent effect on the spin label's mobility, as evidenced by the spectra in Figure 2. EPR spectra recorded in butyl acetate with and without 1% water revealed that the active site conformation was unchanged by water addition even though the enzyme's activity was much higher when 1% water was present. Thus, the increase in activity upon water addition cannot be attributed to a loosening up of the active-site conformation. This result differs from a proposed model of the sequential hydration of dry lysozyme (19), in which restoration of enzyme activity followed a hydration-induced flexibility increase.

It is not possible at present to explain why water has such a pronounced effect on the reaction rates. Although structural differences were not detected as a function of water content, a structural role cannot be completely ruled out. Moreover, the reaction studied is quite complex and involves the oxidation of cinnamyl alcohol coupled with the reduction of octanal (to octanol) to regenerate NAD^+ . The rate-determining step of this sequence is not obvious (hydride transfer or dissociation of the enzyme-octanol complex is a possibility (20), whereas the release of coenzyme is less likely since NAD(H) is expected to remain in the coenzyme binding site). Nonetheless, water apparently accelerated the rate-controlling step, possibly by modifying the electrostatic properties of the active site and/or by facilitating alcohol dissociation, yielding higher rates in solvents with lower affinities for water. Efforts to determine more about the mechanism of the water-induced rate enhancement are now in progress.

Finally, LADH exhibited a higher thermostability in organic solvents (Table 1), which is consistent with previous observations of enhanced enzyme thermostability in organic media (5). However, there was no correlation between structural rigidity, as measured by EPR spectroscopy, and stability against irreversible denaturation at 80°C. This result is relevant to the previous work of Zale and Klibanov (21), which demonstrated that a mechanism expected to stabilize an enzyme against reversible thermal unfolding (for example, increased structural rigidity) will not stabilize the enzyme against irreversible thermal inactivation unless the deactivation temperature is below the unfolding, or transition, temperature of the protein. Since a more rigid structure did not improve the thermostability of LADH at 80°C, either increased rigidity is not a stabilizer of LADH, or 80°C is above the transition temperature of LADH in organic solvents.

Tryptophanase in Reverse Micelles

Two-phase aqueous-organic systems permit enzymatic reactions involving hydrophobic substrates and/or products to be performed. The incorporation of enzymes into organic solvents with reverse micelles provides a promising technique for the synthesis of many organic compounds. The properties of reverse micelles have been

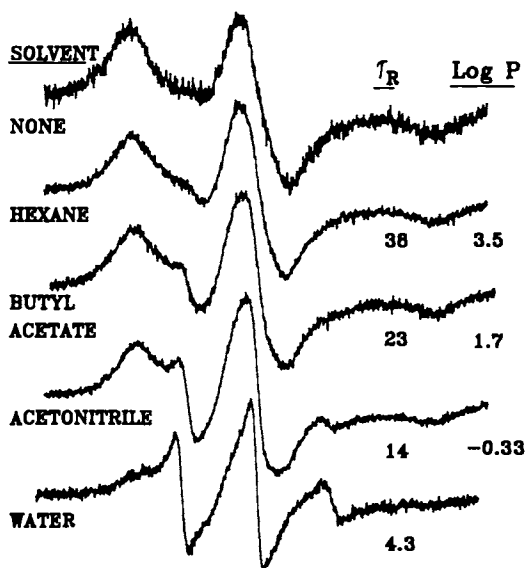


Figure 1. EPR spectra of spin-labeled immobilized LADH in various solvents and in lyophilized form. The water content of each organic solvent ranged from 0.01 to 0.02%. Rotational correlation times are given in nsec. Log P is the logarithm of the partition coefficient of the solvent in an octanol-water mixture.

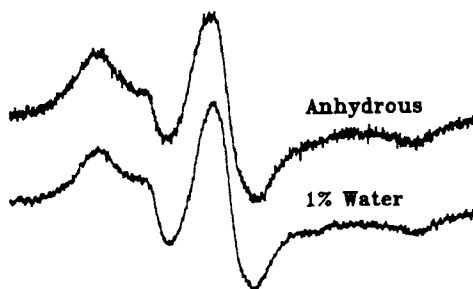
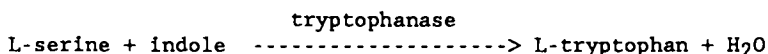


Figure 2. EPR spectra of spin-labeled immobilized LADH in butyl acetate with and without 1% water.

reviewed recently by Luisi and Magid (22). Reports of enzymatic synthesis using reverse-micelle systems include tryptophan synthesis (3), peptide synthesis (23), triacylglycerol synthesis (24) and steroid conversion (25).

Reverse micelles are formed by the addition of a small volume of an aqueous solution to a surfactant-containing organic solvent. The surfactant molecules are orientated at the water-oil interface with the polar "head" groups in the aqueous phase and the nonpolar "tails" in the organic phase. Thus the reverse micelle can encapsulate an enzyme in the aqueous phase. The size of the reverse micelles can be controlled by varying the water-to-surfactant ratio, w_0 .

The model system in this study involves the production of tryptophan from indole and serine using tryptophanase (Figure 3).



This system exploits the advantages offered by reverse micelles. For example, indole is hydrophobic and inhibits tryptophanase at concentrations above 20 mM (3). The reverse-micelle system acts to keep the indole concentration in the aqueous environment of the enzyme low while the organic phase maintains a relatively high indole concentration.

Previous work on the use of a reverse-micelle system for the production of tryptophan reported kinetic data obtained under various conditions (3). Both the water-to-surfactant ratio and the cosurfactant used influenced tryptophan production. The present work reports results from EPR studies of the effect of these parameters on both the water and the enzyme in the reverse micelle. EPR spectra of $\text{Mn}(\text{H}_2\text{O})_6^{2+}$ were recorded to investigate the state of the water in reverse micelles. A nitroxide spin label that reacts with lysine residues was employed to probe the microstructure of tryptophanase in reverse micelles of different w_0 values.

Methods. The purification of crude tryptophanase purchased from Sigma Chemical Company is described elsewhere (3). The preparation of reverse micelles involved several steps and varied slightly depending on the type of experiment. The following describes reverse micelle preparation for kinetic experiments. Serine was first transferred to the organic phase by washing cyclohexane containing 5% v/v Aliquat-336 (tricaprylmethylammonium chloride, obtained from the Henkel Corporation) with an aqueous serine solution (0.20 M), thus exchanging serine for chloride as the anion associated with Aliquat in the organic phase. The aqueous solution was later analyzed to determine the amount of serine transferred to the organic phase. The non-ionic surfactant Brij-56 (Sigma), the cosurfactant 1-hexanol, and the substrate indole were then added to the organic phase at concentrations of 0.15 M, 3% v/v, and 0.10 M, respectively. Finally, an aqueous phase containing 3 mM dithiothreitol, 10 mM pyridoxal-5'-phosphate, and 0.1 M KCl and tryptophanase (freeze dried), pH 9, was added to the organic phase with a micropipette while gently stirring

Table 1. Thermal inactivation of immobilized LADH in water and in nearly anhydrous organic solvents

<u>Solvent</u>	τ_R (ns) of SL-1 in Active Site at 25°C	<u>Percent Activity</u> After 30 min at 80°C
Water	4.3	0.0
Butyl Acetate	23	58 ± 7
Heptane	38	54 ± 8

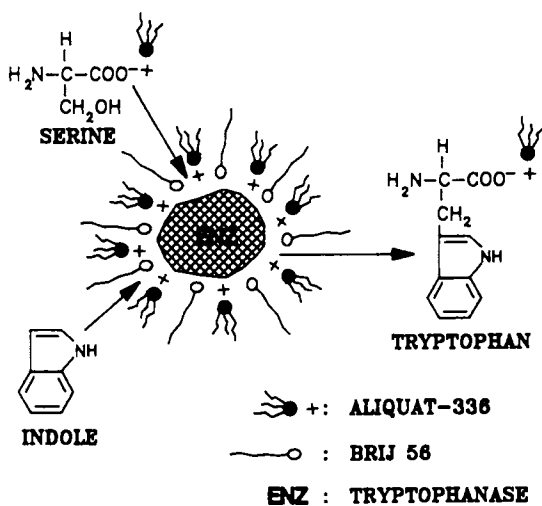


Figure 3. Tryptophan synthesis in reverse micelles.

the solution. Reverse micelles for the EPR experiments were prepared without serine or indole.

Lysine-labelled tryptophanase was prepared by incubating the enzyme with 100-fold molar excess of 2,2,5,5-tetramethyl-3-pyrrolin-1-oxyl-3-carboxylic acid N-hydroxysuccinimide ester (Eastman Kodak Company) in 10 mM bis-tris-propane (Sigma), pH 8 (20% v/v i-propanol), for 24 hours at room temperature. Free spin label was subsequently removed by dialysis. The resulting lysine-labeled enzyme solution was used to make reverse micelles as described above.

The manganese EPR experiments were performed at room temperature without enzyme present. The aqueous phase consisted of a 0.5 mM solution of manganese(II) chloride. EPR spectra were recorded at X-band with a modulation amplitude of 10.0 G and a scan range of 2000 G.

Results and Discussion. Kinetic studies have shown that tryptophan production in reverse micelles is sensitive to w_0 and hence to micelle size (3). Figure 4 shows the effect of w_0 on tryptophan production. Tryptophanase exhibited its highest activity at a w_0 of about 20.

To determine if the properties of micellar water vary with the water content, the EPR spectrum of $MnCl_2$ dissolved in reverse micelles was recorded as a function of w_0 . The results, shown in Figure 5, indicate that the spectrum of $Mn(H_2O)_6^{2+}$ was very sensitive to changes in w_0 . As the water content decreased, the linewidths became increasingly broad, indicating a substantial change in the nature of the water. Such broadening in X-band spectra is consistent with an increase in the rotational correlation time of the manganous ion (26) and hence a more rigid water structure.

The effect of w_0 on the enzyme was examined by comparing the EPR spectra of lysine-labeled tryptophanase. Although the spin label is nonspecific, it can still provide molecular-level information about the enzyme under different conditions. EPR spectra of the spin-labeled enzyme in bulk water and in reverse micelles are shown in Figure 6. Much broader spectra were obtained in reverse micelles, and the calculated rotational correlation time of the attached label (10) increased with w_0 . Thus, the enzyme-bound spin label became more constrained as the water content of the reverse micelle decreased. Since the rotational correlation time of the entire protein in bulk water calculated from the Stokes-Einstein equation is about 200 nsec, the motion of the spin label was still rapid relative to the tumbling rate of the enzyme. Therefore, broadening of the spectrum was apparently caused by a change in the local dynamics of tryptophanase rather than by a decrease in the enzyme's overall rotation rate. The tumbling rate of the enzyme could have decreased as well, however.

In summary, EPR has provided evidence that as the water content in reverse micelles decreases, the water becomes more rigid and the enzyme becomes less flexible. Kinetic studies have shown that there is an optimum water content for enzymatic activity. The link between this optimum and the state of both the water and the enzyme in the reverse micelle is the subject of ongoing research in this laboratory.

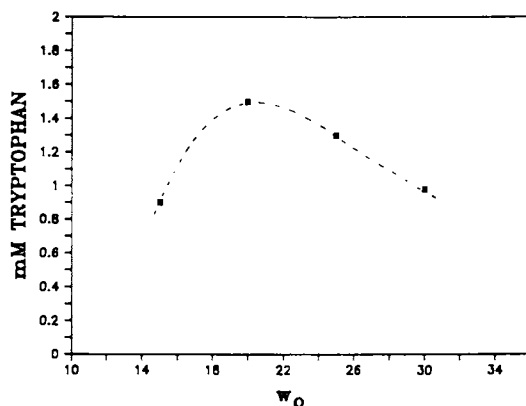


Figure 4. Effect of water content on the amount of tryptophan produced in 20 hrs. w_0 is the molar water-to-surfactant ratio. Experimental conditions: 37°C, pH 9, 0.15 M Brij, 0.05 M indole, 0.83 mg enzyme/ml reactor (data from ref. 3).

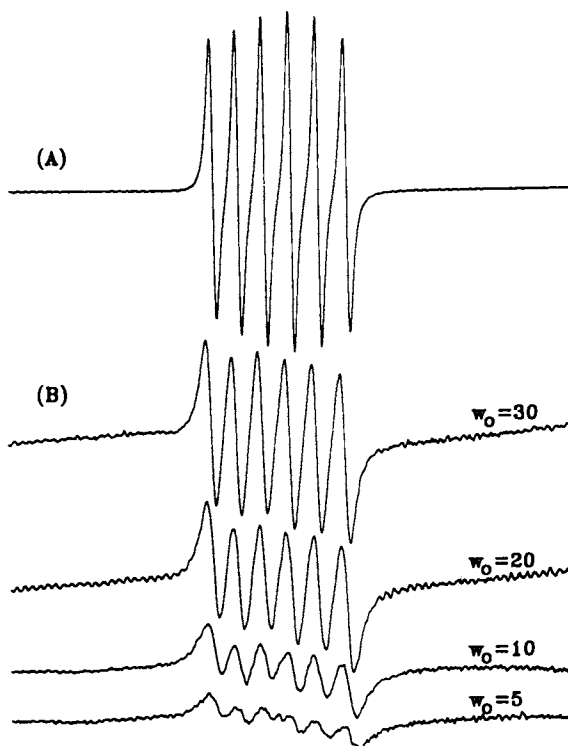


Figure 5. X-band EPR spectra of $MnCl_2$ dissolved in (A) bulk water and (B) reverse micelles.

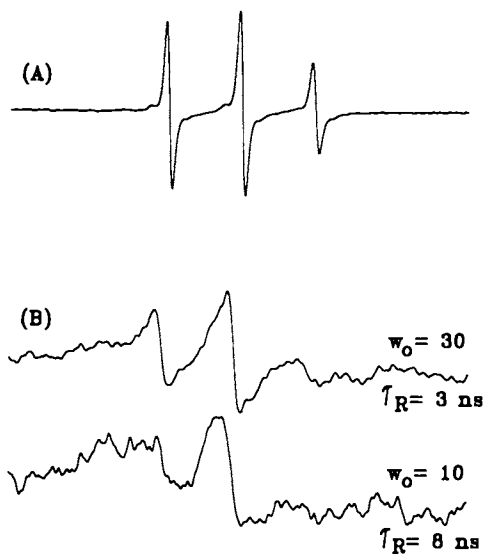


Figure 6. EPR spectra of lysine-labeled tryptophanase in (A) bulk water and (B) reverse micelles.

Literature Cited

1. Klibanov, A.M. Chemtech 1986, 16, 354.
2. Zaks, A.; Klibanov, A.M. Proc. Natl Acad. Sci. USA 1985, 82, 3192.
3. Eggers, D.K.; Blanch, H.W. Bioprocess Eng. 1988, 3, 83.
4. Randolph, T.W.; Clark, D.S.; Blanch, H.W.; Prausnitz, J.M. Science 1988, 239, 387.
5. Zaks, A.; Klibanov, A.M. Science 1984, 224, 1249.
6. Zaks, A.; Klibanov, A.M. J. Am. Chem. Soc. 1986, 108, 2767.
7. Randolph, T.W.; Blanch, H.W.; Prausnitz, J.M. AIChE J. in press.
8. Bello, J. Trends Biochem. Sci. 1985, Volume?, 110.
9. Baker, L.J.; Hansen, A.M.F.; Rao, P.B.; Bryan, W.P. Biopolymers 1983, 22, 1637.
10. Freed, J.H. In Spin Labeling: Theory and Applications; Berliner, L.J., Ed.; Academic: New York, 1976; Chapter 3.
11. Shiotani, M.; Sohma, J.; Freed, J.H.; Macromolecules 1983, 16, 1495.
12. Skerker, P.S.; Clark, D.S.; Biotechnol. Bioeng. 1988, in press.
13. Deetz, J.S.; Rozzell, J.D.; Trends Biotechnol. 1988, 6, 15.
14. Leigh, J.S., Jr. J. Chem. Phys. 1970, 52, 2608.
15. Dalton, L.A.; J.O. McIntyre, J.O.; Fleischer, S. Biochemistry 1987, 26, 2117.
16. Sytkowski, A.J.; Vallee, B.L. Biochemistry 1978, 17, 2850.
17. Clark, D.S.; Skerker, P.S.; Randolph, T.W.; Blanch, H.W.; Prausnitz, J.M. Ann. N.Y. Acad. Sci. in press.
18. Laane, C.; Boeren, S.; Vos, K.; Veeger, C. Biotechnol. Bioeng. 1987, 30, 81.
19. Finney, J.L.; Poole, P.L. Comments Mol. Cell. Biophys. 1984, 2, 129.
20. Fersht, A.; Enzyme Structure and Mechanism, Second Edition; W.H. Freeman: New York, 1985; p 396.
21. Zale, S.E.; Klibanov, A.M.; Biotechnol. Bioeng. 1983, 25, 2221.
22. Luisi, P.L.; Magid, L.J. CRC Crit. Rev. Biochem. 1986, 20, 409.
23. Luthi, P.; Luisi, P.L. J. Am. Chem. Soc. 1984, 106, 7285-86.
24. Morita, S.; Narita, H.; Matoba, T.; Kito, M. JAOCs 1984, 61, 1571.
25. Hilhorst, R.; Laane, C.; Veeger, C. FEBS Lett. 1983, 159, 225.
26. Reed, G.H.; Leigh, J.S. Jr.; Pearson, J.E. J. Chem. Phys. 1971, 55, 3311.

RECEIVED December 5, 1988

Chapter 9

Hydroxylation of C₂, C₃, and Cyclo-C₆ Hydrocarbons by Manganese Porphyrin and Nonporphyrin Catalysts

Richard H. Fish¹, Raymond H. Fong¹, Robert T. Price¹,
John B. Vincent², and George Christou²

¹Lawrence Berkeley Laboratory, University of California,
Berkeley, CA 94720

²Department of Chemistry, Indiana University, Bloomington, IN 47405

Metal complexes that mimic the active site of monooxygenase enzymes and convert carbon-hydrogen bonds to carbon-hydroxyl in the presence of a monooxygen transfer reagents are called biomimetic catalysts. Studies concerning the activation of methane, ethane, propane, and cyclohexane to their respective alcohols with biomimetic catalysts that encompass manganese supramolecule porphyrins and open-faced porphyrins, manganese non-porphyrin tri and tetranuclear clusters, and a mononuclear manganese-substituted Keggin ion in the presence of monooxygen transfer reagent such as iodosylbenzene and t-butyl hydroperoxide will be discussed.

The use of biomimetic catalysts, that mimic monooxygenase enzymes such as cytochrome P-450 and methane monooxygenase by converting C-H to C-OH bonds in the presence of a monooxygen transfer reagent, is an area of intense research interest(1). The monooxygenase enzyme, cytochrome P-450, has a metallo-porphyrin active site(2), while methane monooxygenase has a metallo-non-porphyrin active site(3). These two diverse monooxygenases also have different selectivities for hydrocarbon activation. For example, cytochrome P-450 will activate hydrocarbons greater than C₃, while methane monooxygenase will activate C₁-C₆ and possibly higher homologues.

While the focus of our research is to ultimately activate methane to methanol, as is readily done by methane monooxygenase, we also want to understand what types of biomimics will activate higher homologues as well (C₂, C₃, and cycloC₆). In addition, the bond dissociation energies may play an important role in our ability to activate methane at ambient temperature, since methane has the highest C-H bond dissociation energy (kcal) of all alkanes, i.e., methane(104); ethane(98); propane(96); and cyclohexane (94).

Thus, we have evaluated several biomimetic catalysts, which encompass manganese supramolecule and open-faced porphyrins, manganese tri and tetranuclear clusters, and a mononuclear metal active site in a totally inorganic matrix, a manganese-substituted Keggin ion, with C₁-C₃ and cycloC₆ hydrocarbons in the presence of monooxygen transfer agents, iodosylbenzene and t-butyl hydroperoxide. We will also discuss solvent, catalyst lifetimes, and monooxygen transfer reagent as they effect the C-H activation reaction.

0097-6156/89/0392-0116\$06.00/0

• 1989 American Chemical Society

RESULTS AND DISCUSSION

MANGANESE SUPRAMOLECULE AND OPEN-FACED PORPHYRIN CATALYSTS, 1 AND 2.

Table I shows our results with C₁-C₃ and cycloC₆ hydrocarbons and manganese porphyrin catalysts 1 and 2 (Figure 1), with iodosylbenzene as the monooxygen transfer reagent, at room temperature in methylene chloride. It is evident that the supramolecule and open-faced porphyrin catalysts have similar reactivities with the hydrocarbons studied. Also, it is unfortunate that methane is not activated to methanol; however, ethane, propane, and cyclohexane are converted to their respective alcohols. Hence, we did not see any special reactivity with the supramolecule catalyst, 1, and rationalize that too much flexibility in the "basket handles" does not provide the shape selectivity that we hoped for to gain a kinetic advantage with the difficult to react methane gas.

It is interesting to note that the corresponding iron complexes were less reactive than their manganese analogues, while catalyst lifetimes for 1 and 2 were on the order of 1-2 hr. Thus, both catalyst appear to undergo oxidative degradation and this reaction competes with the conversion of C-H to C-OH bonds. As well, the C-H activation results clearly show a trend of C₆ > C₃ > C₂ and follows the order of the bond dissociation energies(4).

MANGANESE NON-PORPHYRIN CLUSTERS, 1-4

Table II shows the results with C₂, C₃, and cycloC₆ and manganese clusters 1-4 (Figure 1) with t-butyl hydroperoxide at room temperature in acetonitrile (methane did not react under the reaction conditions). The important observation of no catalyst decomposition upon continual addition of t-butyl hydroperoxide to again provide the initial turnover number is an extremely important characteristic of any biomimetic catalyst. It is interesting to note that this increase in catalyst lifetimes occurred in acetonitrile and not methylene chloride and shows the dramatic effect of a coordinating solvent. We did not see any indication of acetonitrile activation.

The Mn₄O₂ clusters were more active than the Mn₃O clusters and the Mn clusters also catalyzed t-butyl hydroperoxide decomposition (@ 1%) to acetone and methanol, which prevented reliable analysis of methane activation results. We could not compare the dinuclear manganese complexes to their tri and tetra analogues because of relative solubility differences; however, we were able to do this with several iron di and tetra clusters and found that the Fe₄O₂ clusters were more active with the hydrocarbons studied. Therefore, higher nuclearity or a variety of ligands may provide the shape selectivity we seek for ultimate methane activation with Mn and Fe clusters.

We also have attempted to inhibit these free radical reactions with 2,6-di-t-butyl-4-methylphenol and found no effect on the formation of cyclohexanol or cyclohexanone using catalyst 4. This latter result strongly suggests that peroxy, alkoxy, or hydroxyl radicals are not intermediates in these reactions. The intermediacy of a putative oxo-manganese complex is further strengthened by the reaction of 1-4 with cyclohexene in the presence of TBHP or iodosylbenzene to provide cyclohexene epoxide and our proposed mechanism is shown in the Equation (5).

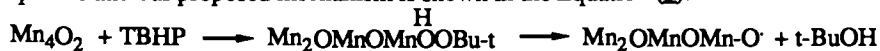


Table I. Carbon-Hydrogen Activation of Hydrocarbons Using Compounds 1 and 2 as Catalysts and Iodosylbenzene as the Monooxygen Transfer Agent^a

Hydrocarbon	Product (%) ^b		Turnover no.	
	1	2	1	2
CH ₄	NPD ^c	NPD	—	—
CH ₃ CH ₃	ethanol (1)	ethanol (2.7)	0.23	0.54
CH ₃ CH ₂ CH ₃	isopropanol (9.6) ^d	isopropanol (13.5) ^e	2.1	2.8
	propanol (0.6)	propanol (1)		
CycloC ₆ H ₁₂	cyclohexanol (72)	cyclohexanol(69.4)	16.7	14
	cyclohexanone (5.2)	cyclohexanone(1)		
	cyclohexyl chloride (4.5)	NPD		

a) Reactions of methane, ethane, and propane were run in a Parr kinetic apparatus at room temperature for 24 h at 100-500 psi with a iodosylbenzene to catalyst ratio of 20:1. Catalyst concentration was .0025 molar in methylene chloride. The cyclohexane reactions were run at room temperature in Schlenk tubes with substrate : iodosylbenzene: catalyst ratios of 1100:20:1 in methylene chloride. Analysis and quantitation of products was obtained via capillary column GC analysis with a 15m · .035 mm DB5 column.

b) Based on the mmoles of iodosylbenzene

c) No product detected

d) Ratio of 2⁰ to 1⁰ C-H bond reactivity on a per H basis is 45:1

e) Ratio is 42:1

Table II. Comparison of the C-H Bond Reactivity of C₂, C₃, and CycloC₆ Hydrocarbons with Mn₃₋₄O₁₋₂L_xL_y Catalysts, 1-4, Using t-Butyl Hydroperoxide as the Monooxygen Transfer Reagent ^a

Hydrocarbon	Catalyst	Products(%) ^b	Turnover No. ^c
CH ₃ CH ₃	1	ethanol(1)	2
	2	ethanol(<1)	<1
	3	ethanol(1)	2
	4	ethanol(<1)	1
CH ₃ CH ₂ CH ₃	1	isopropanol(2) ^d	3
	2	isopropanol(<1)	<1
	3	isopropanol(5)	9
	4	isopropanol(3)	5
CycloC ₆ H ₁₂	1	cyclohexanol(60) cyclohexanone(36)	121
	2	cyclohexanol(50) cyclohexanone(33)	114
	3	cyclohexanol(41) cyclohexanone(39)	126
	4	cyclohexanol(44) cyclohexanone(42)	127

^a Reactions of ethane and propane were reacted in a Parr Kinetic Apparatus at partial pressures of 250 and 90 psi, respectively, at room temperature for 1-3h in acetonitrile. The ratio of t-butyl hydroperoxide (TBHP) to catalyst was 150:1, while the catalyst concentration was .0025M. The cyclohexane reactions were run in Schlenk flasks at room temperature for 1-3h with substrate : oxidant : catalyst ratio of 1100 : 150 : 1 and a catalyst concentration of .001M in acetonitrile. TBHP was added as a benzene solution.

^b The analysis and quantitation was accomplished via capillary column GC and GC-MS analysis. Yields of alcohol and ketone were based on TBHP consumed (iodometric titration). The ketone yields are molar yields multiplied by 2, since two equivalents of TBHP are required to make one equivalent of ketone.

^c Based on the mmoles of oxidizing equivalents/mmoles catalyst.

^d Trace amounts of n-propanol (<<1%) were also formed(GC). As well, trace amounts of acetone were also found; however, a control experiment verified its formation from the Mn cluster-catalyzed decomposition of TBHP. Additionally, small amounts of isopropanol can also be oxidized to acetone under the reaction conditions.

MANGANESE SUBSTITUTED KEGGIN IONS, MnPW₁₁O₃₉⁵⁻

Preliminary results with a manganese-substituted Keggin ion catalyst that has an extremely stable PW₁₁O₃₉⁵⁻ backbone (Figure 1), shows some promise with small hydrocarbons(4). This catalyst can be heated to 65 °C for long periods without decomposition(6). An initial experiment with ethane and t-butyl hydroperoxide in benzene gave 2 turnovers of ethane to ethanol in three hr at 65 °C, while with propane the turnover number was 24 and provided isopropanol and n-propanol in a 5:1 ratio (Table III).

Unfortunately, methane did not provide methanol under these conditions. We are presently evaluating other metal-substituted Keggin ions as C-H activation catalysts for C₁-C₃ hydrocarbons.

Table III. Carbon-Hydrogen Activation of C₁-C₃ Hydrocarbons with a Manganese-Substituted Keggin Ion Catalyst Using t-Butyl Hydroperoxide as the Monooxygen Transfer Reagent in Benzene ^a

Hydrocarbon	Product (%)	Turnover Number
CH ₄	-	-
CH ₃ CH ₃	ethanol (2)	2
CH ₃ CH ₂ CH ₃	isopropanol (30) n-propanol (6)	24

^a Reactions of methane, ethane, and propane were reacted in a Parr Kinetic Apparatus at pressures of 500, 250, and 90 psi, respectively, at 65 °C in benzene. The t-butyl hydroperoxide (TBHP) / catalyst ratio was 177:1 with a catalyst concentration of 2.0 x 10⁻⁴ M. TBHP was added as a benzene solution. Yields were based on TBHP consumed (iodometric titration); ~ 75% in each case.

CONCLUSIONS

Although we have not as yet succeeded in our main goal of activating methane using iodosylbenzene or t-butyl hydroperoxide as monooxygen transfer agents, we have learned how to activate ethane and propane with several manganese mono, tri, and tetranuclear complexes. We hope to use these results as a foundation for the future utilization of oxygen gas as the monooxygen transfer reagent with iron cluster catalysts to give a system that mimics methane monooxygenase enzyme. In fact in a recently published paper, we reported on the synthesis and catalytic activity of a biomimic of methane monooxygenase enzyme, Fe₂O(OAc)₂Cl₂(bipy)₂, with t-butyl hydroperoxide or oxygen gas as the monooxygen transfer agents(7).

ACKNOWLEDGMENTS

The catalysis studies at LBL were supported by the Electric Power Research Institute under U. S. Department of Energy Contract No. DE-AC03-76SF00098, while the manganese cluster synthesis studies at IU were supported by NSF CHE 8507748. We wish to thank Linda Atherton of EPRI for support of the catalysis studies at LBL.

LITERATURE CITED

1. M.J. Nappa and C. A. Tolman, *Inorg. Chem.*, 1985, **24**, 4711 and references therein.
2. F. P. Guengerich and T. L. MacDonald, *Acc. Chem. Res.*, 1984, **17**, 9 and references therein.
3. R. C. Prince, G. N. George, J. C. Savas, S. P. Cramer, and R. N. Patel, *Biochim. Biophys. Acta*, 1988, **952**, 220 and references therein.
4. R. H. Fish, R. T. Price, and R. H. Fong (submitted for publication).
5. R. H. Fish, R. H. Fong, J. B. Vincent, and G. Christou *J. C. S. Chem. Commun.*, 1988, 1504.
6. M. Farji and C.L. Hill, *J. C. S. Chem. Commun.*, 1987, 1487.
7. J. B. Vincent, J. C. Huffman, G. Christou, Q. Li, M. A. Nanny, D. Hendrickson, R. H. Fong, and R. H. Fish, *J. Am. Chem. Soc.*, 1988, **110**, 6898.

RECEIVED November 11, 1988

Chapter 10

Biomimetic Catalytic Oxidation of Lignin Model Compounds

Robert DiCosimo¹ and Hsiao-Chiung Szabo

B.P. America Research and Development, Cleveland, OH 44128

The single-electron-transfer oxidation of model compounds representative of the arylglycerol β -aryl ether and 1,2-diarylpropane linkages of lignin has been examined by using Co(II), Mn(II), or Co(II)/Mn(II) as catalysts. Catalytic oxidation of 1-(3,4-dimethoxyphenyl)-2-(2-methoxyphenoxy)propane-1,3-diol (DMMP) in 80% acetic acid with 500 psi of 4% oxygen in nitrogen and at 170 °C resulted predominantly in products of $\text{C}\alpha$ - $\text{C}\beta$ bond cleavage when using Co(II)/Mn(II) as catalyst. $\text{C}\alpha$ - $\text{C}\beta$ bond cleavage of DMMP results from an initial single-electron oxidation to produce an intermediate aromatic radical cation; in the absence of oxygen and catalyst, acid-catalyzed β -aryl ether cleavage was the predominant reaction pathway. Dihydroanisoin (DHA) and 1,2-bis(4-methoxyphenyl)-propane-1,3-diol (BMPD) were oxidized by stoichiometric quantities of Co(III) to give solely products of $\text{C}\alpha$ - $\text{C}\beta$ bond cleavage, but produced only acid-catalyzed dehydration products under reaction conditions necessary for catalytic oxidation.

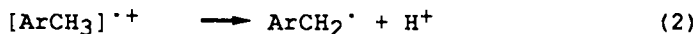
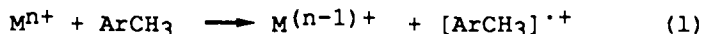
The chemical bleaching of paper pulp is currently performed using chlorine or chlorine dioxide, which for kraft pulp results in the production of between 45 and 90 kg of organic waste/ton of pulp, containing 4-5 kg of organically-bound chlorine/ton. (1,2) Bleaching of paper

¹Current address: Central Research and Development Department, E. I. du Pont de Nemours and Company, Experimental Station, Wilmington, DE 19880-0328

0097-6156/89/0392-0123\$06.00/0
1989 American Chemical Society

pulp whitens the pulp by removal of lignin or by destroying the chromophores of lignin. Lignin is, after cellulose, the principal constituent of higher plants, and is a highly-branched, structurally intricate polymer comprised of phenylpropanoid units.(3) The toxicity of chemical bleaching effluents to fish and other aquatic fauna has been known for some time,(4,5) and regulations that will limit concentrations of polychlorinated aromatics in waste streams will make alternatives to the chemical bleaching of paper pulp with chlorine or chlorine dioxide increasingly desirable. Lignin-degrading enzymes are now being examined as biocatalysts for the bleaching of paper pulp, as well as the pulping of wood. "Ligninase" isolated from the white-rot fungi *Phanerochaete chrysosporium* utilizes hydrogen peroxide to generate an oxy-heme complex, which degrades lignin by oxidizing the aryl groups of lignin or lignin model compounds by a single electron transfer.(6-10) The relatively stable radical cations that result decompose via C α -C β bond cleavage (Figure 1).

One possible problem with using ligninase as a biocatalyst for the degradation of lignin in paper pulp is that the protein has an apparent molecular weight of 41,000,(10) and this may limit its ability to enter into the high molecular weight cellulose-lignin polymer. Faster rates of lignin degradation might be obtained using much smaller "biomimetic" catalysts which function via a similar mechanism. The autoxidation of alkylbenzenes to aldehydes and carboxylic acids, catalyzed by a number of different transition metals, also proceeds by an initial electron transfer, resulting in a one-electron reduction of the metal catalyst and concomitant formation of a substrate radical cation (Equations 1 and 2).(11)



The ease of electron-transfer oxidation of aromatic hydrocarbons to produce radical cations is directly related to the ionization potential of these compounds, with electron-donating substituents such as methoxyl (almost every aryl group of lignin has one or two methoxyl substituents) lowering the oxidation potential. Examination of the ionization potentials for variously substituted aromatic molecules(12) indicates that oxidants such as Mn(III) and Co(III) should be quite efficient in catalyzing the autoxidation of lignin and lignin model compounds via a "biomimetic" mechanism that parallels the oxidation of lignin by ligninase, and we

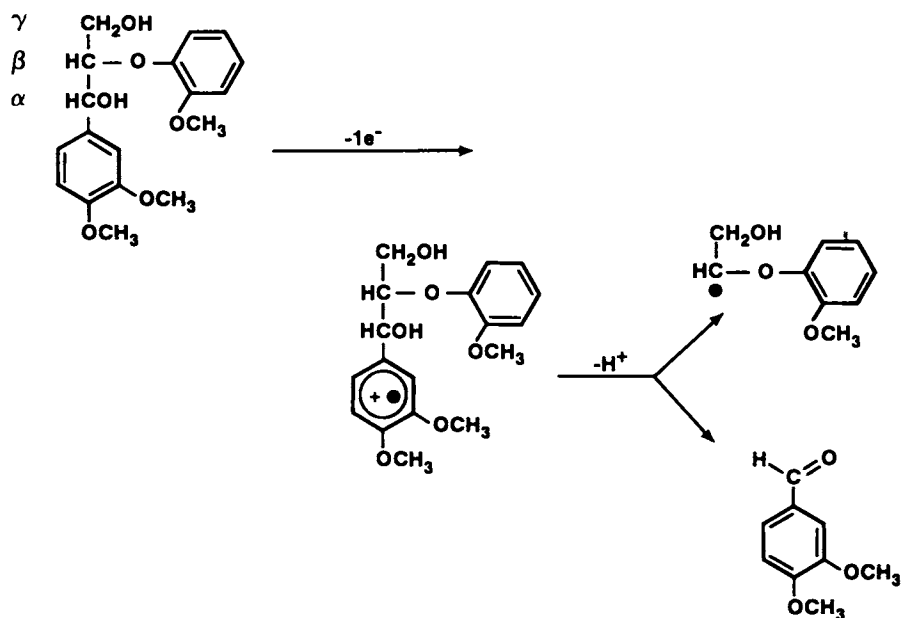


Figure 1. $\text{C}\alpha\text{-C}\beta$ bond cleavage of a lignin model compound by oxidation via single-electron transfer. (Reproduced from Ref. 32. Copyright 1988 ACS)

now report the results of a study of the autoxidation of lignin model compounds by these catalyst systems.

Results and Discussion

The lignin model compounds whose oxidations have now been examined by using autoxidation catalysts have all previously been employed as lignin models in degradative reactions using *Phanerochaete chrysosporium*, which produces the enzyme ligninase, or in reactions that examined the effect of kraft pulping or other chemical or microbial oxidations on lignin model compounds. (13-19) These model compounds represent the arylglycerol β -aryl ether and 1,2-diarylpropane linkages of lignin, which make up 30%-50% and ca. 7%, respectively, of the major types of bonds connecting the phenylpropanoid units of lignin. (3) Figure 2 depicts the four lignin model compounds used in this study and the expected products of the $\text{C}\alpha$ - $\text{C}\beta$ bond cleavage of these compounds by their single-electron-transfer oxidation: dihydroanisoin (DHA), 1,2-bis(4-methoxyphenyl)propane-1,3-diol (BMPD), 1-(4-hydroxy-3-methoxyphenyl)-2-(2-methoxyphenoxy)propane-1,3-diol (HMMP), and 1-(3,4-dimethoxyphenyl)-2-(2-methoxyphenoxy)propane-1,3-diol (DMMP).

Stoichiometric Oxidation of Lignin Model Compounds. The stoichiometric oxidation of the lignin model compounds DHA, BMPD, HMMP, and DMMP was first performed to determine the ability of single-electron-transfer oxidants such as Co(III) to produce $\text{C}\alpha$ - $\text{C}\beta$ bond cleavage of the substrates (Table I). The diarylpropane model DHA was completely oxidized to yield 2 equiv of anisaldehyde. The diarylpropane BMPD produced at least 1 equiv of anisaldehyde; further oxidation of the $\text{C}\beta$ fragment (1-(4-methoxyphenyl)-1,2-ethanediol) produced additional anisaldehyde. The arylglycerol β -aryl ether model compounds HMMP and DMMP were also oxidized by stoichiometric amounts of Co(III), but $\text{C}\alpha$ - $\text{C}\beta$ bond cleavage was only observed for DMMP, which produced DBA and guaiacol. Oxidation of HMMP by Co(III) in acetic acid produced no products of $\text{C}\alpha$ - $\text{C}\beta$ bond cleavage, and no other low-molecular weight (monomeric) products were observed; it is likely that once oxidized to a resonance-stabilized phenoxyl radical, dimerization to biphenyl is the primary reaction pathway. The oxidation of 2-methoxy-4-alkylphenols is known to result in ortho-carbon coupling of two monomers to produce *o,o'*-dihydroxybiphenyl, which are in turn subject to further oxidation. (20)

Table I. Stoichiometric Oxidation of Lignin Model Compounds by Co(III)

compd	[compd]:[Co]	solvent	T(°C)	% conv.	% sel.
DHA	1: 0	AA	25	nr	--
DHA	1: 2	AA	25	100	100
DHA	1: 1	AA	25	53	94
DHA	1: 0	80% AA	25	66	0
DHA	1: 2	80% AA	25	100	62
BMPD	1: 0	AA	25	10	0
BMPD	1: 2	AA	25	100	97
BMPD	1: 2	AA	50	100	100
BMPD	1: 2	50% AA	50	88	54
HMMP	1: 0	AA	25	1	0
HMMP	1: 2	AA	25	88	0
HMMP	1: 0	50% AA	25	7	0
HMMP	1: 2	50% AA	25	73	0
DMMP	1: 0	AA	118	2	0
DMMP	1: 2	AA	118	99	67
DMMP	1: 0	50% AA	reflux	18	0
DMMP	1: 2	50% AA	reflux	40	38

[compd] = 1.0 mM, AA = acetic acid

Catalyst Regeneration Using Peracetic Acid. After having used stoichiometric amounts of electron-transfer oxidants for the oxidation of DHA, BMPD, and DMMP to α - β bond-cleavage products, the generation of catalytic amounts of electron-transfer oxidants was first demonstrated by using peracetic acid to oxidize Co(II) to Co(III) in situ (Table II). Five equivalents of BMPD were oxidized with 1 equiv of Co(III) in glacial acetic

Table II. Regeneration of Co(III) with Peracetic Acid

	Co(III) (mM)	CH ₃ CO ₃ H(mM)	% conv.	% sel.
BMPD	0.20	1.6	100	100
BMPD	0	1.0	87	30
DMMP	0.25	1.0	90	48
DMMP	0	1.0	8	0

[BMPD], [DMMP] = 1.0 mM, solvent = AA, 25 °C

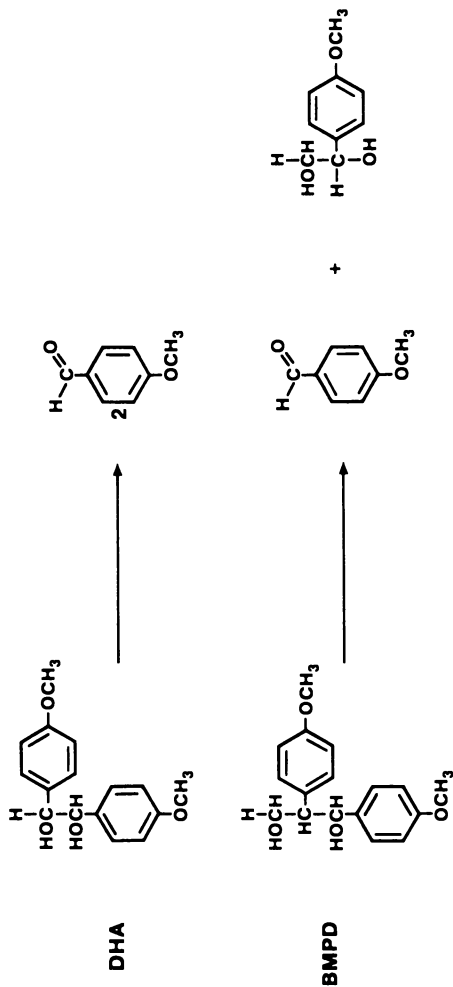


Figure 2. Model compounds representing 1,2-diarylpropane and arylglycerol β -aryl ether linkages of lignin. (Reproduced from Ref. 32. Copyright 1988 ACS). (Continued on next page.)

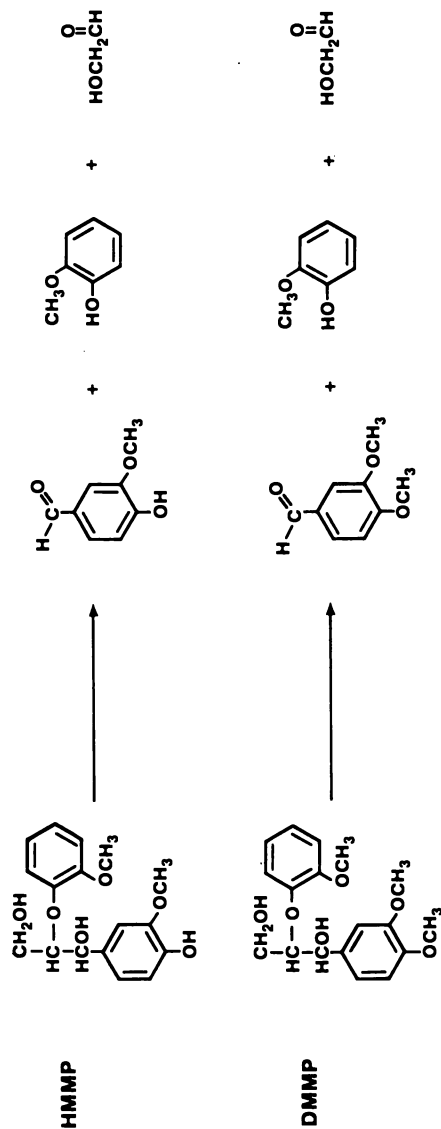


Figure 2. Continued.

acid at 25 °C by using 8 equiv of peracetic acid to regenerate Co(III). Anisaldehyde was produced with 100% selectivity at 100% conversion of BMPD. The reaction of 1 equiv of BMPD with 1 equiv of peracetic acid in the absence of added catalyst gave only 30% selectivity to anisaldehyde at 87% conversion. The catalytic oxidation of DMMP using peracetic acid as the cooxidant was also demonstrated: 4 equiv of DMMP was oxidized in the presence of 1 equiv of cobalt(II) acetate by using 4 equiv of peracetic acid as the cooxidant. A 48% selectivity to DMB at 90% conversion was obtained, and three turnovers of Co(II) were achieved. DMMP is very stable in the presence of peracetic acid under the same conditions: a 92% recovery was obtained at 25 °C after 5 h. Because of the expense of using of stoichiometric quantities of peracetic acid for lignin degradation, and the large quantities of peracid that would be required for the application of this type of catalytic oxidation to a process such as paper pulp bleaching, an alternative method of catalyst oxidation is desirable. The most economical way to generate the desired electron-transfer oxidants in situ would use oxygen as the ultimate oxidant, and alkylperoxy or peroxyacid intermediates formed during the reaction of oxygen with the α - β bond-cleavage products of lignin (in this case, lignin model compounds) could reoxidize the catalyst.

Acid-Catalyzed Dehydration of Lignin Model Compounds.

In addition to α - β bond cleavage, both the diarylethane- and diarylpropanediols and the arylglycerol β -aryl ethers are subject to acid-catalyzed dehydration reactions. DHA and BMPD could be oxidized with stoichiometric amounts of Co(III) to give good to excellent selectivity to α - β bond-cleavage products under reactions conditions that would otherwise produce only the acid-catalyzed dehydration products desoxyanisoin and trans-4,4'-dimethoxystilbene, respectively, but these same model compounds were not stable at the higher reaction temperatures and pressures (>150 °C, 500 psi 4% oxygen in nitrogen) required to obtain catalytic reaction with oxygen and the Co(II), Mn(II), or Mn(II)/Co(II) catalysts. HMMP was unsuitable as a model compound since it did not undergo α - β bond cleavage when oxidized by Co(III). In contrast, the arylglycerol β -aryl ether DMMP could be catalytically oxidized to give predominantly α - β bond-cleavage products under the required high-temperature, high-pressure reaction conditions, where in the absence of catalyst and oxygen, acid-catalyzed dehydration and β -aryl ether cleavage were also observed. (21)

The stability of the lignin model compound DMMP under the reaction conditions and in the solvents to be

used for catalytic oxidations was first determined in the absence of added catalyst. After heating for 3 h at 170 °C and under 4% oxygen in nitrogen in glacial acetic acid, no DMMP remained, and the products were the diacetate 1-(3,4-dimethoxyphenyl)-2-(2-methoxyphenoxy)propane-1,3-diol diacetate (DMPD, 66% yield), the monoacetate 3-(3,4-dimethoxyphenyl)-3-hydroxy-2-(2-methoxyphenoxy)propyl acetate (DHMA, 2.2% yield) (where acetylation of the primary hydroxyl group of DMMP has taken place), 3,4-dimethoxybenzaldehyde (DMB, 7.6%), 3,4-dimethoxybenzoic acid (DBA, 9.9%), and guaiacol (7.3%). A minor product also formed is the monoacetate at the secondary hydroxyl group. In 80% aqueous acetic acid, 5% DMMP remained, and DMPD (5.8%), DHMA (12%), DMB (20%), dimethoxybenzaldehyde (DBA, 16%), and guaiacol (35%) were produced; similar yields were observed in 50% acetic acid, except for guaiacol (56%). The production of DHMA and DMPD as byproducts was observed in most reactions of DMMP with Co(II) or Mn(II)/Co(II) (1:9), oxygen, and acetaldehyde (added as a cooxidant for the generation of Mn(III)/Co(III), *vide infra*). DMPD and DHMA were considered to be unreacted starting material when determining conversions of DMMP and selectivity to products.

Catalytic Oxidations. The effect of the addition of oxygen and Co, Mn, and Mn/Co (1:9) oxidation catalysts on the reaction of DMMP in 80% acetic acid at 170 °C is illustrated by the examples listed in Table III.

Table III. Catalytic Oxidation of DMMP^a

catalyst	reaction gas	conv. (%)	% selectivity		
			DMB	DBA	guaiacol
	N ₂	92	4	6	77
	4% O ₂ in N ₂	77	26	21	49
Co(II)	4% O ₂ in N ₂	49	34	28	54
Mn(II)	4% O ₂ in N ₂	89	41	33	0
Mn(II)/Co(II)	4% O ₂ in N ₂	79	29	42	9
Mn(II)/Co(II)	N ₂	53	6	5	64

^aReactions were run for 3 h in 80% acetic acid at 170 °C and 500 psi of nitrogen or oxygen/nitrogen, using 10 mM DMP and 100 mM catalyst; Mn(II)/Co(II) ratio was 1:9. DMB = 3,4-dimethoxybenzaldehyde, DBA = 3,4-dimethoxybenzoic acid.

Heating a 10 mM solution of DMMP in 80% acetic acid in the absence of catalyst or oxygen results in acid-

catalyzed β -aryl ether cleavage to produce guaiacol and 3-(3,4-dimethoxyphenyl)-2-oxo-1-hydroxypropane, (21) with very little α - β bond cleavage. Adding oxygen but no catalyst leads to an increase in α - β bond cleavage and decrease in β -aryl ether cleavage, while adding both oxygen and catalyst produces the highest selectivities (60-70% combined selectivities for DMB and DBA) to α - β bond cleavage. Running the reaction with catalyst but no oxygen leads to acid-catalyzed β -aryl ether cleavage as the predominant reaction pathway, but conversions (related to the rate of reactions) are much lower than in the absence of catalyst, indicating a possible stabilization of DMMP to acid-catalyzed reactions by chelation to the catalyst.

Acetaldehyde was added to the reaction mixtures as a cooxidant for catalyst regeneration; acetaldehyde is oxidized under these reaction conditions to peracetic acid, which is capable of reoxidizing Co(II) to Co(III) and Mn(II) to Mn(III). (22, 23) Increasing the concentration of acetaldehyde from 1.0 mM to 100 mM in reaction mixtures containing DMMP (10 mM) and Mn/Co(100 mM) resulted in only a small increase in the conversion of DMMP and the selectivity to DMB and DBA (Figure 3), and a similar effect on conversion and selectivity was obtained when using Mn(II) as catalyst. When using Co(II) as catalyst, a marked increase in conversion was observed between reactions run with no added acetaldehyde and those containing 1-100 mM acetaldehyde.

Of the different catalyst used (Co(II), Mn(II), and Mn(II)/Co(II) (1:9)), the mixed catalyst Mn/Co (1:9) gave the best selectivities and conversions in the presence of added acetaldehyde; a similar synergistic effect when using Co(II) and Mn(II) for the autoxidation of *p*-xylene has been previously reported. (24) Mn(II) alone gave higher selectivity to α - β bond-cleavage products than Co(II), but the combination of Mn(II)/Co(II) (1:9) generally resulted in the highest conversion and selectivities to the desired products. The catalytic oxidation of 10 mM DMMP using various concentrations of Mn/Co (1:9) (0-500 mM) in 80% acetic acid with 100 mM acetaldehyde at 170 °C and 500 psi 4% oxygen in nitrogen was examined (Figure 4). Selectivity to products of α - β bond cleavage increased from 39% with no added catalyst to 71% with 100 mM Mn/Co (1:9); further increases in catalyst concentration only produced moderate increases in selectivity at this partial pressure of oxygen. Conversions of DMMP remained fairly constant up to Mn/Co concentrations of 100 mM, but were slightly lower at higher concentrations.

Increasing the concentration of DMMP while maintaining the concentration of catalyst, acetaldehyde, and oxygen constant resulted in a decrease in

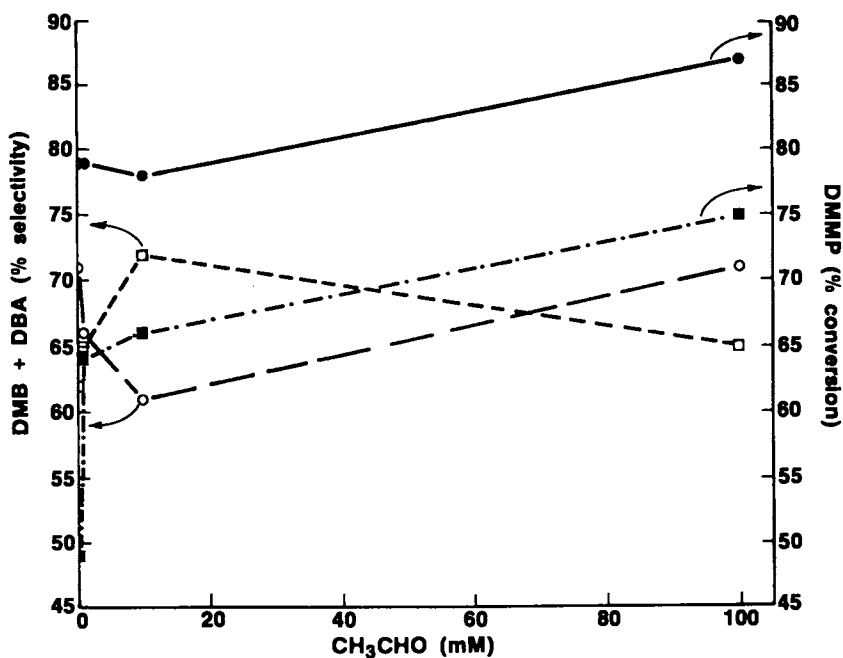


Figure 3. Selectivity to DMB and DBA and conversion of DMMP, as a function of acetaldehyde concentration. Reactions were performed by using 500 psi of 4% O₂ in nitrogen and either Mn(II)/Co(II) (1:9, 0.10 M; ●, conversion of DMMP; ○, selectivity, to DMB and DBA) or Co(II) (0.10 M; ■, conversion; □, selectivity), in 80% acetic acid with DMMP (0.010 M) at 170 °C for 3 h. (Reproduced from Ref. 32. Copyright 1988 ACS)

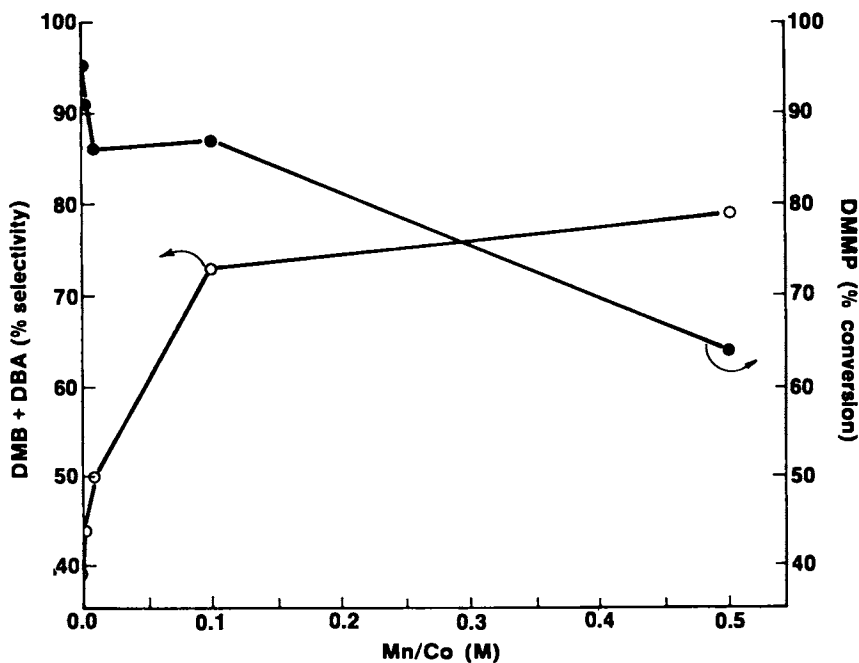


Figure 4. Selectivity to products of $C\alpha-C\beta$ bond cleavage (○) and conversion of DMMP (●) as a function of catalyst concentration. Reactions were performed by using 500 psi of 4% O_2 in nitrogen in 80% acetic acid with DMMP (0.010 M) and acetaldehyde (0.10 M) at 170 °C for 3 h; $Mn(II)/Co(II) = 1:9$. (Reproduced from Ref. 32. Copyright 1988 ACS)

selectivity to the C α -C β bond-cleavage products DBA and DMB. A concomitant increase in the production of guaiacol was observed with increasing concentration of DMMP, indicating that the acid-catalyzed decomposition of DMMP becomes the predominant reaction pathway as the concentration of oxygen becomes limiting: increasing the partial pressure of oxygen in the reaction produces an increase in the selectivity to DBA and DMB at any given concentration of DMMP. The optimum ratio of reactants favoring C α -C β cleavage in 80% acetic acid was 10 Mn/Co (1:9):10 acetaldehyde:1 DMMP using 10 mM DMMP and 8% oxygen in nitrogen; a 78% yield of DMB and an 18% yield of DBA at 100% conversion of DMMP were obtained. When the concentrations of all reactants except oxygen were increased at this same ratio, higher concentrations again gave lower selectivities to DMB and DBA. The rate of conversion of DMMP decreased slightly with increasing concentration of DMMP, all other reaction parameters being held constant.

The transition metal-catalyzed electron-transfer oxidation of DMMP requires oxygen for catalyst reoxidation. A blank check performed by heating a solution of 10:10:1 Mn/Co(1:9):acetaldehyde:DMMP (10 mM) in 80% acetic acid and at 500 psi of nitrogen and 170 °C for 3 h produced selectivities of 4% DMB and 11% DBA at 47% conversion, with a 64% selectivity to guaiacol; with no oxygen present, the predominant reaction of DMMP was acid-catalyzed dehydration and β -aryl ether cleavage. In contrast, the same reaction with 8% oxygen in nitrogen gave 63% selectivity to DMB and 21% selectivity to DBA at 100% conversion, and no guaiacol was observed. Similar results were obtained when using either Co(II) or Mn(II) alone as catalysts. The conversions of DMMP and yields of DMB, DBA, and guaiacol were approximately the same when solutions of DMMP were heated to 170 °C in either the presence or absence of added catalyst and/or acetaldehyde in the absence of oxygen.

Using a ratio of Mn(II)/Co(II):acetaldehyde:DMMP of 10:10:1 and 100 mM Mn/Co(1:9), running the reaction at 170 °C and 500 psi of 4% oxygen in nitrogen gave high selectivities to DMB and DBA at almost complete conversion of DMMP in glacial, 80%, and 50% aqueous acetic acid. In glacial acetic acid, the selectivity to DMB and DBA was 82% and 16%, respectively, at 97% conversion. In 80% acetic acid, the selectivity to DMB and DBA was 58% and 29%, respectively, at 99% conversion. In 50% acetic acid, the selectivity to DMB and DBA was 58% and 24%, respectively, at 100% conversion. These same reactions were examined at temperatures of 100 °C, 130 °C, and 150 °C. Low conversions (10-20%) were obtained when running reactions at 100 °C or 130 °C for 3-5 h; at 150 °C, DMMP

conversions increased to 50-60% at selectivities similar to those obtained at 170 °C.

Conclusions

Under appropriate reaction conditions, i.e. high catalyst and oxygen concentration and low DMMP concentration, the catalytic oxidation of the lignin model compound DMMP proceeds almost completely by α -C β bond cleavage of the arylglycerol β -aryl ether. Although DMMP undergoes autoxidation to produce some products of α -C β bond cleavage in the presence of oxygen alone, significant increases in α -C β bond cleavage are produced by the addition of catalysts capable of one electron-transfer oxidation of α -aryl group. The mechanism of this catalytic oxidation mimics the oxidation of the same lignin model compound by the enzyme ligninase. The development of a "biomimetic" catalyst for the oxidative degradation of lignin, which does not depend on hydrogen peroxide for catalyst reoxidation (as is found for ligninase and heme proteins), would provide a distinct advantage for the use of such systems over ligninase or other peroxide-dependent microbial or enzymatic systems. It is possible that hydroperoxy-lignin intermediates are produced during the aerobic microbial degradation of lignin, but because the heme is enzyme-bound, it is not readily accessible to reoxidation by the hydroperoxy intermediates; metal acetates such as cobalt(II) or manganese(II) acetate should easily react with these same hydroperoxy intermediates and be reoxidized. Also, the microbial and enzyme systems are currently limited to temperatures below 40 °C and are used in aqueous systems at an optimum pH of 4.5-5.0, while the catalyst systems that have already been developed for the selective oxidation of alkylaromatics (such as *p*-xylene to terephthalic acid), and which may be adapted to the oxidative degradation of lignin, can be run in organic or acidic or basic aqueous solvents at temperatures up to 200 °C.

One disadvantage of this "biomimetic" catalyst system for lignin degradation is that only the nonphenolic arylglycerol β -aryl ether DMMP was oxidized via α -C β bond cleavage. Under the conditions for catalytic oxidation employed, models of 1,2-diarylpropane structures of lignin (DHA and BMPD) gave primarily acid-catalyzed dehydration products, while the phenolic arylglycerol β -aryl ether HMMP was oxidized but did not produce products of α -C β bond cleavage. The enzyme ligninase can oxidize these same diarylpropane structures via α -C β bond cleavage, and as a substitute for the chlorine bleaching of paper pulp for residual lignin removal, the enzymatic reaction may produce

greater amounts of delignification than catalytic oxidation. However, both the studies of ligninase and biomimetic models of ligninase have focused primarily on reactions of arylglycerol β -aryl ethers, which are representative of the major type of structures found in lignin, but the structure of residual lignins remaining in paper pulps after cooking is not well-known.(25) Kraft cooking of pulp is believed to degrade β -aryl ether structures to styryl aryl ethers, diaryl ethers, and biphenyls, which are not easily degraded and are removed in a subsequent chemical bleaching step.(26,27) Rather than breaking carbon-carbon bonds for dissolution of residual lignin, oxidation by a biomimetic catalyst, or by ligninase itself, may result in further polymerization of the β -aryl ether degradation products. The treatment of kraft pulp with *P. chrysosporium* has been reported, and although treatment did not result in any bleaching, the remaining pulp was easier to bleach by conventional chlorine treatment due to degradation of some of the residual lignin.(28) An examination of the catalytic oxidation of residual lignin in paper pulp which utilizes oxygen and Mn/Co acetates in aqueous acetic acid needs to be performed before the efficacy of such a method can be judged in comparison to chlorine bleaching.

Experimental Section

General Remarks. Extreme caution should be taken when working with peroxides or peracids directly or when employing reaction conditions where peroxides or peracids will be generated in situ. No metal-ware (e.g. syringe needles) should be employed. Only all-glass reaction vessels, gas-tight syringes with Teflon luer-loc hubs, and Teflon syringe needles and cannulas were used. Dihydroanisoin (1,2-bis(4-methoxyphenyl)ethane-1,2-diol, DHA)(23) and 1,2-bis(4-methoxyphenyl)propane-1,3-diol (BMPD)(24) were prepared as previously described, whereas 1-(4-hydroxy-3-methoxyphenyl)-2-(2-methoxyphenoxy)propane-1,3-diol (HMMP) and 1-(3,4-dimethoxyphenyl)-2-(2-methoxyphenoxy)-propane-1,3-diol (DMMP) were prepared according to slight variations of published procedures.(29,30) Cobalt(III) acetate was prepared by the ozonation of cobalt(II) acetate according to a reported procedure.(31) Reactions using oxygen/nitrogen mixtures at greater than atmospheric pressure were performed in Parr Model 4740 Hastelloy C high pressure reaction vessels equipped with glass liners and Teflon-coated stirring bars. Product selectivities were calculated on the basis of product yields and the amount of substrate reacted (conversion). Yields of products and recovered starting materials were determined quantitatively by HPLC.

Stoichiometric Oxidation of Lignin Model Compounds with Cobalt(III) Acetate. In a typical procedure, a solution of DMMP (6.8 mg, 0.018 mmol) and cobalt(III) acetate (84.3%, 10.5 mg, 0.037 mmol) in 18 mL of glacial acetic acid was heated to reflux in 20 min with stirring. One hour later, the color turned from greenish black to pink. The solution was cooled to room temperature and veratrole (10.2 mg, 0.074 mmol) was added as an internal standard for HPLC analysis. A 67% selectivity to DMB at 99% conversion of DMMP was obtained. For reactions where cobalt(III) acetate still remained, an aqueous solution of ferrous sulfate was added dropwise until the color of the solution turned from green to pink; then veratrole was added as internal standard.

Catalytic Oxidation of Lignin Model Compounds. In a typical procedure, a Pyrex glass liner containing a Teflon-coated magnetic stirring bar, DMMP (8.4 gm, 0.025 mmol), manganese(II) acetate (4.3 mg, 0.025 mmol), cobalt(II) acetate (39.8 mg, 0.23 mmol), and acetaldehyde (14 μ L, 0.25 mmol) in 2.5 mL of 80% acetic acid was placed in a 71-mL Parr Hastelloy C high pressure reaction vessel (Model 4740). The reactor was sealed, purged three times by pressurizing to 320 psi of N₂ and then venting to atmospheric pressure, and then charged with 336 psi of 4% O₂ in N₂). The reactor was put in a heating block preheated at 170 °C and the reaction mixture stirred for 3 h; at 170 °C, the reactor pressure increased to 500 psi. The reactor was then rapidly cooled to room temperature by placing it in an ice/water bath and the vessel subsequently vented to atmospheric pressure. Veratrole (11.2 mg, 0.081 mmol) was added to the reaction mixture as an HPLC internal standard and the mixture was analyzed to yield DMB (37%), DBA (25%), and guaiacol (2.4%) at 87% conversion.

Literature Cited

1. Erickson, K. E.; Kolar, M. C.; Ljungquist, P.O.; Kringstad, K. P. Environ. Sci. Technol. 1985, **19**, 1219-1224.
2. Kringstad, K. P.; Lindstrom, K. Environ. Sci. Technol. 1984, **18**, 236A-248A.
3. Sarkanen, K. V. In Lignins: Occurrence, Formation, Structure and Reactions; Sarkanen, K. V., Ludwig, C. H., Eds.; Wiley: New York, 1967; Chapters 3 and 4.
4. Walden, C. C. Water Res. 1976, **10**, 639-664
5. Dence, C. W.; Annergren, G. E. In The Bleaching of Pulp, 3rd rev.ed.; Singh, R. P., Ed.; TAPPI Press: 1979; Chapter 3, pp 74-75.

6. Kuwahara, M.; Glenn, J. K.; Morgan, M. A.; Gold, M. H. FEBS Lett. 1984, 169, 247-250.
7. Kirk, T. K.; Mozuch, M. D.; Tien, M. Biochem. J. 1985, 226, 455-460.
8. Schoemaker, H. E.; Harvey, P. J.; Bowen, R. M.; Palmer, J. M. FEBS Lett. 1985, 183, 7-12.
9. Paterson, A.; Lundquist, K. Nature (London) 1985, 316, 575-576.
10. Farrell, R. L. Ann. N.Y. Acad. Sci. 1987, 501, 150-158.
11. Sheldon, R. A.; Kochi, J. K. Metal-Catalyzed Oxidations of Organic Compounds; Academic Press; New York, 1981; pp 122-133, 315-328.
12. Fukuzumi, S.; Kochi, J. K. J. Am. Chem. Soc. 1981, 103, 7240-7252.
13. Shimada, M.; Gold, M. H. Arch. Microbiol. 1983, 134, 299-302.
14. Kirk, T. K.; Nakatsubo, F. Biochim. Biophys. Acta 1983, 756, 376-384.
15. Oki, T.; Okubo, K.; Ishikawa, H. J. Jpn. Wood Res. Soc. 1974, 20, 549-557.
16. Adler, E.; Falkehag, I.; Marton, J.; Halvarson, H. Acta Chem. Scand. 1964, 18, 1313-1314.
17. Tien, M.; Kersten, P. I.; Kirk, T. K. Appl. Environ. Microbiol. 1987, 53, 242-245.
18. Huynh, V. B.; Paszczynski, A.; Olson, P.; Crawford, R. Arch. Biochim. Biophys. 1986, 250, 186-196.
19. Enoki, A.; Goldsby, G. P.; Gold, M. H. Arch. Microbiol. 1980, 125, 227-232.
20. Kratzl, K.; Gratzl, J.; Claus, P. Adv. Chem. 1966, 59, 157-176.
21. Adler, E.; Lundquist, K.; Miksche, G. E. Adv. Chem. Ser. 1966, 59, 22-35.
22. Hendriks, C. F.; van Beeek, H. C. A.; Heertjes, P. M. Ind. Eng. Chem. Prod. Res. Dev. 1978, 17, 260-264.
23. Allen, G. C.; Aguilo, A. Adv. Chem. Ser. 1968, 76, 363-381.
24. Kurokawa, A.; Osaki, N.; Shigeyasu, M. J. Chem. Soc. Jpn. 1985, 207-213.
25. Gierer, J.; Wannstrom, S. Holzforschung 1984, 38, 181-184.
26. Gellerstedt, G.; Lindfors, E. L. Holzforschung 1984, 38, 151-158.
27. Gellerstedt, G.; Lindfors, E. L.; Lapiere, C.; Monties, B. Sven. Papperstidn. 1984, 87, R61-R67.
28. Kirk, T. K.; Yang, H. H. Biotechnol. Lett. 1981, 1, 374-51.
29. Hosoya, S.; Kanagawa, K.; Kaneko, H.; Nakano, J. Makuzai Gakkaishi 1980, 26, 118-121.

30. Vyas, G. N.; Shah, N. M. In Organic Syntheses; Rabjohn, N., Ed.; Wiley: New York, 1963; Collect. Vol. 4, p 836-838.
31. Tang, R.; Kochi, J. K. J. Inorg. Nucl. Chem. 1973, 35, 3845-3856.
32. DiCosimo, R.; Szabo, H.-C. J. Org. Chem. 1988, 53, 1673-1679.

RECEIVED November 4, 1988

Chapter 11

Zeolite Catalysts as Enzyme Mimics

Toward Silicon-Based Life?

Norman Herron

**Central Research and Development Department, E. I. du Pont de Nemours
and Company, Wilmington, DE 19880-0328**

The similarity between the rigid framework of a silico- aluminate zeolite having internal voids of molecular dimensions and the tertiary protein structure of an enzyme having a molecular sized substrate binding site has led to the development of 3 remarkable zeolite mimics of enzyme functions. A size encapsulated "ship-in-a-bottle" cobalt complex demonstrates oxygen binding behavior with evidence of cooperativity between the binding sites in an analogue of hemoglobin. Oxidizing systems which use zeolite supported Fe and Pd species to activate molecular oxygen at room temperature and pressure, demonstrate selectivities for hydrocarbon oxidation which are unrivaled in all but natural systems such as the cytochromes P450. Finally, semiconductor clusters arranged in a hyperlattice within zeolite frameworks display photoinduced electron transfer in analogy to the iron-sulfur proteins whose core structure they mimic.

The widespread use of their ion-exchange properties in the water-softening/detergent industry and their strong acid catalysis properties in petroleum-refining have made zeolites the workhorse materials in both applications. While this has attracted many researchers to the zeolite field, it has also had the effect of typecasting these remarkable materials into a limited number of chemical roles. The work reported below is a brief review of our own work here at Du Pont which attempts to dispel this stereotype by demonstrating that there are many remarkable similarities between zeolite structures and those of protein portions of natural

0097-6156/89/0392-0141\$06.00/0

© 1989 American Chemical Society

enzymes(1). By taking advantage of these similarities one can develop some exciting new catalysts which combine the attractive features of the robust, chemically inert zeolite with the tremendous selectivity and activity of enzymes.

What is a zeolite?(2) These materials possess open framework structures constructed of SiO_4 and AlO_4 tetrahedra linked through oxygen bridges. The open framework possesses pores and cavities of molecular dimensions 3-13Å making these the ultimate extrapolation of the quest for ever smaller reaction vessels. These "nano-bottles" are such that chemistry carried out inside them is itself affected by the confines in which it is being performed. One negative charge per aluminum is present on the framework and is compensated by loosely attached, and hence ion-exchangeable, cations. These cation-exchange sites allow the straightforward introduction of active metal sites for catalysis (for a comprehensive discussion of ion-exchange and metal active sites in zeolites please see reference 2).

What is an enzyme? Let us hypothesize that the actual chemical transformation performed by a generic metallo-enzyme is carried out solely at the metal active site in a very non-selective catalytic reaction, typical of traditional homogeneous catalysis. However, nature demands much higher selectivity in her chemistry and so has constructed a very special environment in which to carry out this chemistry - the protein tertiary structure. The protein wraps around the active site performing several crucial functions a) protecting the active site from deleterious reactions such as self-destruction via bimolecular pathways b) sieving of substrate molecules so that only those capable of passing through the protein channels can gain access to the embedded prosthetic group. This can give the enzyme a high substrate-selectivity and c) providing a very stereochemically demanding void space in the vicinity of the active site where the substrate must reside during reaction. This leads to transformations at specific bonds within the substrate molecule. Presented in this fashion, the similarities between a metallo-enzyme and a metal ion containing zeolite become striking.

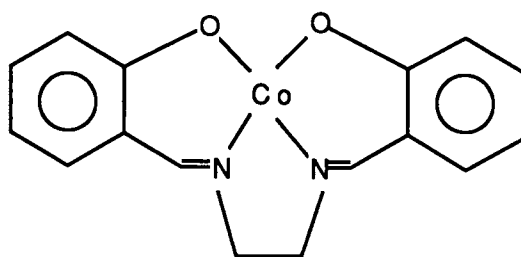
The following sections review 3 systems which we have developed to explore the generality of these concepts: mimics of hemoglobin, cytochrome P450 and of iron-sulfur ferredoxins. While the use of zeolites as enzyme mimics is an under-studied area it is certainly not new as evidence a previous volume in this series (1). The intent here is to emphasize the general concepts of zeolite biomimicry by highlighting the key results we have obtained. Interested readers are referred to the

detailed publications referenced below for full experimental procedures and characterizational details.

Hemoglobin Analogue

Binding and transport of molecular oxygen is the first step in the respiratory chain and this function is performed in mammals by the iron proteins hemoglobin and myoglobin. Many synthetic models (3) and mimics(4) of this chemistry have been prepared using coordination complexes of iron, cobalt, manganese and other metal ions but all suffer from the same problems as the natural systems - namely autoxidation of the active sites with concurrent loss of oxygen binding behavior. Many of the autoxidation mechanisms identify oxo or peroxy dimer formation as the deleterious reaction(5). In addition to severely retarding this dimerization, the protein portion of hemoglobin also engenders a fascinating property known as cooperativity(6). Hemoglobin is a 4 subunit enzyme where each subunit has an iron oxygen binding site and these 4 sites interact such that binding of oxygen to the first subunit facilitates the binding of oxygen to the remaining 3 subunits of the tetramer.

Our synthetic mimic (7) consists of the well known oxygen binder cobalt salen (I) (8) constructed inside zeolite Y. This material is an example of the



SALEN I

"ship-in-a-bottle" (9) synthetic approach to encapsulated catalyst complexes in zeolites. Ion-exchange of cobalt(II) ions into the crystallite voids at a concentration of $\sim 1\text{Co}$ per 2 supercages followed by sublimation of the flexible free ligand Salen into the same voids leads to assembly of the rigid complex. This complex involves square-planar coordination of the tetradentate salen ligand such that the complex has dimensions greater than the window size of the zeolite - once constructed inside the pores the complex is physically trapped on the basis of its size: a true ship-in-a-bottle (Figure 1). This complex as its pyridine adduct does indeed form an oxygen adduct as judged by the characteristic epr signal (Figure 1) generated upon exposure to dioxygen.

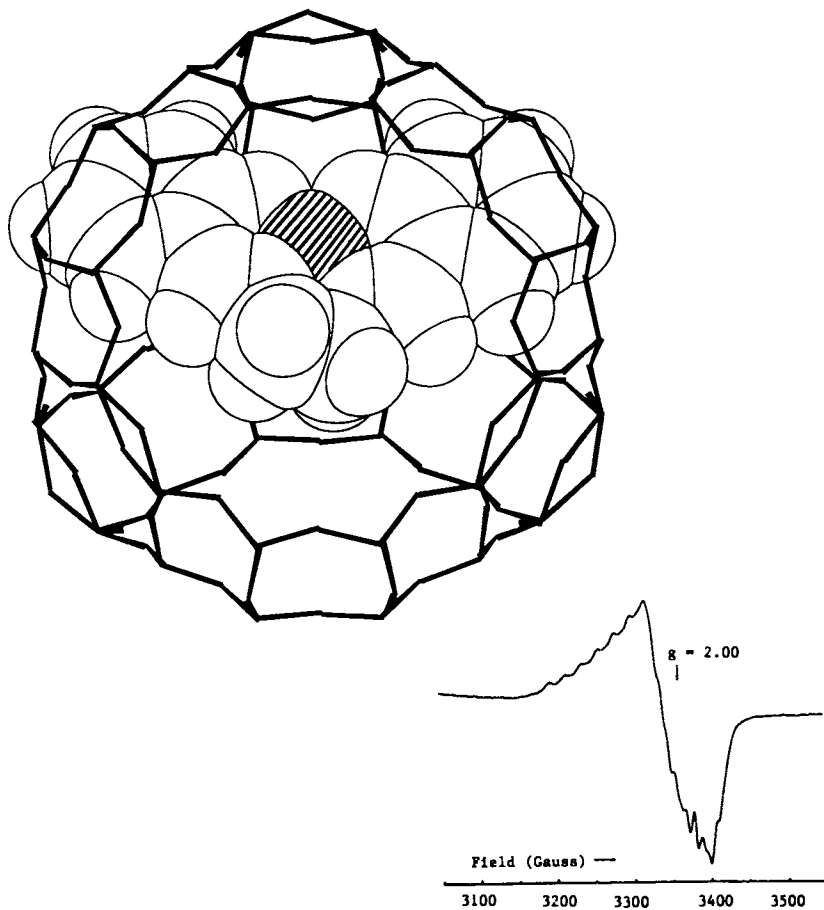


Figure 1. Representation of Co-salen inside zeolite Y supercage. Zeolite framework has been reduced to stick bonds for clarity, Co atom is shaded. Inset shows epr spectrum of oxygen adduct at 298K and 760 torr oxygen.

Two of the remarkable features of this zeolite entrapped adduct are:

Firstly, compared to the same complex in free solution or as a crystalline solid, the zeolite encapsulated material displays quite remarkable stability towards autoxidation and peroxy-dimer formation(10). For example the half-life for the oxygen adduct epr signal at room temperature in air is ~4weeks when entrapped in the zeolite compared to several minutes in free solution (10) (in the crystalline Co-salen solid, peroxy-dimers are formed exclusively (10)). This is a manifestation of the extremely effective site-isolation achieved by entrapping the complexes inside the pores of the zeolite leading to elimination of the normal autoxidation mechanism.

Secondly, an examination of the thermodynamics of oxygen binding as plotted in a Hill plot (Figure 2) at 4 different temperatures shows evidence of a negative cooperativity between cobalt binding sites (slope<1) (11). This result means that binding of oxygen to the first few cobalt sites makes it progressively more difficult for subsequent oxygen to bind to other sites. This is the reverse of hemoglobin's behavior. The explanation is still unclear, but may well result from progressively more difficult oxygen binding as one progresses from the exterior to the interior of each zeolite crystallite. Binding of oxygen at the cobalt sites in the outermost cages of the crystallite is easiest but binding becomes more difficult as the oxygen has to diffuse toward the interior sites. A van't Hoff plot of the data reveals an enthalpy of binding of -11.4Kcal/mol and an entropy of -51e.u. which compare with values of -12.4Kcal/mol and -47e.u. for the same complex in pyridine solution(12). The lower oxygen binding constants inside the zeolite therefore appear to result from a reduced exothermicity consistent with the oxygen being bound at a restrictive site where the sterics of interaction of bound oxygen with the zeolite cavity walls are important.

This example demonstrates the ability of zeolites to reproduce the control (typical of enzyme proteins) of both the interactions between active sites and the thermodynamics of reactions at those active sites. The next example demonstrates the zeolite's ability to kinetically control product selectivity in an oxidation reaction typical of the monooxygenase enzymes.

Cytochrome P450 Analogue

Further on down the respiratory chain from hemoglobin lie the monooxygenase enzymes, cytochromes P450, which perform the function of selectively oxidizing organic materials to usable or excretable

hydrophilic compounds. Their unique ability to convert, for example, unactivated alkanes to alcohols with unusual selectivities using only molecular oxygen and a reducing cofactor (while in aqueous solution and at room temperature) has made these materials the envy of synthetic organic chemists. There have been numerous attempts to model the heme-iron active site of the enzymes(13) so as to reproduce some of their selectivity by including multiple bulky peripheral substituents upon the basic porphyrin nucleus. While these models have undoubtedly contributed tremendously to an understanding of the mechanistic features of the monooxygenases they have yet to demonstrate the phenomenal selectivities.

The enzyme cycle is represented in Figure 3, emphasizing only the redox and coordination at the iron center. If one accepts the tenet that the FeO^{3+} species is the active potent oxidant then the selectivity of the enzyme is dictated by how the protein sieves and directs substrates toward this indiscriminate oxidant. How does nature produce this oxidant? she takes molecular oxygen, two electrons and two protons and eliminates water! Our mimic(14) is designed to do the same thing except that we will take the two electrons and two protons together as molecular hydrogen and combine it with oxygen over Pd(0) to generate hydrogen peroxide. This hydrogen peroxide can then be reacted at an iron site to eliminate water and give the desired FeO^{3+} unit. If all of this is done inside the stereochemically demanding pores of a zeolite then any substrate which is simultaneously in those pores should suffer selective oxidation by the FeO^{3+} as directed by the zeolite framework.

The mimic is prepared by sequential ion-exchanges with iron(II) and Pd(II) tetrammine cations followed by calcinations and reduction of the Pd(II) to Pd(0) as previously described(14). A material with ~2wt% Fe(II) and 1wt% Pd(0) is used by immersing the dry zeolite solid in neat substrate alkane and then pressuring the reaction vessel with a 3:1 mixture of oxygen:hydrogen. After shaking this mixture at room temperature for 4 hours the products are analyzed by capillary GC. As a control to assess the intrinsic selectivity of such a Pd/Fe system in the absence of steric effects of the zeolite, catalysts prepared with amorphous silico-aluminate supports were run for comparison. In these cases all reactions must take place at the particle surface since there is no interior pore structure available. In addition, comparison of reaction selectivities of this catalysts with our zeolite materials allows us to ascertain that the Fe active sites must be actually inside (and not on the exterior surface) of the zeolite crystallites.

The first zeolite host explored was zeolite A which is a very selective

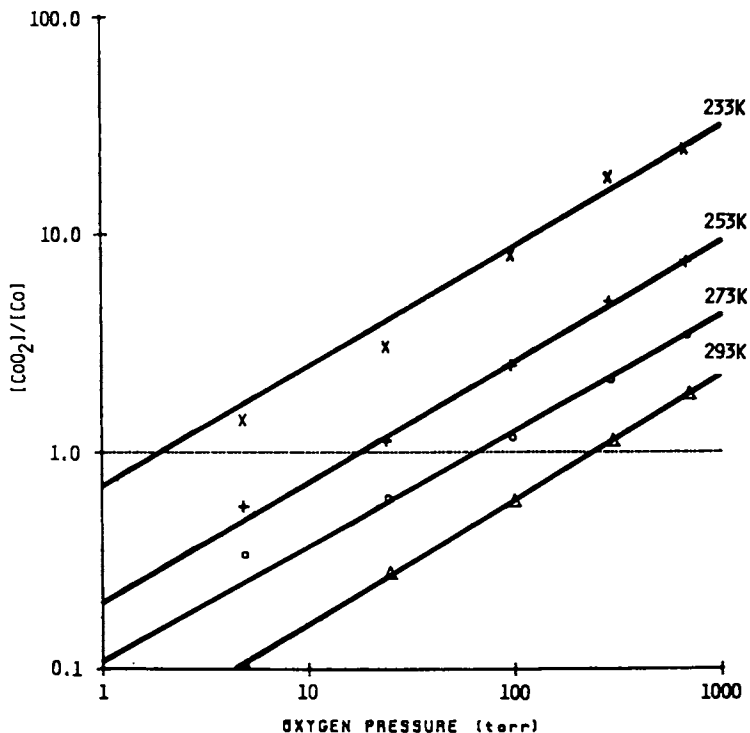


Figure 2. Hill plot of oxygen binding to Co-salen.py in zeolite Y.

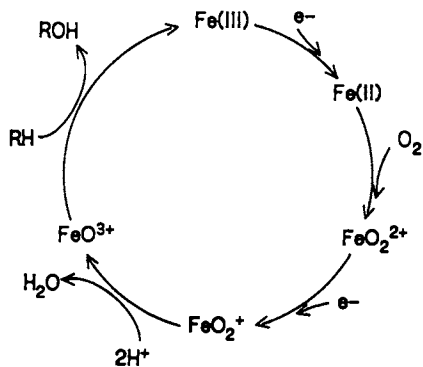


Figure 3. Enzyme cycle of Cytochrome P450.

absorbent of linear alkanes to the exclusion of branched or cyclic hydrocarbons(15). It was therefore expected that extreme examples of substrate selectivity could be achieved in competitive oxidation of linear alkanes vs. cyclic alkanes.

Figure 4a confirms this expectation. While the selectivity for oxidation of n-octane in the presence of cyclohexane is slight (55:45) over the control silicoaluminate support, the selectivity over the A zeolite is tremendous (>200:1) in favor of the linear alkane.(plots are of total of all oxidation products from each substrate) This indicates that the zeolite is exerting its sieving effect and therefore the desired chemistry is occurring inside the zeolite pores. Indeed, not only is the chemistry occurring there but the vast majority of the octanol products are remaining there at the end of the reaction and can only be released for analysis by complete destruction of the framework using conc. sulfuric acid! This trapping of products is more than simple absorption since they are not released simply by displacement with a more polar molecule (eg. water) The production of secondary alcohols as part of the product mix means that the pores of the zeolite rapidly become filled with molecules which are too large to escape from the interior and remain trapped. These molecules then act as plugs for escape of even the linear alcohol products so that the entire zeolite interior becomes saturated with products and the catalytic activity is shut down.

The incredible substrate selectivity of this system pales in comparison to the regioselectivity displayed by the octane oxidation products! In Figure 4b the dramatic increase of products derived from terminal methyl group oxidation in the zeolite system is apparent (plots are normalized to a "per hydrogen" basis and represent the total of products (alcohols and ketones) at each position in the chain). Over the control catalyst the primary/ secondary oxidation ratio is 0.05 while in the zeolite A this ratio is 0.6. This selectivity for oxidation toward the end of the alkane chain probably arises from the very close fit between the alkane and the A pore size which essentially constrains it to have an extended "linear" conformation. It is therefore the methyl end groups which are the first to encounter and so be oxidized by the iron active sites which tend to be located in the six ring faces of the zeolite cage (illustrated schematically in Figure 5).

While the selectivities of this system are dramatic the activity is low (~1 turnover on Fe in a 4 hr. batch run) and the necessity of running all reactions in an explosion rated environment (because of the H₂/O₂ mixtures) combined with the need to dissolve away the zeolite to reclaim products make this a very impractical synthetic method for alkane

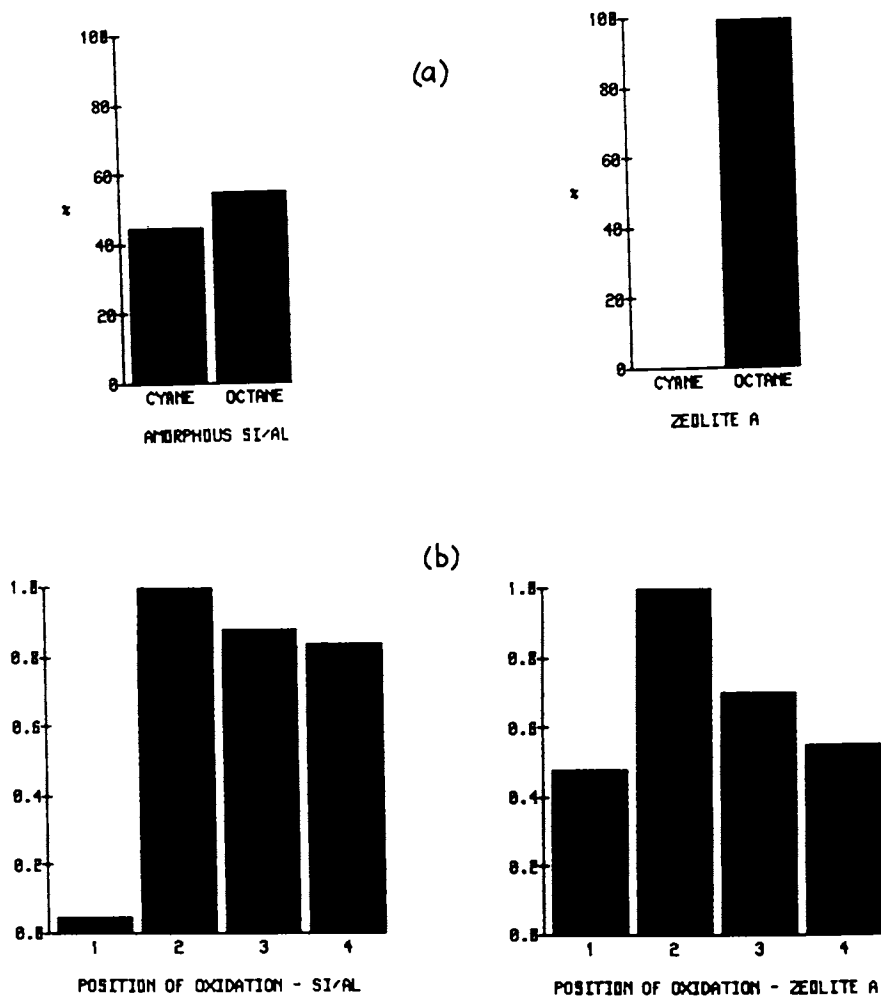


Figure 4. Selectivity of alkane oxidation with Fe/Pd/A zeolite and H_2/O_2 . a) substrate selectivity between n-octane and cyclohexane and b) regioselectivity of n-octane oxidation.

oxidation. These problems can each be addressed as follows. The low turnover and product trapping are really the same problem since we believe that it is the plugging of the pore system by products which leads to the shut down of the reaction since at that point no further substrate can get to the active sites - this is a familiar problem with zeolite catalysis (Herron, N. J. Coord. Chem., in press) and should be solved by two changes. 1) a larger pore system will permit egress of product secondary alcohols (at the obvious expense of lowered substrate selectivity) 2) a higher Si/Al ratio zeolite is more hydrophobic and at a ratio above ~20 begins to favor absorption of the reactant alkane over the product alcohols (at the expense of ion exchange sites). These criteria can be met by the ZSM-5 zeolite with its 10-ring channels and high Si/Al ratio. The inconvenience of using hydrogen/oxygen mixtures can be circumvented by using preformed hydrogen peroxide rather than making it in situ by combination over Pd(0). The ideal system is therefore a simple Fe ion-exchanged high silica ZSM-5 zeolite fed hydrogen peroxide (either aqueous or in organic solvents at low concentration). Oxidation of n-octane with this system does indeed lead to all products being recovered from the supernatant solution without zeolite dissolution and the system becoming truly catalytic with ~4 turnovers on Fe in 4 hours. Remarkably, the regioselectivity of the ZSM-5 system is even more pronounced for oxidation towards the terminus of the alkane chain with a primary/secondary oxidation ratio of 3.3. This material is now in the ballpark of a viable ω -hydroxylase mimic. This enzyme is capable of regioselective oxidation of terminal methyl groups of alkanes or linear carboxylic acids with a prim/sec oxidation ratio of ~10.

Iron-sulfur Protein Analogue

One of the essential cofactor enzymes in the cytochrome P450 network provides electrons to reduce iron and or oxygen to generate the active oxidant. These natural electron-transfer materials are typified by the iron-sulfur proteins(16). Work by Holm and others has modeled the basic iron-sulfur cores of these proteins and a variety of structure types have been modeled. One of these types, an iron-sulfur cubane like cluster consists of interpenetrating tetrahedra of iron and sulfide ions.

The fascination with using zeolites as very small reaction chambers for production of novel species which are not available in normal environments had led us to explore the possibility of synthesizing extremely small particles of semiconductor materials within the pores (Herron, N.; Wang, Y.; Stucky, G. D.; Eddy, M. M.; Cox, D. E.; Bein, T.;

Moller, K. *J. Am. Chem. Soc.* in press.)⁽¹⁷⁾. This is of interest from the standpoint that such small pieces of a bulk semiconductor lattice cannot fully develop the normal semiconductor band structure and so reside in the so called size-quantized or quantum-confined regime. This is where the electron-hole pair of an excited semiconductor particle has a radius⁽¹⁸⁾ larger than the actual particle size. The electron then behaves as a particle in a box and novel optical properties result. We decided, therefore, to look at preparation of CdS inside the zeolite cavities and then to explore the photo-oxidation chemistry of these species with absorbed olefins.

Cadmium ion-exchange of zeolite Y followed by calcination in flowing oxygen leads to materials having from 0 to 90% of the original sodium ions replaced by Cd. Treatment of the dry calcined zeolite with hydrogen sulfide gas (1atm) at 100°C generates the CdS clusters inside the zeolite pores⁽¹⁷⁾. The quantum confinement effects are manifest in that the material is typically white or pale cream rather than the yellow-orange of bulk CdS. The actual structure of the CdS units in the zeolite is revealed by a detailed study of the powder x-ray diffractograms and EXAFS data. These techniques reveal the basic unit to be a cubane Cd_4S_4 cluster of interpenetrating Cd and S tetrahedra - (Figure 6) very reminiscent of the Fe_4S_4 cluster core discussed above. These clusters are located in the small sodalite cages of the framework and are strongly interacting with it through Cd-O bonds (Figure 6). What is particularly interesting is how these clusters begin to interact with one another as the loading density begins to rise above the percolation threshold of 15 vol%. At this point the absorption spectra begin to reveal a new absorption band and luminescence behavior starts to switch on as the three dimensionally interconnected array (cluster-cluster distance of $\sim 6\text{\AA}$) of quantum dots begins to develop a semiconductor like band structure (Figure 6).

Since all of the CdS clusters reside in the sodalite cages of the zeolite Y framework, the larger supercages of the structure are still available for absorption of substrate molecules - in this case olefins for photo-oxidation via electron transfer. Colloidal CdS in free solution has been used for such oxidations previously⁽¹⁹⁾ and in a competitive oxidation of styrene and 1,1-diphenylethylene we find that unconfined bulk CdS will effect oxidation in a ratio of 1:2 for these two olefins (irradiation at 365nm). In the zeolite confined system we find however that the ratio becomes 1:1 ie a slight shift in selectivity toward the smaller substrate as may be expected on the basis of size/diffusion effects. From the viewpoint of the enzyme mimic, we have here a system

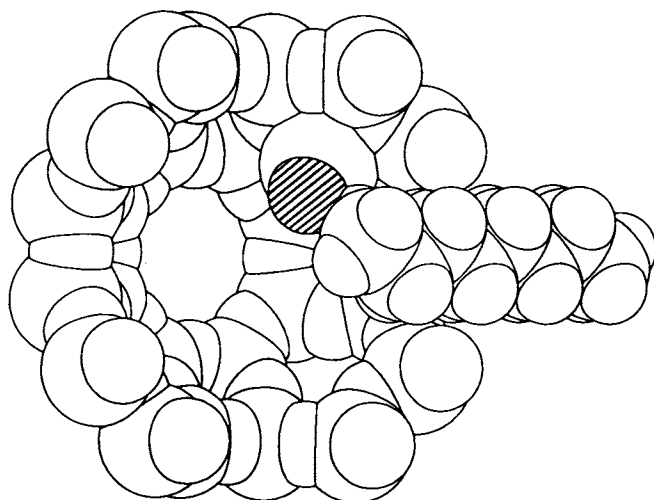


Figure 5. Cutaway representation of n-octane proceeding through the 8-ring window of zeolite A towards the iron active site for oxidation. Cross hatched atom is the active oxygen on iron.

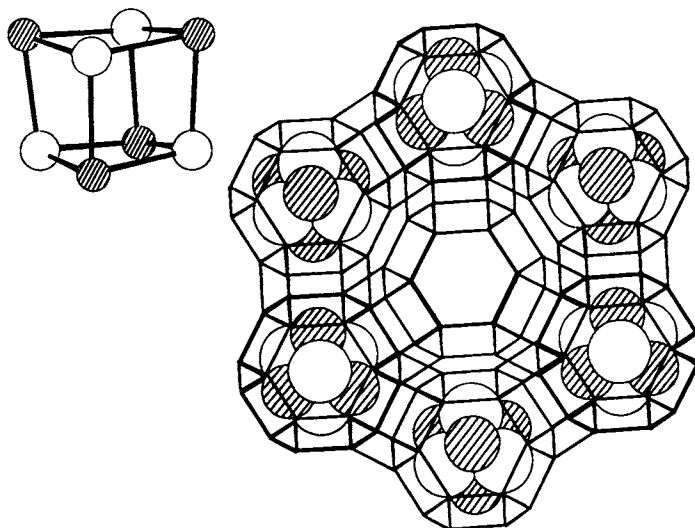


Figure 6. CdS clusters in the sodalite cages of zeolite Y. The zeolite has been reduced to sticks connecting only the tetrahedral atoms for clarity. Inset shows the structure of an individual CdS cubane-like cluster. Cd atoms are cross hatched.

which mimics the core structure of iron sulfur proteins while also undergoing electron transfer (photo stimulated) with substrate molecules in analogy with these same proteins.

The future of this line of research lies not in the enzyme mimicry described above but more in the novel optical and especially non-linear optical properties of quantum confined semiconductor systems - the production of optical computer elements such as optical transistors, spatial light modulators and phase conjugate materials. From the biomimetic perspective we are moving in the direction of the silicon-based brain!

Conclusion

The above examples have demonstrated that viable enzyme mimics of hemoglobin, cytochrome P450 and iron-sulfur proteins can indeed be produced by making use of the analogy between protein tertiary structure and the pore structure of inorganic "Si-based" zeolite systems. These examples represent only the tip of a potentially enormous mountain of novel, robust and highly practical enzyme mimics. It only requires that biochemists view zeolites as sterically demanding supports for active sites and that zeolite chemists view zeolites as something other than acid catalysts or ion-exchangers. If that can be communicated by this and similar articles there may be considerable "life" left in these old rocks yet.

Acknowledgments

The technical assistance of J. B. Jensen, S. Harvey, J. D. Nicholson and J. E. Macdougall was invaluable while contributions of Drs. C. A. Tolman, Y. Wang, D. R. Corbin, R. D. Farlee, G. D. Stucky, M. M. Eddy, W. E. Farneth, T. Bein and K. Moller to various aspects of this work were likewise dramatic. The assistance of E. Jayne Allen in preparing this manuscript is greatly appreciated.

Literature Cited

- 1) Dyer, A; Hayes, G. G.; Phillips, G. O.; Townsend, R. P. Molecular Sieves; ACS Adv. Chem. Ser., American Chemical Society: Washington, DC, 1973, No.121, 299.
- 2) Breck, D. W. Zeolite Molecular Sieves; Wiley: New York, 1974.

- 3) Collman, J. P.; Gagne, R. R.; Halbert, T. R.; Marchon, J. C.; Reed, C. A. J. Am. Chem. Soc. 1973, **95**, 7868.
- 4) see Jones, R. D.; Summerville, D. A.; Basolo, F. Chem. Revs., 1979, **79**, 139.
- 5) Alben, J. O.; Fuchsmayr, W. H.; Beaudreau, C. A.; Caughey, W. S. Biochemistry, 1968, **7**, 624.
- 6) Baldwin, J. M. Brit. Med. Bull. 1976, **32**, 213.
- 7) Herron, N. Inorg. Chem. 1986, **25**, 4717.
- 8) Wilmarth, W. K.; Aranoff, S.; Calvin, M. J. Am. Chem. Soc. 1946, **68**, 2263.
- 9) This term was first coined in Herron, N.; Stucky, G. D.; Tolman, C. A. Inorg. Chim. Acta 1985, **100**, 135.
- 10) Floriani, C.; Calderazzo, F. J. Chem. Soc. A 1969, 946.
Ochiai, E. I. J. Inorg. Nucl. Chem. 1973, **35**, 1727.
Barklelew, C. H.; Calvin, M. J. Am. Chem. Soc. 1946, **68**, 2257.
- 11) Hill, A. V. J. Physiol. (London) 1910, **40**, IV-VII.
- 12) Tazher, G.; Amiconi, G.; Antonini, E.; Brunori, M.; Costa, G. Nature (London) New Biol. 1973, **241**, 222.
- 13) see for example Cook, B. R.; Reinert, T. J.; Suslick, K. S. J. Am. Chem. Soc. 1986, **108**, 7281.
- 14) Herron, N.; Tolman, C. A. J. Am. Chem. Soc. 1987, **109**, 2837.
- 15) Barrer, R. M. in Zeolite and Clay Minerals as Sorbents and Molecular Sieves, Academic Press: New York, 1978.
- 16) Tsibris, J. C. M.; Woody, R. D. Coord. Chem. Revs 1970, **5**, 417.
Kimura, T. Structure and Bonding, 1968, **5**, 1.
- 17) Wang, Y.; Herron, N. J. Phys. Chem. 1987, **91**, 257.
- 18) Brus, L. E. J. Phys. Chem. 1986, **90**, 2555.
- 19) Fox, M. A. Acc. Chem. Res. 1983, **16**, 314.

RECEIVED November 7, 1988

Chapter 12

Immobilization of Proteins and Enzymes onto Functionalized Polypropylene Surfaces by a Gaseous Plasma Modification Technique

R. Sipehia, J. Daka¹, A. S. Chawla¹, and T. M. S. Chang

Artificial Cells and Organs Research Centre, Faculty of Medicine, McGill University, Montreal, Quebec H3G 1Y6, Canada

Polypropylene membranes or beads were treated in gaseous plasma of anhydrous ammonia in order to add amino groups on to their surfaces. The presence of the amino groups was detected by FT-IR-ATR spectrometry. Through these amino groups in one batch of the samples, albumin was immobilized. The presence of immobilized albumin on the polymer surface was confirmed by FT-IR-ATR spectrometry. Glucose oxidase and peroxidase were immobilized individually onto two separate batches of polypropylene beads with amino groups on their surfaces. With the help of calibration curves, it was found that 40-55% of the immobilized enzymes were in the active form. Beads and membranes bearing enzymes and other proteins are important materials for biotechnology. This technique demonstrates that even inert polymers can be activated easily for attachment of these biomolecules.

Gaseous plasma generated by an electrical discharge at low pressure provides a unique and powerful method for the modification of surfaces of biomaterials without altering their bulk properties. This modification could be made by plasma polymerization wherein a thin, highly cross-linked and pin hole free film of filler free silicone polymer could be added onto a variety of substrate materials in order to prepare improved blood compatible surfaces (1). Alternatively, gaseous plasma could be used to add new chemical groups to a material surface which could then be used for attaching a variety of biomolecules. By anhydrous ammonia plasma, amino groups can be added to the surface of polypropylene membranes or to the surface of polypropylene beads. These amino groups can then be employed to bind albumin to polypropylene as was done in our previous work in which a quantitative measure of bound protein was

¹Current address: Bureau of Radiation and Medical Devices, Health and Welfare Canada, Ottawa, Ontario K1A 0L2, Canada

0097-6156/89/0392-0155\$06.00/0
© 1989 American Chemical Society

done using ^{125}I -labelled albumin (2,3). It was found that immobilized albumin was strongly bound and had a higher surface concentration of $275 \mu\text{g}/\text{cm}^2$ compared with $28 \mu\text{g}/\text{cm}^2$ obtained by a chemical immobilization method (4). To show the versatility of the plasma technique, we have extended the work to enzymes; glucose oxidase and peroxidase, which were attached to two separate batches of polypropylene beads.

In the present studies, a Fourier-transform infra-red spectrometer in attenuated total reflectance mode (FT-IR-ATR) was used to characterize the albuminated polymer membrane surface. FT-IR-ATR is a powerful surface analysis technique in which a spectrum of only a few micron thick surface layer is obtained. As albumin or enzymes were attached only on the surfaces of polypropylene, FT-IR-ATR technique was ideally suited for their analysis.

MATERIALS AND METHODS

Glucose oxidase (from *Aspergillus niger*, specific activity 20 unit/mg), was purchased from Boehringer Mannheim Canada Ltd. (Dorval, Quebec, Canada). Bovine albumin (Fraction V), peroxidase (from Horseradish, specific activity 44 unit/mg) and O-dianisidine dihydrochloride (purified crystals) were purchased from Sigma Chemical Company (St. Louis, MO, USA). A 0.5M phosphate buffer at pH 7.5 was used in these studies.

Anhydrous ammonia was purchased from Matheson Canada Ltd., Whitby, Ontario. The substrate materials used were polypropylene membrane (Celgard-2400, Celanese Corp., Summit, NJ) and polypropylene beads (Hercules Canada Ltd., Montreal, Quebec). The Celgard-2400 was a $25.4 \mu\text{m}$ thick porous membrane with an effective pore size of $0.02 \mu\text{m}$ with a 38% porosity. The beads as purchased were slightly flattened spheres having a diameter of about 2.5-3 mm and being about 3.5 mm thick. The membranes and the beads were washed with distilled water, then with absolute ethanol in an ultrasonic cleaner and were finally dried in a vacuum oven, at about 70°C . These substrate materials were ready for use as a control or for further treatment. The further treatment involved the attachment of NH_2 groups onto the surface of the substrate material in an ammonia plasma reactor, perhaps by free-radical reaction, as reported in our previous report (2).

The detailed discussions of the plasma reactor used has already been given (5) Briefly, it was a cylindrical glass vessel of about $60 \times 10 \text{ cm}$ O.D. The radio frequency (RF) plasma generator (Tegal Corp., Richmond, California) was capacitatively coupled to the plasma reactor by placing flat strips of copper electrodes along the outside circumference. The substrate polymer membrane was placed 7.5 cm downstream from the gas outlets.

In order to activate polypropylene beads, 40 beads were placed inside a cylindrical container ($28 \times 8 \text{ cm}$ O.D.) which was then inserted in the plasma reactor. This container had an attached glass rod ($18 \times 1 \text{ cm}$ O.D.) the free end of which was coupled to an electric motor by which the container, and hence polypropylene beads, could be rotated inside the plasma reactor. The speed of rotation was 3 rpm during the process of attachment of NH_2 groups onto the surfaces of the beads.

The plasma reactor was evacuated using a rotary vacuum pump. The attachment of amino groups onto the surfaces of the membranes or beads was carried out at 0.4 mm Hg, because at this pressure, the attachment of NH_2 groups was found to be greatest (4). The 0.4 mm Hg pressure was maintained by anhydrous NH_3 feed. When the pressure inside the reactor had stabilized at 0.4 mm Hg a pulsed RF power of 30 W was applied. The times of power-on and power-off were equal. At the end of a 30-min reaction period, the plasma was switched off and the feed of anhydrous ammonia gas was stopped. The propylene beads were evacuated for an additional 30 min to remove the unreacted species. The beads exposed to ammonia gaseous plasma are referred to as PPB- NH_2 . To characterize the surfaces of the control and the modified membranes, the FT-IR spectrometry (Nicolet 7000 Series) with an ATR attachment was used. KRS-5 reflection plate at an incident angle of 45° was employed for FT-IR-ATR work. Control or modified membrane samples were applied on both sides of the reflection plate. This allowed spectra of only few micron thick layer of the surfaces contacting the KRS-5 reflection plate to be obtained. Immobilization of albumin onto membrane having surface amino groups has been described (2,3).

Attachment of glucose oxidase to the amino groups on the polypropylene beads was carried out as follows: a 5-mL solution of glucose oxidase, containing 20 mg of enzyme in phosphate buffer, (0.5M, pH 7.5) was prepared. Thirty beads (PPB- NH_2) were soaked in this solution for one hour. After removing the beads, the concentration of the remaining enzyme solution was measured and was used in calculating the initial concentration of the enzyme on the bead surface.

The beads removed from enzyme solution were washed several times with phosphate buffer solution in order to remove loosely bound glucose oxidase. They were then soaked in the cross-linking solution of 1.5% glutaraldehyde in phosphate buffer for 2 h. The beads were removed from the cross-linking solution, washed with phosphate buffer and left in 0.13 M glycine for 24 h to eliminate the remaining free aldehyde groups on their surface. These polypropylene beads, with immobilized glucose oxidase, were referred to as GO-PPB.

The procedure used to prepare immobilized peroxidase was the same as described above for the glucose oxidase. The polypropylene beads with immobilized peroxidase on their surface were designated as P-PPB.

In order to determine the quantity of enzyme which had been covalently immobilized onto the beads, calibration curves relating enzyme activities to enzyme concentrations were prepared. Various concentrations of each enzyme (glucose oxidase and peroxidase) were employed in these calibrations. O-Dianisidine was used as an enzyme reactant. The appearance of absorbency due to the oxidation of O-dianisidine at 460 nm, by the catalytic activity of the enzymes, was followed with the help of the Bausch & Lomb, Double Beam, Spectronic 2000 spectrophotometer. The rate of reaction increased with the increased amount of enzyme employed.

RESULTS AND DISCUSSION

The FT-IR-ATR absorption spectrum of the control polypropylene (untreated) is shown in Figure 1. It is a typical polypropylene spectrum with absorption bands due to asymmetric and symmetric stretching of CH_3 and CH_2 groups around 2900 cm^{-1} . The absorption bands at 1460 cm^{-1} and at 1380 cm^{-1} represent the asymmetric and symmetric bending of CH_3 , respectively. Absorption bands at 2878 cm^{-1} (CH_3 stretching) and at 841 cm^{-1} (Methylene rocking modes) suggest that the polypropylene membrane is of the isotactic form.

The FT-IR-ATR spectrum of the polypropylene membrane with amino groups on its surface is shown in Figure 2. The spectrum shows the appearance of a broad absorption bands between 3100 and 3600 cm^{-1} representing asymmetric stretching for NH_2 groups. The absorption band at about 1670 cm^{-1} represents the carbonyl stretching of an amide group (the amide I band). The band at about 1550 cm^{-1} represents the bending vibrations of $-\text{NH}_2$ group (the amide II band). These bands suggest that residual oxygen in the plasma reactor was taking part in the reactions to produce amide groups on the polymer surface.

FT-IR-ATR spectra of the control membrane and of the albuminated membrane are shown in Figures 3A and 3B, respectively. Only a part of the spectra of interest are shown. The amide I band of bovine albumin (highly α -helical) occur at 1658 cm^{-1} which is due to $\text{C}=\text{O}$ stretch. The amide II band appears at 1540 cm^{-1} representing $-\text{NH}$ bending.

The appearance of amide I and amide II bands in the FT-IR-ATR spectrum of the albuminated membranes (Figure 3B) confirms that albumin is indeed immobilized. The above band did not appear in the FT-IR-ATR spectrum of the control membrane (Figure 3A).

According to our activity-enzyme calibration curve, the total amounts of the immobilized glucose oxidase and peroxidase on the bead surface were found to be $52.0\text{ }\mu\text{g}/\text{cm}^2$ and $43\text{ }\mu\text{g}/\text{cm}^2$, respectively. To assess the stability of enzyme-polypropylene linkage (GO-PPB and P-PPB), the beads were washed with buffer for up to six hours. The results of washing GO-PPB and P-PPB are shown in Figure 4 and Figure 5, respectively. It can be seen from these figures that after the initial removal of the physically adsorbed enzymes, the concentrations of the enzymes tend to reach a steady state. After washing with a buffer for six hours, the amounts of glucose oxidase and peroxidase retained on the beads were found to be $20.36\text{ }\mu\text{g}/\text{cm}^2$ and $23.7\text{ }\mu\text{g}/\text{cm}^2$ respectively on the basis of calibration curves. Therefore, enzymes immobilized on polypropylene beads using anhydrous ammonia plasma varied between 39-55% of the original amounts. Control beads, which had no NH_2 groups on the surface but were exposed to enzyme solutions showed no attachment of the enzymes. This suggests that the NH_2 group is essential in the binding of enzymes to the bead surfaces and the binding force between the enzymes and the activated polypropylene support was strong.

CONCLUSION

The results of the present ammonia plasma treatment show that a polypropylene surface can be functionalized with NH_2 groups by the ammonia plasma technique. The resultant polymer is fairly suitable

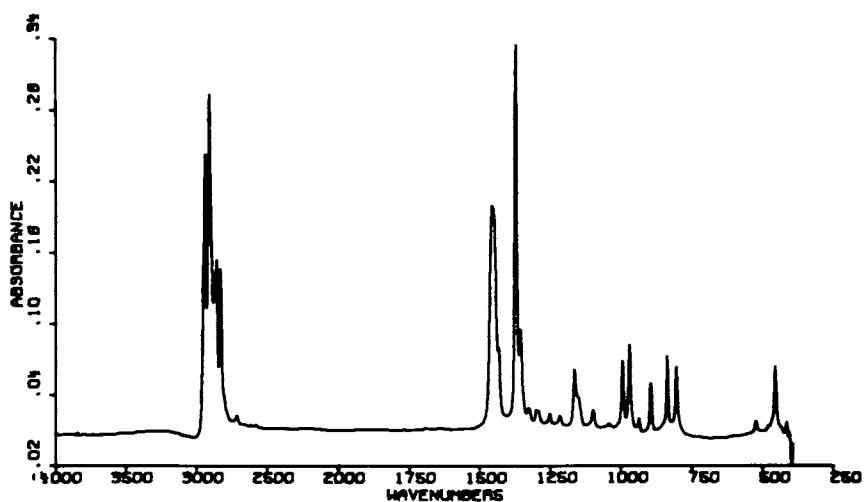


Figure 1. FT-IR absorption spectrum of an untreated polypropylene surface (control).

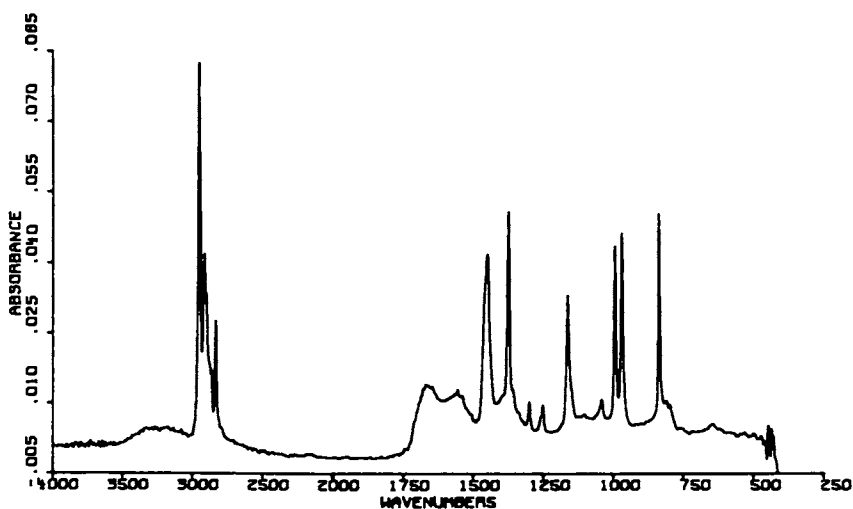


Figure 2. FT-IR spectrum of the polypropylene membrane with amino groups attached to its surface.

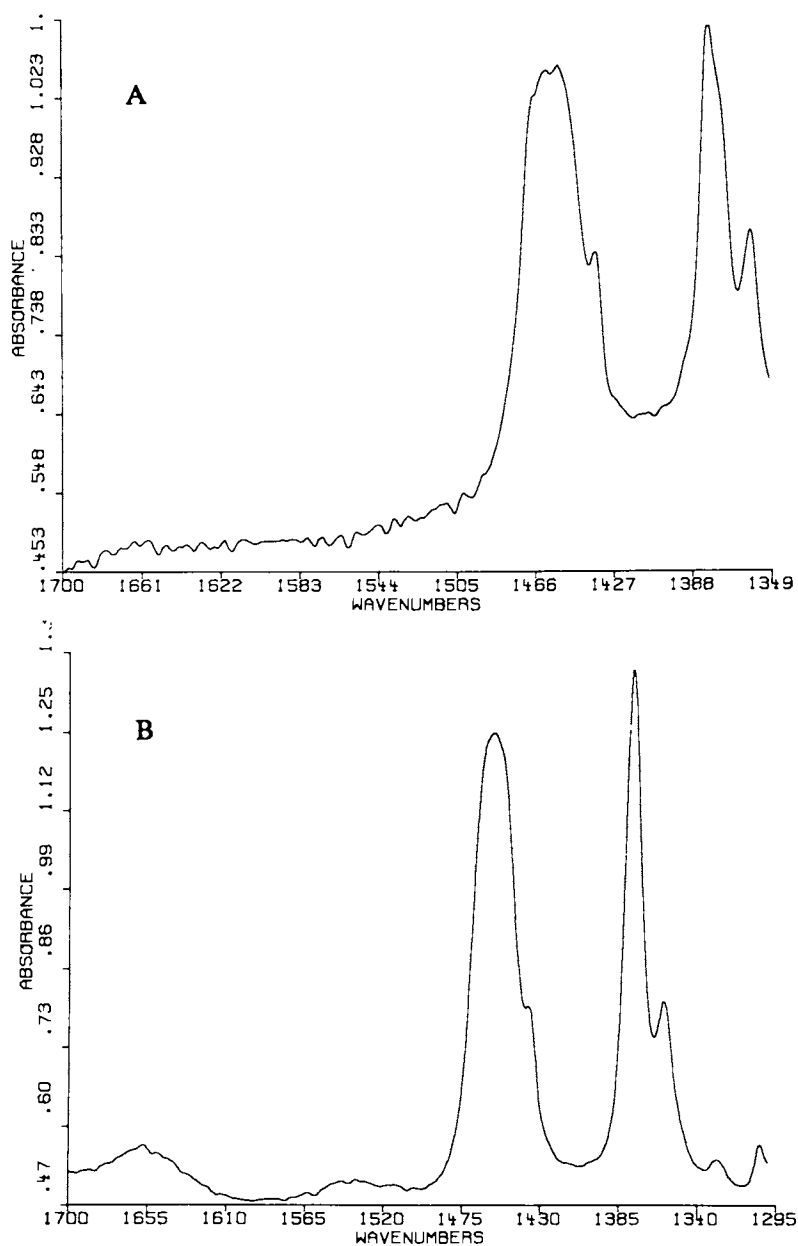


Figure 3. Comparison of the FT-IR spectra of a control polypropylene membrane (A) with that of the albuminated polypropylene membrane (B).

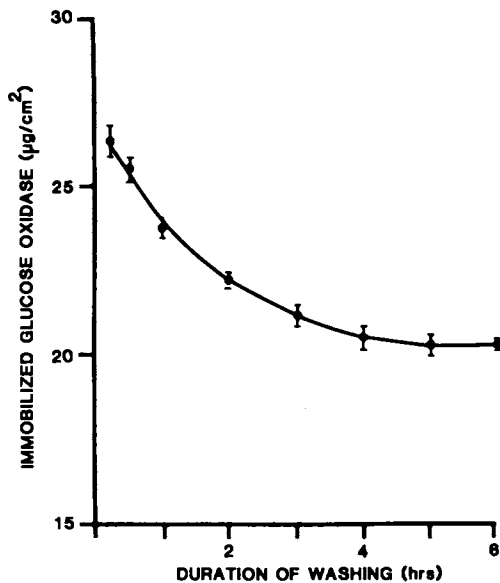


Figure 4. Concentration of immobilized glucose oxidase remaining on polypropylene beads (GO-PPB) after washing with phosphate buffer for various time intervals ($n=3$).

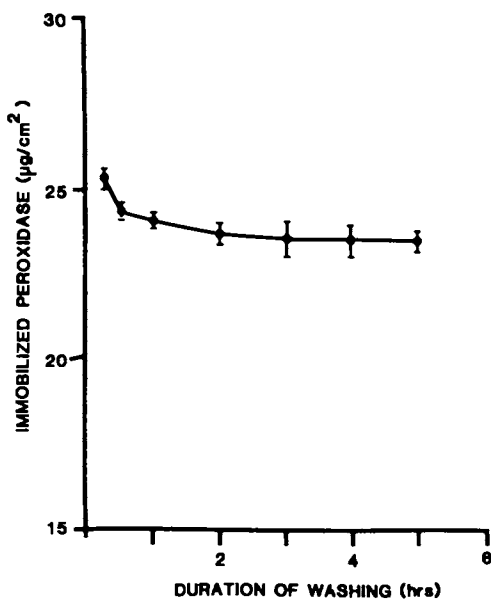


Figure 5. Concentration of immobilized peroxidase remaining on polypropylene beads (P-PPB) after washing with phosphate buffer for various time intervals ($N=3$).

for attachment of proteins, including those with catalytic properties such as enzymes. Thus the immobilization of proteinous antigens and antibodies to originally inert polypropylene can also be achieved by this method.

ACKNOWLEDGMENT

The financial support provided by the Medical Research Council of Canada, and the designation of grant support as a center of excellence in science and technology by the Ministry of Higher Education, Science and Technology of Quebec (to TMS Chang) is appreciated.

REFERENCES

1. Chawla, A.S.; Sipehia, R. J. Biomed. Mater. Res. 1984, 18, 537-545.
2. Sipehia, R.; Chawla, A.S. Biomat., Med. Dev., Art. Org. 1982, 10, 229-246.
3. Sipehia, R.; Chawla, A.S.; Chang, T.M.S. Biomaterials 1986, 7, 471-473.
4. Hoffman, A.S.; Schmer, G.; Harris, C.; Kraft, W.G. Trans. Amer. Soc. Artif. Int. Organs 1972, 18, 10-16.
5. Chawla, A.S. Trans. Amer. Soc. Artif. Int. Organs 1979, 25, 287-293.

RECEIVED November 28, 1988

Author Index

- Alber, Thomas C., 34
Blanch, Harvey, 104
Burrington, James D., 1
Chang, T. M. S., 155
Chawla, A. S., 155
Christou, George, 116
Clark, Douglas S., 104
Creagh, Louise, 104
Daka, J., 155
Davenport, Robert C., Jr., 34
DiCosimo, Robert, 123
Farber, Gregory K., 34
Ferguson, H. D., 90
Fish, Richard H., 116
Folkman, Judah, 19
Fong, Raymond H., 116
Giammona, D. Ann, 34
Glasfeld, Arthur M., 34
Gleason, K. K., 90
Goddard, William A., III, 65
Good, Mary L., xi
Guinn, Mark, 104
Hatton, T. A., 90
Herron, Norman, 141
Horrocks, William D., 34
Kanaoka, Masaharu, 34
Klopman, Gilles, 52
Lolis, Elias, 34
Naylor, Adel M., 65
Petsko, Gregory A., 34
Prausnitz, John, 104
Price, Robert T., 116
Ringe, Dagmar, 34
Shield, J. W., 90
Sipehia, R., 155
Skerker, Paul, 104
Szabo, Hsiao-Chiung, 123
Tiraby, Gerard, 34
Venegas, Ruben E., 52
Vincent, John B., 116
Weisz, Paul B., 6,19

Affiliation Index

- Allied-Signal, Inc., xi
B.P. America Research and Development, 1,123
California Institute of Technology, 65
Case Western Reserve University, 52
E. I. du Pont de Nemours and Company, 141
Harvard Medical School
and Children's Hospital, 19
Indiana University, 116
Massachusetts Institute of Technology, 34,90
McGill University, 155
University of California-Berkeley, 104,116
University of Pennsylvania, 6,19

Subject Index

A

- Acetaldehyde, effect on catalytic
oxidation, 132,133f
Acid-catalyzed dehydration, lignin model
compounds, 130-131
Activating fragments, definition, 54
Activity, determination in peptide
fragments, 54
 β -Alanine dendrimers
cascade growth pattern, 67,68f
minimum diameter vs. generation, 71,72f
molecular dynamic simulations, 67,69
monomer unit, 67

Author Index

- Alber, Thomas C., 34
Blanch, Harvey, 104
Burrington, James D., 1
Chang, T. M. S., 155
Chawla, A. S., 155
Christou, George, 116
Clark, Douglas S., 104
Creagh, Louise, 104
Daka, J., 155
Davenport, Robert C., Jr., 34
DiCosimo, Robert, 123
Farber, Gregory K., 34
Ferguson, H. D., 90
Fish, Richard H., 116
Folkman, Judah, 19
Fong, Raymond H., 116
Giammona, D. Ann, 34
Glasfeld, Arthur M., 34
Gleason, K. K., 90
Goddard, William A., III, 65
Good, Mary L., xi
Guinn, Mark, 104
Hatton, T. A., 90
Herron, Norman, 141
Horrocks, William D., 34
Kanaoka, Masaharu, 34
Klopman, Gilles, 52
Lolis, Elias, 34
Naylor, Adel M., 65
Petsko, Gregory A., 34
Prausnitz, John, 104
Price, Robert T., 116
Ringe, Dagmar, 34
Shield, J. W., 90
Sipehia, R., 155
Skerker, Paul, 104
Szabo, Hsiao-Chiung, 123
Tiraby, Gerard, 34
Venegas, Ruben E., 52
Vincent, John B., 116
Weisz, Paul B., 6,19

Affiliation Index

- Allied-Signal, Inc., xi
B.P. America Research and Development, 1,123
California Institute of Technology, 65
Case Western Reserve University, 52
E. I. du Pont de Nemours and Company, 141
Harvard Medical School
and Children's Hospital, 19
Indiana University, 116
Massachusetts Institute of Technology, 34,90
McGill University, 155
University of California-Berkeley, 104,116
University of Pennsylvania, 6,19

Subject Index

A

- Acetaldehyde, effect on catalytic
oxidation, 132,133f
Acid-catalyzed dehydration, lignin model
compounds, 130-131
Activating fragments, definition, 54
Activity, determination in peptide
fragments, 54
 β -Alanine dendrimers
cascade growth pattern, 67,68f
minimum diameter vs. generation, 71,72f
molecular dynamic simulations, 67,69
monomer unit, 67

- β -Alanine dendrimers—*Continued*
solvent-accessible surface, 69,70f
structures for early generations, 67,69
structures for higher generations, 69,70f
- Albuminated polypropylene membrane,
FT-IR-ATR spectra, 158,160f
- Aldehyde, isomerization to
ketone, 34–35,36f
- Alkylbenzenes, autoxidation to
aldehydes, 124
- Amino acids, IUPAC coding system, 54r
- Angiogenesis
consequences, 20
definition, 20
inhibition, 20–30
physiological process, 20
relationship between chemical engineering
and biomedicine, 16
schematic representation, 20,25f
- Antiangiogenic effectiveness
dose–response study, 24,25f
examples, 23r
- Aromatic molecules, ionization
potentials, 124
- Artificial biocatalytic systems, design for
fuel and chemical feedstock
production, 65
- B**
- Biocatalysis, barriers to
commercialization, 3–4
- Biochemistry, focus of interest, 9
- Biological catalysts, selectivity
advantage, 3
- Biomaterial surfaces, modifications by
gaseous plasma, 155–162
- Biomedicine, interrelationship with chemical
engineering, 9–10,11f,12
- Biomimetic catalysts
activation of hydrocarbons, 117–121
definition, 116
- Biomimetic catalytic oxidation
disadvantages, 136–137
selectivity to C α –C β bond cleavage vs.
catalyst concentration, 132,134f,135–136
- Biomimetics, possible applications, 4
- Bleaching of paper pulp, use of
lignin-degrading enzymes, 124
- C**
- Cannizzaro reaction, description, 49
- Catalysis
advantages of reactivity control, 2
impact, 2–3
- Catalysis—*Continued*
role in functional and specialty
chemicals, 3
role in petroleum industry, 3
technical advances, 4
- Catalytic oxidation, 1-(3,4-dimethoxyphenyl)-
2-(2-methoxyphenoxy)propane-
1,3-diol, 131–136
- Catalytic processes, selectivity, 2
- Chemical bleaching effluents, toxicity, 124
- Chemical engineering science
design of catalysts for chemical
processes, 9
focus of interest, 9
interrelationship with
biomedicine, 9–10,11f,12
- Chemistry, focus of interest, 9
- Chick embryo bioassay, experimental
procedure, 23
- Chorioallantoic membrane assay, experimental
procedure, 23
- α -Chymotrypsin
enzyme mimic, 12,13–14f
hydrolysis kinetics of
substrates, 94,96–97,98f
- Cobalt salen
Hill plot of oxygen binding, 145,147f
representation inside zeolite Y
supercage, 143,144f
structure, 143
- Computer-automated structure evaluation
program
application to snake venom toxicity
studies, 55–63
methodology for amino acid sequence
studies, 53,54r,55
relation between peptide sequences and
biological activity, 52
- Corneal neovascularization,
inhibition, 24,26–27f
- Cyclodextrins
bonding to cell surface, 22–23
description, 22
stability constants for steroids, 22
- Cytochrome P–450
active site, 116
enzyme cycle, 146,147f
function, 145–146
preparation of mimic, 146
schematic representation, 65,66f
- Cytotoxins of snake venom
backbone, typical, 60,62f
description, 52
examples, 57,58r
fragments responsible for activity, 60,63
fragments with toxicity function, 57,59f
quantitative structure–activity
relationship, 57,59

D

- Deactivating fragments, definition, 54
- Dihydrofolate reductase
 active site of binary complex, 74,75f
 active site residue of natural mutants, 79,80r
 binding of methotrexate, 77,78f
 catalytic properties, 73
 conformation of bound inhibitor, 82,83f
 conformation of bound substrate, 82,84,85f,86
 docked active site regions, 79,81f
 effect of site mutation on rate, 74,77,78f
 Gibbs free energy plot of kinetic profiles, 77,78f
 role in cell metabolism, 73
 steady-state kinetic cycle, 74,76f
 structure, 73
 surface comparison of natural mutants, 79,81f,82
- Dihydroxyacetone phosphate, binding conformation, 43
- 1-(3,4-Dimethoxyphenyl)-2-(2-methoxyphenoxy)propane-1,3-diol, catalytic oxidation, 131–136
- Dipeptide formation
 influence of localization and concentration of species in reaction medium, 94,95f
 reaction mechanism in reversed micelles, 94,95f
 time course of reaction, 92,93f,94
- Dopamine
 complex with sequestered dendrimers, 69,71,72f
 structure, 69
- Dopamine–dendrimer systems,
 structure, 71,75f

E

- Endothelial cells
 control of growth, 20
 growth, 19–20
- Enzymatic reactions, role of water at low water concentration, 104–113
- Enzymatic reactions in reversed micelles
 dipeptide formation, 92,93f,94,95f
 effect of substrate localization, 97,99–103
 experimental procedures, 91–92
 kinetics of model substrates, 94,96–100
 materials, 91

Enzyme(s)

- advantages, 3
 definition, 142
 immobilization onto functionalized polypropylene surfaces, 155–162
- Enzyme-catalyzed reactions in organic solvents, potential advantages, 90
- Enzyme mimics, zeolite catalysts, 141–153

F

- Fourier-transform infrared spectrometry in attenuated total reflectance mode (FT-IR-ATR), description, 156
- Fragment, description, 12,15
- Functionally invariant residues,
 definition, 53

G

- Gaseous plasma, biomaterial surface modification, 155–162
- Glucose isomerase
 applications, 35
 chemical mechanism, 38–39
 conformational change on substrate binding, 42–43
 crystal structure of enzyme–substrate complex, 48
 enzyme–substrate complex without metals, 48
 isomerization of ketone to aldehyde, 35,37f
 kinetic parameters, 38
 mechanism of isomerization catalysis, 48–50
 reaction rate, 38
 structure, 40,41f
 structure of enzyme–substrate complexes, 40,42,47–50
- Glucose oxidase
 experimental procedures for immobilization, 156–157
 immobilized, concentration on polypropylene beads, 158,161f
- Glycosaminoglycan, fragment, 15

H

- Hemoglobin
 composition, 143
 function, 143
 synthetic mimic, 143–145

Heparin

- composition, 21
 - effective replacement for angiogenic control, 23*r*,24,25*f*
 - fragment, 15
 - fragment activity, 21
 - use in angiogenesis inhibition, 20–21
- Hyaluronic acid, fragments, 15
- Hydrocarbon activation, biomimetic catalysts, 117–121
- Hydrocortisone, use in angiogenesis inhibition, 20

I

- Immobilized glucose oxidase, concentration on polypropylene beads, 158,161*f*
- Immobilized horse liver alcohol dehydrogenase in organic solvents active site structure determination by spin-labeling, 106
- effect of solvent water content on activity, 105–108,110
- effect of solvent water content on thermal inactivation, 107,110*r*
- electron paramagnetic resonance spectroscopy, 106–107,108*f*
- experimental procedures, 105
- Immobilized peroxidase concentration on polypropylene beads, 158,161*f*
- preparation, 157
- Inhibition of angiogenesis antiangiogenic effectiveness, 23*r*,24,25*f*
- corneal neovascularization inhibition, 24,26–27*f*
- measurement in chick embryo bioassay, 20–21
- mechanism, 20
- model and mechanism, 24,28,29*f*,30
- simplest model approach, 21–22
- use of hydrocortisone and heparin, 20–21
- Interdisciplinary research, advantages, 6–7
- Iron–sulfur protein function, 150
- mimic preparation, 151,152*f*,153
- Isomerization, aldehyde to ketone, 34–35,36*f*
- IUPAC coding system, amino acids, 54*r*

K

- Keggin ions, manganese-substituted catalysts, 121*r*
- Ketone, isomerization to aldehyde, 34–35,36*f*

L

- Leuckart reaction, description, 49
- Lignin, description, 124
- Lignin model compounds acid-catalyzed dehydration, 130–131
- catalyst regeneration using peracetic acid, 127*r*,130
- catalytic oxidations, 131–136
- experimental procedures for catalytic oxidation, 138
- preparation, 137
- products of C_α–C_β bond cleavage, 126,128–129*f*
- stoichiometric oxidation, 126,127*r*
- stoichiometric oxidation with cobalt(III) acetate, 138
- structures, 126,128–129*f*
- Ligninase C_α–C_β bond cleavage, 124,125*f*
- limitation in lignin degradation in paper pulp, 124
- Long neurotoxins of snake venom, description, 52
- Lung surface, bacterial clearance, 12,13*f*

M

- Manganese nonporphyrin catalyst carbon–hydrogen bond reactivity of hydrocarbons, 117,120*r*
- mechanism of hydrocarbon activation, 117
- structures, 117,119*f*
- Manganese open-faced porphyrin catalyst carbon–hydrogen activation of hydrocarbons, 117,118*f*
- structure, 117,119*f*
- Manganese-substituted Keggin ions carbon–hydrogen activation of hydrocarbons, 121*r*
- structure, 119*f*,121
- Manganese supramolecule porphyrin catalyst carbon–hydrogen activation of hydrocarbons, 117,118*r*
- structure, 117,119*f*
- Medicine, focus of interest, 9
- Merrwein–Ponndorf–Verley–Oppenauer reaction, description, 49–50
- Methane monooxygenase, active site, 116
- Methotrexate binding, 77,78*f*
- structure, 73–74
- Micelle volume fraction, calculation, 96
- Molecular biology, focus of interest, 9
- Molecular complexes, representation, 7,8*f*
- Molecular encapsulation, starburst dendrimers, 67–72

- Molecular entities**
 chemical composition, 7
 structure, 7
 systems of molecules, 7
 systems of systems, 7
- Molecular systems**
 challenges, 15–16
 representation, 7,8f
 trends, 12,13–14f,15
- Molecules**
 representation, 7,8f
 systems, 7
- Myoglobin**, function, 143
- Myosin**, subfragments, 15
- N**
- Neurotoxins**, invariant residues, 53
- P**
- Paper pulp**, chemical bleaching, 123–124
- Partition coefficient**, definition, 94,96
- Pasteur**, Louis, father of biomedical science and technology, 7
- Peptide(s)**, small, applications, 91
- Peptide data base**, fragmentation, 54
- Peptide fragments**, activity
 determination, 54–55
- Peroxidase**, immobilized
 concentration on polypropylene
 beads, 158,161f
 preparation, 157
- Polypropylene**, FT-IR-ATR absorption
 spectrum, 158,159f
- Polypropylene membrane with amino groups**,
 FT-IR-ATR spectrum, 158,159f
- Proteins**, immobilization onto functionalized
 polypropylene surfaces, 155–162
- R**
- Reversed micellar system**
 bimolecular rate constant vs. micelle
 volume fraction, 97,98f
 chemical shifts, 99r,100f
 comparison of solubility of
 substrates, 96,97f
 effect of substrate configuration, 101
 effect of substrate localization on
 reaction rate, 97–103
 hydrolysis rates vs. those in aqueous
 solution, 96–97,98f,100f
 kinetics of model substrates, 94,96–100
- Reversed micellar system—Continued**
 schematic representation of substrate
 interaction with surfactant head
 groups, 101,102f
 spin–lattice relaxation rates, 97,99,101r
- Reversed micelles**
 applications, 107,109
 definition, 90–91
 enzymatic reactions, 91–103
 formation, 109
 schematic representation, 91,93f
 tryptophan synthesis, 109,110f
- S**
- Sequestered dendrimers**, complex with
 dopamine, 69,71,72f
- Short neurotoxins of snake venom**
 backbone, typical, 60,61f
 description, 52
 examples, 55,56r
 fragments responsible for activity, 60
 fragments with toxicity function, 55f,57r
 primary structure, 59f,60
 quantitative structure–activity
 relationship, 55,57
- Simplest model approach**, description, 21
- Small peptides**, applications, 91
- Snake venom toxins**
 categories, 52
 computer-automated structure evaluation of
 activity, 52–63
 elucidation of active site, 53
- Starburst dendrimers**
 cascade growth pattern, 67,68f
 molecular encapsulation, 67–72
- Steroid–saccharide–cell system**
 effectiveness, 28
 mechanism, 28,29f,30
 model for interaction, 24,28
- Structurally invariant residues**,
 definition, 53
- Sulfate**, role in strong cell adhesion, 22–23
- T**
- 5,6,7,8-Tetrahydrofolate**, structure, 73
- Toxins**, elucidation of active site, 53
- Triose phosphate isomerase**
 active site, 40
 active site in enzyme–substrate
 complex, 44,45f
 chemical mechanism, 38–39
 conformational change on substrate
 binding, 42–43

Triose phosphate isomerase—*Continued*
crystal structure, 46
free energy profile, 35,38
isomerization of ketone to aldehyde, 35,36f
kinetic parameters, 35,38
minimum perturbation approach to complex
structure determination, 43–44
reaction rate, 38
replacement of His–95 with Gln, 46
structure, 39–40,41f
structure of enzyme–substrate
complexes, 40,42–47
Tryptophan, synthesis, 109,110f
Tryptophanase in reversed micelles
effect of solvent water content on
spin-label, 111,113f
effect of water content on amount of
tryptophan production, 111,112f
electron paramagnetic resonance
spectroscopy, 111,112–113f
experimental procedures, 109,111
tryptophan synthesis, 109,110f

W

Water, effect on enzyme reaction
rate, 104–113

Z

Zeolite(s)
ability to control active site interactions
and thermodynamics, 143–145,147
applications, 141
description, 142
preparation of cytochrome P–450
mimic, 146
Zeolite A
representation of *n*-octane proceeding
toward Fe active site for
oxidation, 148,152f
selectivity for alkane
oxidation, 148,149f,150
**Zeolite catalysts, use as enzyme
mimics, 141–153**
Zeolite Y
CdS clusters in sodalite
cages, 151,152f,153
cobalt salen inside supercage, 143,144f

*Production by Rebecca Hunsicker
Indexing by Deborah H. Steiner*

*Elements typeset by Hot Type Ltd., Washington, DC
Printed and bound by Maple Press, York, PA*